

# Early-age Fracture Response of Concrete with Hybrid Steel and Macro-synthetic Polypropylene Fiber Blends

Jayakrishnan R

CE14MTECH11004

A Dissertation Submitted to  
Indian Institute of Technology Hyderabad  
In Partial Fulfillment of the Requirements for  
The Degree of Master of Technology



भारतीय प्रौद्योगिकी संस्थान हैदराबाद  
Indian Institute of Technology Hyderabad

Department of Civil Engineering

## Declaration

I declare that this written submission represents my ideas in my own words. and where others' ideas or words have been included, I have adequately cited and referenced the original sources. I also declare that I have adhered to all principles of academic honesty and integrity and have not misrepresented or fabricated or falsified any idea/data/fact/source in my submission. I understand that any violation of the above will be a cause for disciplinary action by the Institute and can also evoke penal action from the sources that have thus not been properly cited, or from whom proper permission has not been taken when needed.

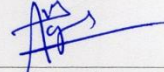


Jayakrishnan R

CE14MTECH11004

## Approval Sheet

This thesis entitled **Early Age Fracture Response of Concrete with Hybrid Steel and Macro Polypropylene Fiber Blends** by Jayakrishnan R is approved for the degree of Master of Technology from IIT Hyderabad.



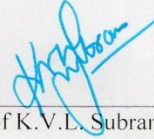
---

Dr. Anil Agarwal  
Examiner



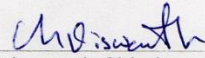
---

Dr. S. Suriya Prakash  
Examiner



---

Prof K.V.L. Subramaniam  
Adviser



---

Dr. Vishwanath Chinthapenta  
Chairman

## Acknowledgements

I would like to convey my gratitude to my advisor, Dr. K.V.L.Subramaniam for his guidance throughout this project. His suggestions during the three stages of my research, i.e. experimental, analytical and numerical work, have contributed to my knowledge and have vastly improved the quality of this thesis. I would also like to thank Dr. S.Suriya Prakash for his feedback on my experiments.

I extend my special gratitude to my fellow student, James Jose, K. Chiranjeevi Reddy, G. Sahith Reddy, for his guidance and help in conducting experiments. Thanks are also due to G.V.P. Bhagath Singh for his valuable support in the laboratory.

Finally, my friends, Smriti P Hareendran, G Jyotsna and G Prithvi Raj provided me good company during this period. I will always cherish the time spent with them.

Dedicated to

My Parents

## Nomenclature

$P_1$	First peak load
$P_u$	Peak load in load deflection response
$\delta_u$	Deflection corresponding to $P_u$
$P_{crit}$	Load corresponding to immediate lowest point after peak load
$\delta_u$	Deflection corresponding to $P_{crit}$
$\delta_p$	Net deflection at peak
$\delta_1$	First-peak loads
$F_p$	Peak Strength
$f_1$	First-Peak Strength
$PD600$	Residual load at net deflection of $L/600$
$AD600$	Residual Strength at net deflection of $L/600$
$PD150$	Residual load at net deflection of $L/150$
$AD150$	Residual Strength at net deflection of $L/150$
$TD150$	Area under the load vs. net deflection curve 0 to $L/150$
$RT,D150$	Equivalent flexural strength
$TJSCE$	Toughness
$FJSCE$	Toughness factor
$CMOD$	Crack mouth opening displacement
$LOP$	Limit of proportionality
$FL$	Load corresponding to LOP
$f_{ct,Lf}$	Strength corresponding to LOP
$F_i$	Load corresponding to with $CMOD = CMOD_j$ or $\delta = \delta_i$ ( $i = 1,2,3,4$ )
$f_{R,j}$	Residual flexural Tensile Strength corresponding with $CMOD = CMOD_j$ where ( $i = 1.5, 2.5, 3.5, 4.5$ )
$CTOD$	Crack Tip opening displacement

PIf	First crack load
$f_{If}$	First crack strength
PPFRC	Polypropylene Nylon Fiber Reinforced Concrete.
SFRC	Steel Fiber Reinforced Concrete.
HyFRC	Hybrid Fiber Reinforced Concrete.

# Contents

List of figures.....	11
List of Tables.....	16
Chapter 1: Introduction.....	17
1.1 Introduction.....	18
1.2 Objectives.....	19
Chapter 2: Review of Standard Test Methods and Literature.....	20
2.1 Introduction.....	20
2.2 Review of fibers.....	21
2.2.1 Steel fibers.....	24
2.2.2 Polypropylene fibers.....	26
2.3 Hybrid Fiber Reinforced Concrete.....	29
2.4 Standard Test Methods.....	34
2.4.1 ASTM 1609 Test Procedure.....	35
2.4.2 ASTM 1018 Test Procedure.....	37
2.4.3 JSCE SF4 Test Procedure.....	39
2.4.4 RILEM TC 162 Test Procedure.....	41
2.4.5 UNI 11039-2 Test Procedure.....	42
2.4.6 EN 14651 Test Procedure.....	44
Chapter 3: Materials and Methods.....	47
3.1 Introduction.....	47
3.1.1 Cement.....	47
3.1.2 Fly Ash.....	47
3.1.3 Aggregates.....	47



3.1.4 Synthetic Fibers.....	47
3.1.5 Steel Fibers.....	48
3.1.6 Admixtures.....	49
3.2 Experimental Program.....	49
3.2.1 Casting and Curing Specimen.....	50
3.3 Test Methods.....	51
3.3.1 Slump.....	51
3.3.2 Compressive Strength Testing.....	52
3.3.3 Four Point Bending Test.....	52
3.4 Test Matrix.....	54
Chapter 4: Experimental Results.....	55
4.1 Introduction.....	55
4.2 Compressive Strength.....	56
4.3 Flexural Test Results as per ASTM C1609 (For unnotched beam).....	57
4.4 Flexural Test Results as per EN 14651-2005 (For notched beam).....	65
4.5 Analysis of Data.....	68
4.6 Summary of Findings.....	74
Chapter 5: Digital Image Correlation Results.....	74
5.1 Introduction.....	74
5.2 Background.....	76
5.3 Results.....	77
5.4 Analysis of results.....	95
5.5 Summary and findings.....	96
Chapter 6: Analytical Model.....	97

6.1 Introduction.....	97
6.2 Load deflection curve from moment curvature analysis.....	101
6.3 Proposed Analytical Formulation for multi-linear softening.....	102
6.4 Inverse Analysis.....	106
Chapter 7: Summary of findings and future works.....	113
References.....	116
Appendix.....	123

## List of Figures

Figure 2.1: The composite stress-strain curves for fiber-reinforced brittle matrix: (a) Low fiber volume content; (b) intermediate volume fraction; and (c) high volume fraction.....	22
Figure 2.2: Strain hardening response of polypropylene fiber composites.....	24
Figure 2.3: Effect of steel fiber shape on the load response in flexure.....	26
Figure 2.4: Various types of synthetic fibers tested in the present study.....	28
Figure 2.5: Comparison of absorbed energies from pullout tests for various fiber types [23].....	28
Figure 2.6: Load-deflection curves for Hooked end steel fibers and Synthetic fibers.....	29
Figure 2.7: Load-deflection plots for various fiber combinations.....	32
Figure 2.8: Plastic shrinkage crack in the steel-polypropylene hybrid concrete.....	34
Figure 2.9: Diagrammatic View of a Suitable Apparatus for Flexure Test of Concrete by Third-Point Loading Method.....	36
Figure 2.10: Example of Parameter Calculations.....	36
Figure 2.11: Important Characteristics of the Load-Deflection Curve.....	38
Figure 2.12: Definition of Toughness Indices for Elastic-Plastic Material Behavior.....	39
Figure 2.13: Definitions of JSCE Toughness and Toughness Factor.....	40
Figure 2.14: Schematic diagram of the UNI 11309 four-point bending test setup.....	42

Figure 2.15: (a) Basic concrete load-CTOD, (b) Load-CTOD (UNI 11309).....	43
Figure 2.16: Typical arrangement of measuring CMOD (EN 14651).....	44
Figure 2.17: Load-CMOD and $F_j$ ( $j=1.5, 2.5, 3.5, 4, 5$ ).....	46
Figure 3.1: Macro polypropylene fibers.....	48
Figure 3.2: 3D Dramix Steel fibers.....	48
Figure 4.1 Compressive Strength Results for 0.5% Volume fraction at 3, 7 and 28 days.....	56
Figure 4.2 Compressive Strength Results for 0.94% Volume fraction at 3, 7 and 28 days.....	57
Figure 4.3 Load deflection response of control specimen.....	58
Figure 4.4 Load Deflection response from flexure test for 0.5% Polypropylene FRC at 3, 7 and 28 days.....	59
Figure 4.5 Load Deflection response from flexure test for 0.94% volume fraction of Polypropylene FRC at 3, 7 and 28 days.....	59
Figure 4.6 Variation of MOR as the age of Polypropylene FRC increases. (a) 0.5% VF (b) 0.94% VF.....	60
Figure 4.7 Load Deflection response from flexure test for 0.5% Steel FRC at 3, 7 and 28 days.....	60
Figure 4.8 Load Deflection response from flexure test for 0.94% Steel FRC at 3, 7 and 28 days.....	62
Figure 4.9 Load Deflection response from flexure test for 0.5% Hybrid FRC at 3, 7 and 28 days.....	62
Figure 4.10 Load Deflection response from flexure test for 0.94% Hybrid FRC at 3, 7 and 28 days.....	62
Figure 4.11 Load Deflection response of Polypropylene, Steel and Hybrid FRC beams at 0.5% Volume fraction on (a) 3 Day, (b) 7 Day and (c) 28 Day.....	64

Figure 4.12 Load Deflection response of Polypropylene, Steel and Hybrid FRC beams at 0.94% Volume fraction on (a) 3 Day, (b) 7 Day and (c) 28 Day.....	65
Figure 4.13 Load CMOD response of Polypropylene, Steel and Hybrid FRC of 0.5% Volume Fraction at (a) 3 Day, (b) 7 Day and (c) 28 Day.....	67
Figure 4.14 Load CMOD response of Polypropylene, Steel and Hybrid FRC of 0.94% Volume Fraction at 3 Day.....	68
Figure 4.15 Residual Strength at L/600 as per ASTM C1609.....	69
Figure 4.16 Residual Strength at L/150 as per ASTM C1609.....	70
Figure 4.17 Equivalent Flexural Strength Ratio as per ASTM C 1609 at (a) 3 day (b) 7day and (c) 28 day.....	71
Figure 4.18 Toughness Factor as per JSCE SF4 at (a) 3 day (b) 7day and (c) 28 day.....	72
Figure 4.19 Residual Flexural Strength as per EN 14651.....	74
Figure 5. 1: (a) Load-CMOD of plot of Hybrid specimen with 0.5% volume fraction (b) $\epsilon_{xx}$ at 12.54 kN (pre-peak); (c) $\epsilon_{xx}$ at 14.51 kN (pre-peak); (d) $\epsilon_{xx}$ at 15.45 (peak); (e) $\epsilon_{xx}$ at 14.06 kN (post-peak); (f) $\epsilon_{xx}$ at 12.92 kN (post-peak); and (g) $\epsilon_{xx}$ at 12.56 kN (post-peak).....	78
Figure 5. 2: The strain profile showing the multiple cracking of hybrid and steel FRC at 0.94% volume fraction and the load CMOD response; (a) Blend at 3 day (b) Blend at 7 day (c) Blend at 28 day (d) Steel FRC at 3 day (e) Steel FRC at 7 day (f) Steel FRC at 28 day .....	81
Figure 5.3 Horizontal strips for strain computations.....	82
Figure 5.4 (a) Typical load response of control; (b) Displacement profile at line 1; (c) Strain profile at line 1 at distinct load points.....	83
Figure 5.5: (a) Typical load response of 0.5% Hybrid FRC at 3 days; (b) Displacement profile at line 1; (c) Strain profile at line 1 at distinct load points.....	84

Figure 5.6: (a) Typical load response of 0.5% Hybrid FRC at 7 days; (b) Displacement profile at line 1; (c) Strain profile at line 1 at distinct load points.....	84
Figure 5.7: (a) Typical load response of 0.5% Hybrid FRC at 28 days; (b) Displacement profile at line 1; (c) Strain profile at line 1 at distinct load points.....	84
Figure 5.8: (a) Typical load response of 0.5% Polypropylene FRC at 3 days; (b) Displacement profile at line 1; (c) Strain profile at line 1 at distinct load points.....	85
Figure 5.9: (a) Typical load response of 0.5% Polypropylene FRC at 7 days; (b) Displacement profile at line 1; (c) Strain profile at line 1 at distinct load points.....	85
Figure 5.10: (a) Typical load response of 0.5% Polypropylene FRC at 28 days; (b) Displacement profile at line 1; (c) Strain profile at line 1 at distinct load points.....	86
Figure 5.11: (a) Typical load response of 0.5% Steel FRC at 3 days; (b) Displacement profile at line 1; (c) Strain profile at line 1 at distinct load points.....	86
Figure 5.12: (a) Typical load response of 0.5% Steel FRC at 7 days; (b) Displacement profile at line 1; (c) Strain profile at line 1 at distinct load points.....	87
Figure 5.13: (a) Typical load response of 0.5% Steel FRC at 28 days; (b) Displacement profile at line 1; (c) Strain profile at line 1 at distinct load points.....	87
Figure 5.14: (a) Typical load response of 0.94% Hybrid FRC at 3 days; (b) Displacement profile at line 1; (c) Strain profile at line 1 at distinct load points.....	88
Figure 5.15: (a) Typical load response of 0.94% Hybrid FRC at 7 days; (b) Displacement profile at line 1; (c) Strain profile at line 1 at distinct load points.....	88
Figure 5.16: (a) Typical load response of 0.94% Hybrid FRC at 28 days; (b) Displacement profile at line 1; (c) Strain profile at line 1 at distinct load points.....	89

Figure 5.17: (a) Typical load response of 0.94% Polypropylene FRC at 3 days; (b) Displacement profile at line 1; (c) Strain profile at line 1 at distinct load points.....	89
Figure 5.18: (a) Typical load response of 0.94% Polypropylene FRC at 7 days; (b) Displacement profile at line 1; (c) Strain profile at line 1 at distinct load points.....	90
Figure 5.19: (a) Typical load response of 0.94% Polypropylene FRC at 28 days; (b) Displacement profile at line 1; (c) Strain profile at line 1 at distinct load points.....	90
Figure 5.20: (a) Typical load response of 0.94% Steel FRC at 3 days; (b) Displacement profile at line 1; (c) Strain profile at line 1 at distinct load points.....	91
Figure 5.21: (a) Typical load response of 0.94% Steel FRC at 7 days; (b) Displacement profile at line 1; (c) Strain profile at line 1 at distinct load points.....	91
Figure 5.22: (a) Typical load response of 0.94% Steel FRC at 28 days; (b) Displacement profile at line 1; (c) Strain profile at line 1 at distinct load points.....	92
Figure 5.23 Variation of Strain value ( $\epsilon_{xx}$ ) on lines along the depth of section at distinct loads for control Specimen.....	93
Figure 5.24 Variation of Strain value ( $\epsilon_{xx}$ ) on lines along the depth of section at distinct loads for Hybrid FRC with 0.5% volume fraction at 28 days.....	95
Figure 6.1 Geometry, loading, and deformation of Cracked Incremental Horizontal Strip of hinge.....	98
Figure 6.2 Definition of Parameters of Bilinear Stress-Crack opening relationship.....	99
Figure 6.3 Distinct Phases of Stress Distribution during propagation of the crack in the section.....	100
Figure 6.4 Model representation of simply supported beam after cracking.....	101
Figure 6.5 Definition of Parameters of Multi linear Stress-Crack relationship.....	103

Figure 6.6 General Stress distribution for multi linear case.....	104
Figure 6.9 Stress crack opening relationship of steel, polypropylene and hybrid FRC at 0.5% volume fraction at 3 day.....	108
Figure 6.10 Stress crack opening relationship of steel, polypropylene and hybrid FRC at 0.5% volume fraction at 7 day.....	108
Figure 6.11 Stress crack opening relationship of steel, polypropylene and hybrid FRC at 0.5% volume fraction at 28 day.....	109
Figure 6.12 Experimental and matched theoretical curves for 0.5% Polypropylene FRC at 28 days.....	111
Figure 6.13 Crack Depth vs Crack Width for the mean crack opening parameters for polypropylene, steel and hybrid FRC at 3 day.....	112
Figure 6.14 Crack Depth vs Crack Width for the mean crack opening parameters for polypropylene, steel and hybrid FRC at 7 day.....	113
Figure 6.15 Crack Depth vs Crack Width for the mean crack opening parameters for polypropylene, steel and hybrid FRC at 28 day.....	114
 List of Tables	
Table 2.1: Properties of the different fibers.....	21
Table 2.2: Properties of various types of polypropylene fibers.....	27
Table 2.3: Properties of the fibers investigated.....	31
Table 2.4: Properties of the fibers investigated.....	33
Table 3.1: Batch weights of the constituents.....	50
Table 3.2: Test matrix of the experimental program.....	54
Table 5.1 Locations of lines.....	82
Table 6.1 Mean (Std Dev) values of Crack Opening parameters of Polypropylene, Blend and Steel FRC.....	109



# Chapter 1

## Introduction

### 1.1 Introduction

Concrete is the most widely used construction material as it offers low cost, general availability, and wide applicability. Concrete being a quasi-brittle material and it exhibits an increase in brittleness with increasing strength. Plain concrete has low tensile strength and toughness. Failure in concrete under applied tensile loading is associated with cracking. A crack is produced at low tensile stress and once formed it grows rapidly in the material. Concrete in the hardening state (after setting) develops tensile stress if volume changes due to shrinkage and thermal strains are restrained. Damage in tension develops at low tensile stress in the form of microcracks. The microcracks are formed even before the application of load. Under applied load, these micro-cracks coalesce to form visible cracks. Cracking leads to premature deterioration often resulting in a dramatic reduction in the service life and an increase in the life-cycle maintenance costs; cracks also accelerate deterioration by permitting the ingress of aggressive agents thereby producing corrosion of the steel reinforcement. Therefore improving the ability of concrete to carry tensile stresses is important to improve the service performance of structures.

Adding short and randomly distributed fibers to concrete has been shown to increase the tensile strength, ductility and toughness of the material. Fibers bridge cracks and suppress the propagation of the crack which imparts post cracking ductility. In a concrete beam containing fibers, damage is produced by gradual development of single or multiple cracks with increasing deflection, while a beam without fibers fails suddenly by breaking

into two pieces at small deflection. Inclusion of fibers increases the energy absorption property of the composite, thereby increasing the toughness.. This results in the enhancement of toughening effect due to several fiber-matrix interactions. Main fiber matrix interactions are fiber bridging, fiber debonding, fiber pullout and fiber rupture as the crack propagates through the matrix.

Today a variety of fibers are available for use in concrete for different applications. Most widely used fibers are made of steel, synthetic (polypropylene and polyethylene), glass and carbon. Synthetic fibers are typically softer and used in small volume fractions to control shrinkage cracking. Synthetic fibers provide limited potential for use in structural applications. Steel fibers are used in a wide range of structural applications, in general, when the control of concrete cracking is important such as industrial pavements [2, 3] precast structural elements [4] and tunnel linings [5]. Steel fibers have high elastic modulus and stiffness and produce increase in toughness and improvements in tensile strength and toughness of concrete [6, 7]. In general, addition of steel fibers influence the compressive strain at ultimate load and ductility in flexure more significantly than the improvements in strength [8]. Steel fibers, however, increase structure weight of concrete and exhibit balling effect during mixing, which lowers the workability of the mix. In addition, steel fibers corrode, cannot be used in the presence of conductive electric and magnetic fields.

The improvement in the material performance obtained from a single type of fiber is usually within a limited range. Incorporation of two or different types of fibers provide superior properties and is known as hybrid fiber reinforced concrete. The main reason for hybridization is to control the cracks at different zones of the concrete during different loading stages. Functional blending of fibers has been shown to produce overall improvements in properties of concrete due to synergistic effects beyond the influence of a single fiber type. In particular, blends of steel and synthetic fibers have been shown to produce significant improvements in early age cracking response due to restrained

shrinkage. In this fiber blend the synthetic fiber is intended to improve the fresh and early age properties such as ease of production and plastic shrinkage, while the second fiber leads to improved toughness and post-cracking load carrying capacity. While the benefit of using blends to improve early age cracking behavior of concrete has been established, the synergy of the fibers on the fracture behavior and crack bridging stresses has not been investigated and this forms the basis of this study.

## 1.2 Objectives

The broad objective of the work reported in this thesis is to investigate the influence of hybridization of macro steel and synthetic fibers on the early age mechanical behavior of fiber reinforced concrete. Specific objectives of the thesis include

1. To study the influence of crack bridging on the flexural response of hybrid fiber reinforced concrete as a function of age.
2. To evaluate the influence of hybrid fiber reinforced concrete on the toughness and ductility of the concrete as a function of age.
3. To provide an interpretation for the observed tension response of hybrid fiber reinforced concrete in flexure in terms of crack propagation and toughening mechanisms in the composite.
4. To determine the crack bridging stresses contributed by hybrid macro-synthetic fibers as a function of age.

# Chapter 2

## Review of Standard Test methods and Literature

### 2.1 Introduction

Concrete is a brittle material with a low strain capacity. Reinforcing the concrete with short randomly distributed fibers can help to tackle the brittleness and enhances resistance to crack propagation. The fibers help mainly by bridging the crack formed in the concrete, thereby increasing the toughness and post crack ductility in tension. Fibers in concrete can be effective in bridging cracks in both micro and macro levels. Usually micro cracks coalesce to form macro cracks which finally leads to the failure of the structure. Thus the fibers can play an important role in reinforcing the concrete to improve its properties. While fiber bridging enhances the load carrying capacities which is achieved due to transfer of stress after cracking. The earliest documented use of fibers has been the incorporation of chopped hay and camel hair in adobe bricks by the Egyptians. Since then different types of fibers have been developed, which can broadly be classified as metallic, synthetic, glass, and mineral. Properties of the different fibers commonly available today are listed in Table 2.1.

Table 2.1: Properties of the different fibers

Fiber	Diameter (μm)	Specific Gravity	Tensile Strength (GPa)	Elastic Modulus (GPa)	Fracture Strain (%)
Steel	5-500	7.84	0.5-2.0	210	0.5-3.5
Glass	9-15	2.6	2.0-4.0	70-80	2.0-3.5
Fibrillated Polypropylene	20-200	0.9	0.5-0.75	5-77	8.0
Cellulose		1.2	0.3-0.5	10	
Carbon(high strength)	9	1.9	2.6	230	1
Cement matrix		2.5	3.7x10 <sup>-3</sup>	10-45	0.02

There are various factors that influence the properties of fiber reinforced concrete. Fiber volume content or fiber volume fraction is the primary variable which has a significant influence on the behavior of the material in tension. For small volume fraction, after the first crack, there is a drop in the load. There are small number of fibers bridging the crack that sustain the load. The capacity provided by the number of fibers crossing the crack is significantly less than the first crack load and load carrying capacity decreases rapidly with increasing deformation. For intermediate volume fraction, after the drop in load associated with the formation of a crack, the load carrying capacity provided by the fibers produces a progressive yet gradual decrease in the load carrying capacity. For high volume fraction, after first crack, there are a large number of fibers bridging the crack and the resistance to crack opening provided by the fibers is larger than the first crack load. As the load increases, more cracks form along the length of specimen.

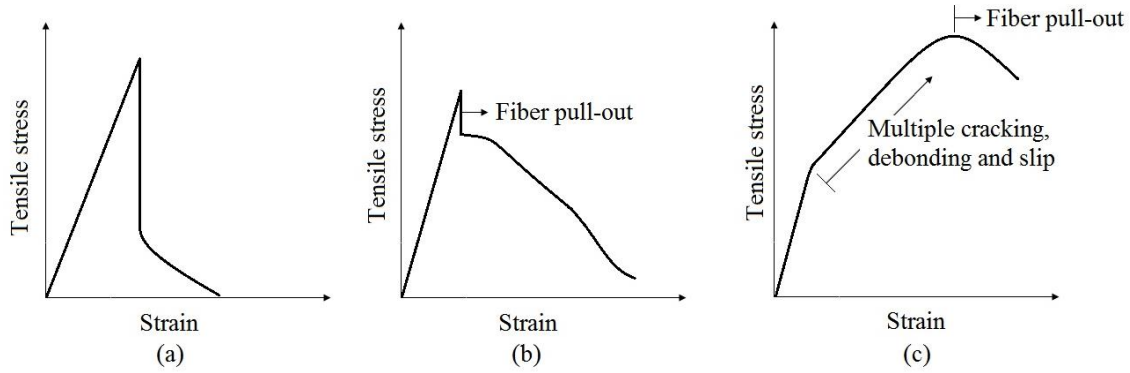


Figure 2.1: The composite stress-strain curves for fiber-reinforced brittle matrix: (a) Low fiber volume content; (b) intermediate volume fraction; and (c) high volume fraction.

The composite behavior of the fiber reinforced concrete (FRC) depends on the interaction between the fibers and the cementitious matrix. Main fiber matrix interactions are: fiber bridging, fiber debonding, fiber pullout and fiber rupture as the crack propagates through the matrix (Fig 2.1). The observed load response at the different volume fractions is associated with the pullout response of fibers from the concrete matrix averaged over the crack. The mechanical behaviour of the FRC are influenced by reinforcing mechanisms or the ability of the fibers to transfer stress across the crack. In short randomly distributed fibers at low and intermediate fiber volume fractions (typically up to 2%) the contribution of fibers is after strain localization, which occurs close to the peak tensile load. The tensile strength in these cases is comparable to that of the unreinforced matrix. The strain softening is influenced by the cracking closing pressure provided by the fibers as a function of the crack opening displacement. The toughening provided by the fibers depends upon the pull out resistance of the fibers embedded in the matrix. During crack propagation, debonding and sliding contribute significantly to the pull out resistance of the fibers and hence contribute to the total energy consumption when a large crack develops in the matrix. Fiber breakage has not been considered to contribute significantly to the energy dissipated during crack propagation in FRC [24]. Several fracture based formulations which consider the debonding behaviour of fibers from the cementitious matrix have been proposed [10].

At higher volume fractions, which are usually achieved using special processing techniques, the pre-peak behaviour is fundamentally altered due to stabilization of micro cracking in the matrix. A uniform distribution of micro cracks in the matrix leads to significant enhancement in the strain capacity of the matrix [11]. The load response of such composites exhibits strain hardening response as shown in Fig 2.2. There is a point in the load response identified as the bend-over-point (BOP) where the matrix contribution to the tensile load response reaches a maximum. The load response following the BOP is characterized by multiple cracking in the matrix. In this stage the incremental loading of the fibers at the location of the crack is transferred to the matrix through the interfacial bond, which results in a build-up of tensile stress in the matrix. More cracks are produced in the matrix when the tensile stress in matrix reaches the tensile strength of the matrix. Mechanistic and fracture based approaches which consider fiber-matrix interaction in high volume composites where the localization of crack is suppressed is very complex and is still developing.

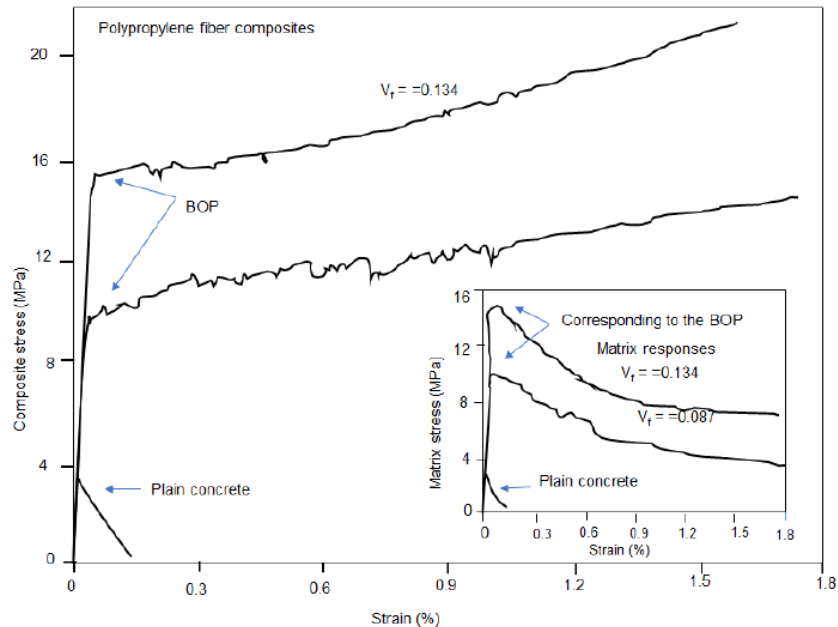


Figure 2.2: Strain hardening response of polypropylene fiber composites

## 2.2 Review of Fiber Types

### 2.2.1 Steel fibers

Steel fibers have a relatively high strength and modulus and are available in aspect ratios ranging from 20 to 100 and length ranging from 6.4 mm to 75 mm. The process of manufacture varies from cut sheets, cold drawn wires or hot melt extraction and are available in different cross-sections and shapes depending on the method of manufacture and use.

While steel fibers improve the strength of concrete under all load actions, their effectiveness in improving strength varies among compression, tension and flexure. There is an insignificant change in the ultimate compressive strength upon the addition of steel fibers; There is an increase of up to 15 percent for volume of fibers up to 1.5 percent by volume [12] [13]. There is a significant improvement in strength in tension with an increase of the order of 30 to 40 percent reported for the addition of 1.5 percent by volume of fibers in mortar or concrete [14]. Strength data [15] shows that the flexural strength of SFRC is about 50 to 70 percent more than that of the unreinforced concrete matrix in the normal third-point bending test [15, 16].

The ability of steel fibers to serve as reinforcement is determined by the resistance of the fibers to pullout from the matrix resulting from the breakdown of the fiber-matrix interfacial bond. Improvements in ductility depend on the on the type and volume percentage of fibers present [17, 18]. In conventionally mixed SFRC, high aspect ratio fibers are more effective in improving the post-peak performance because of their high resistance to pullout from the matrix. However, at high aspect ratio there is a potential for balling of the fibers during mixing [19]. Techniques such as enlarging or hooking of ends, roughening their surface texture, or crimping to produce a wavy rather than straight fiber profile allow for retaining high pullout resistance while reducing fiber aspect ratio. These types are more effective than equivalent straight uniform fibers of the same length



and diameter. Consequently, the amount of these fibers required to achieve a given level of improvement in strength and ductility is usually less than the amount of equivalent straight uniform fibers [19, 20].

The fiber pullout behaviour is influenced by the type of fiber as seen in the load response obtained from steel fiber reinforced concrete with 50 kg/m<sup>3</sup> fibers in Fig 2.3. For hooked end steel fiber, after first crack, there is drop but that drop is less than the other two fibers, deformed end fiber and corrugated fiber. For deformed end fiber and corrugated fiber, after first crack there is a continuous decrease in the load carrying capacity with increasing deformation. Hooked end fibers, which provide the highest pullout resistance from the matrix provide the highest load carrying capacity with increasing deformation after crack formation.

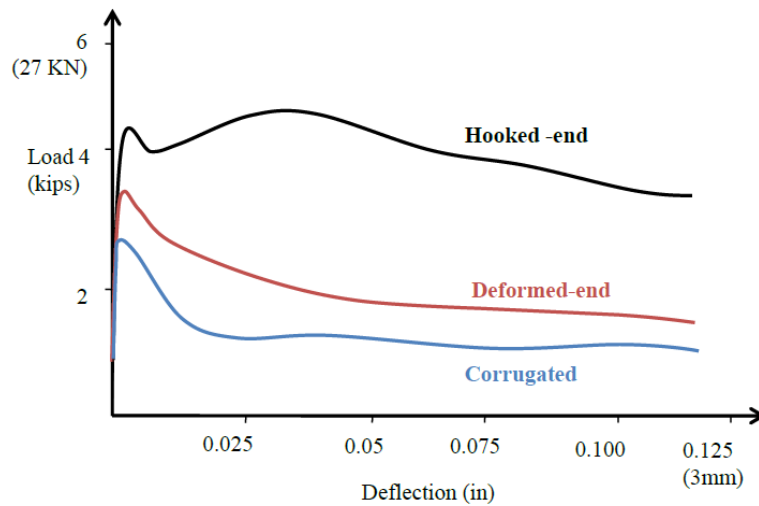


Figure 2.3: Effect of steel fiber shape on the load response in flexure

Improvements in post-crack ductility under tension result in significant improvements in flexural response. Ductile behaviour of the SFRC on the tension side of a beam alters the normally elastic distribution of stress and strain over the member depth. The altered stress distribution is essentially plastic in the tension zone and elastic in the compression zone, resulting in a shift of the neutral axis toward the compression zone [21].

### 2.2.2 Polypropylene fibers

Polypropylene (PP) fibers are available in two different forms; Monofilaments and Fibrillated. Monofilament fibers are single strand of fibers having uniform cross-sectional. Fibrillated fibers are manufactured in the form of films or tapes that are slit in such a way that they have net like physical structure. Most commercial applications of polypropylene fibers have used low volume percentage (0.1 percent), monofilament or fibrillated fibers in non-structural applications such as control of plastic shrinkage cracking. Typical properties of monofilament and fibrillated polypropylene fibers is given in Table 2.2.

Table 2.2: Properties of various types of polypropylene fibers

Fiber type	Length	Diameter	Tensile strength	Modulus of Elasticity	Specific Surface	Density
	(mm)	(mm)	(MPa)	(MPa)	(m <sup>2</sup> /kg)	(kg/cm <sup>3</sup> )
Mono filament	30-50	0.3-0.5	547-658	3.5-7.5	91	0.9
Micro filament	12-20	0.05-0.20	330-414	3.9-5.5	225	0.91
Fibrillated	19-40	0.20-0.30	500-750	5.0-10.0	58	0.95

At dosages considered by the industry, of 1.2 kg/m<sup>3</sup>, PP fibers have been shown to influence the fracture behaviour; the influence of the fibres was especially felt in the tail of the load-deflection curve, showing a wider softening branch in the case of the FRC mixes, which corresponds to a more ductile behaviour of the concrete. The effect of the fibre is more remarkable in the case of the low strength concrete, where the stresses in the cohesive zone are lower, and the bridge effect of the fibre has a greater effect due to the higher level of deformation. It was shown that the fibres with the highest elongation and

lowest strength (i.e. the most ductile fibres) presented the highest values of fracture energy. In the case of high strength concrete the higher level of the cohesive stresses mitigates the bridge effect of the fibres. In low- and normal-strength concrete the main mechanism of failure of the fibres was by pull-out while in high strength concrete it was due to fiber breakage [22].

### *Macro-synthetic Polypropylene fiber*

Structural synthetic fibers are available in different geometries and shapes as shown in Fig 2.4. The energy absorption capacities from pullout tests on the different shape synthetic fiber obtained from pullout tests are shown in Fig 2.5. [23]. Test results indicate that the crimped-shape structural synthetic fibers exhibit the highest energy absorption capacity.

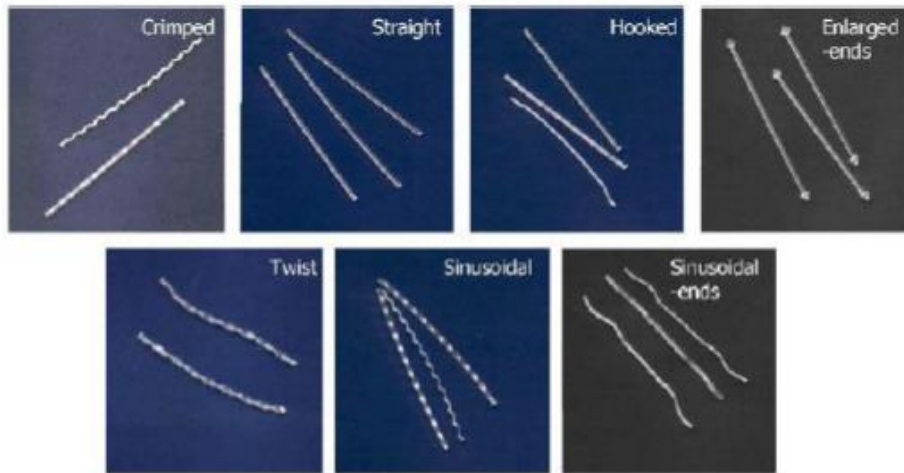


Figure 2.4: Various types of synthetic fibers tested in the present study

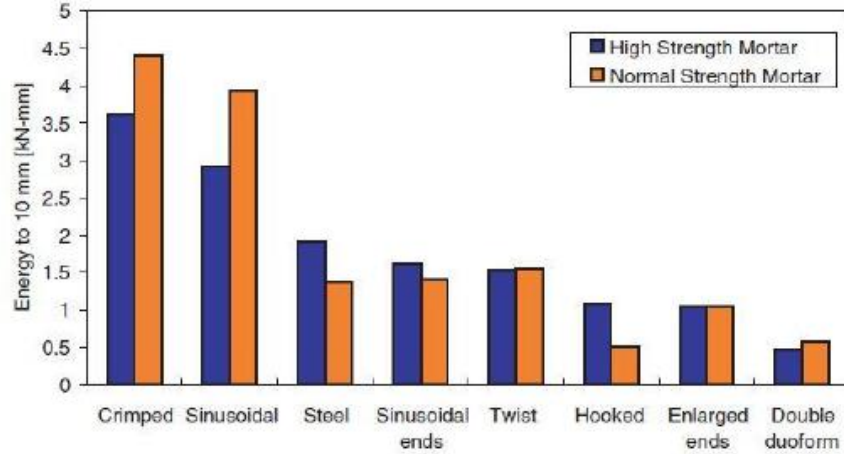


Figure 2.5: Comparison of absorbed energies from pullout tests for various fiber types [23].

The energy absorption capacity and thus the toughening effect of FRC is the result of fiber matrix interactions such as fiber pullout, fiber debonding and also due to fiber rupture. Shukla et al [24] in his investigation to understand the pullout behavior of polypropylene fibers found that the embedded length and interfacial bond affects the pullout of fiber from matrix.

A comparison of the load response in flexure between hooked end steel fibers and synthetic fibers is shown in Fig 6. Data obtained from [25] are plotted in the Fig 2.6. Steel fibers at dosages up to 50 kg/m<sup>3</sup>, show in a drop in load immediately after formation of the crack, followed by a gradual decrease in load carrying capacity. In case of synthetic fiber, at fiber dosage rate of 4.6 kg/m<sup>3</sup>, there is sudden drop (the load drop decreases in fiber dosage rate 5.3 kg/m<sup>3</sup>), after first crack, there is continuously decreasing load and increasing the deflection (slowly fiber pull out start from the matrix).

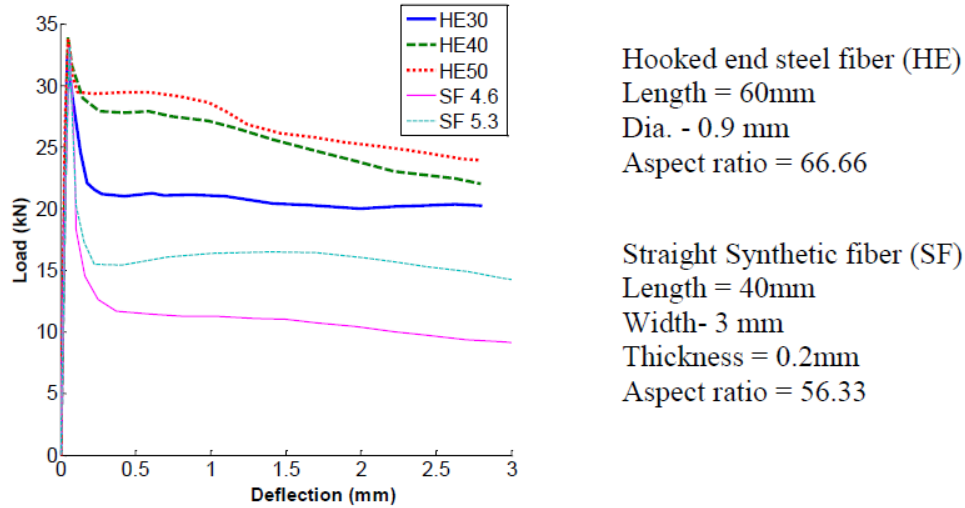


Figure 2.6: Load–deflection curves for Hooked end steel fibers and Synthetic fibers

### 2.3 Hybrid Fiber Reinforced Concrete

Considering the fiber matrix interaction, in unloaded stage, stresses in both the matrix and fiber are assumed to be zero. Applying the tensile or compressive load to the composite results in the development of stresses and deformations that must remain compatible. When the load is applied to the matrix, a part of load is transferred to the fiber along the surface, by the development of shear stresses. This happens because of the difference in stiffness of both matrix and fiber. If the fiber is stiffer than the matrix, deformations at and around the fibers will be smaller and if the stiffness is smaller than matrix, then the deformation around the fiber will be higher. This is the case when the matrix is in uncracked condition. Once the matrix cracks, load transfer is carried out by the fibers. Several fibers will bridge the crack, transferring the load across the crack and if the fibers can transmit sufficient load across the crack, multiple cracks are developed in the matrix.

Conventional reinforced concrete consists of reinforcing bars which are continuous throughout the specimen. While the fiber reinforced concrete consists of short and random distribution of fibers which are discontinuous in nature. The conventional reinforcing bars

addresses crack arrest at only specific sections and at a single scale. While the fiber reinforcement ensures a random distribution of crack arrest zones within concrete.

Fiber reinforced concrete containing one type of fiber has many limitations in terms of cracking opening resistance and toughness enhancement. This leads to the concept of hybridization. A hybrid fiber reinforced concrete consists of two or more different fibers, which can help to achieve superior properties to the composite. On adding different types of fibers, the nature of fiber matrix interaction results in the enhancement of the properties. If there is a positive interaction between the fiber and the matrix, the resulting hybrid performance can exceed the sum of individual fiber performances, and this phenomenon is termed as synergy. It is very important for a hybrid fiber reinforced concrete to achieve synergy.

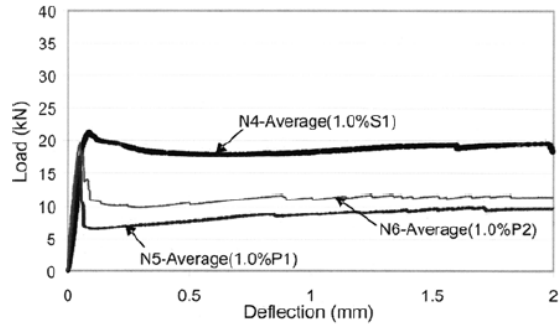
Banthia and Gupta [49] proposed three ways of classifying fiber hybrids based on fiber interaction leading to synergy:

- a. Hybrids based on fiber constitutive response: This hybrid consists of combination of a stiffer fiber and a flexible fiber. Stiffer fiber provides the reasonable first crack strength and ultimate strength while the flexible fiber imparts improved toughness and strain capacity in the post cracking zone.
- b. Hybrids based on fiber dimensions: This hybrid is combination of large and small fibers. Smaller fiber bridges the micro crack thereby controls the growth and delays coalescence. This results in an improved tensile strength of the composite. Larger fiber is responsible for arresting the macro-cracks, which leads to improve the fracture toughness of the composite.
- c. Hybrids based on fiber function: In this type one type of fiber is intended to improve the fresh and early age properties such as ease of production and plastic shrinkage, while the second fiber leads to improved mechanical properties capacity in the post-crack zone.

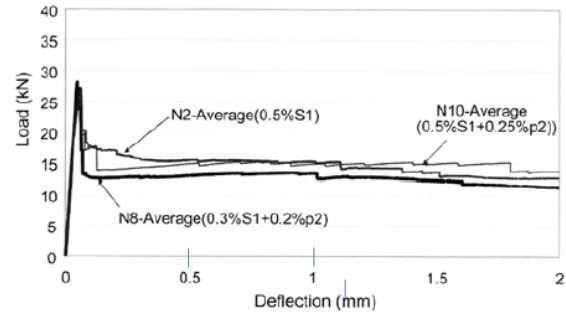
Banthia et al. [49] investigated steel and polypropylene fibers individually and also hybrid combinations at both micro and macro levels. Fibers used in the study are shown in table 2.3. Figure 2.7 shows comparison between various individual and hybrid combinations of steel and polypropylene at micro and macro level. It was found that at same volume fractions, deformed steel provides better toughness than the crimped or self-fibrillating polypropylene macro-fibers. Between the two polypropylene macro-fibers, the self-fibrillating fiber was shown to perform better than the crimped macro-fiber. Also the hybrids of steel and polypropylene demonstrated better synergy. FRCs with low toughness are better candidates for hybridization than composites with a higher toughness. Considering this, the  $V_f$  in the hybrids was a maximum of 1.3%.

Table 2.3: Properties of the fibers investigated

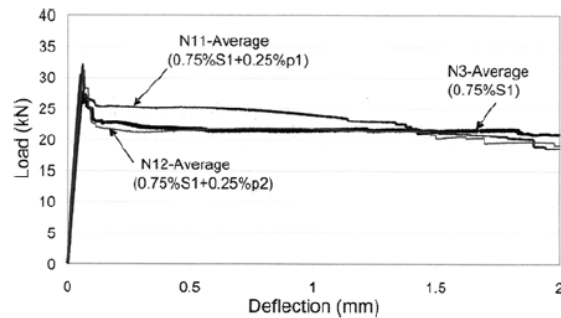
Fiber code	Type		Diameter	Geometry	Cross sectional shape
S1	Flat-ended steel	50		Flat-end	Circular
P1	Macro polypropylene	50	1 mm	Crimped	Rectangular
P2	Self-fibrillating Polypropylene	50	1 mm	Straight	Fibrillated
c	Carbon fiber (Mesophase pitch-based)	12.5	9-11 $\mu\text{m}$	Straight	Circular
p1	Micro polypropylene	12.5	2-denier	Straight	Circular
p2	Micro polypropylene	12.5	3-denier	Straight	Circular



Comparison of mixes with steel (S1) and polypropylene macro-fibers (P1 and P2) at 1%



Comparison of mixes with steel macro-fiber (S1) and its two-fiber hybrids with polypropylene micro-fiber (p1)



Comparison of two polypropylene micro-fibers (p1 and p2) for hybridization with 0.75 S1

Figure 2.7: Load-deflection plots for various fiber combinations

Hybrid combination of steel and micro polypropylene fiber have been shown to increase the ultimate compressive strain of the composite [50]. Combination of steel and micro polypropylene fibers showed that the stronger and stiffer steel fiber improved the ultimate strength, while the more flexible and ductile polypropylene fibers improved toughness and strain [51]. The steel macro-fibers with highly deformed geometry produce better hybrids than those with a less deformed geometry [52]. Bantia et al reported a positive synergy of hooked end steel fibers with cellulose fibers. On comparing with double deformed fibers, hooked end fibers provided better synergy [55]. Lawler et al. [56] reported hybridization showed a reduction in permeability of cracked hybrid fiber reinforced mortar under load containing steel and polypropylene.



Shivakumar and Santhanam [53] investigated the plastic shrinkage cracking on high strength fiber reinforced concrete. They used a fiber volume fraction of 0.5%. Individual steel as well as hybrid combinations of steel as well as other non-metallic fibers like polypropylene, polyester and glass fibers were used to investigate the plastic shrinkage response of concrete. The properties of the fibers used in the study are given in Table 2.4. In this study the crack measurements were performed using an image analysis technique. The crack measurements included crack length, crack width and the total crack area. It was found that the plastic shrinkage cracks were reduced significantly. Hybrid fibers were more effective in crack reduction, hybrids provided 50-99% reduction in crack area when compared to plain concrete. Among the hybrid combination, steel-polypropylene fibers provided a crack reduction of 80-97%, turned to be the better hybrid combination. The workability of concrete have an adverse effect on addition of non-metallic fibers in hybridization.

Table 2.4: Properties of the fibers investigated

Property	Hooked steel	Polypropylene	Glass	Polyester
Length (mm)	30	20	6	12
Diameter (mm)	0.5	0.1	0.01	0.05
Aspect ratio (l/d)	60	200	600	240
Specific gravity	7.8	0.9	2.72	1.35
Tensile strength (MPa)	1700	450	2280	970
Elastic modulus (GPa)	200	5	80	15
Failure strain (%)	3.5	18	3.6	35



Figure 2.8: Plastic shrinkage crack in the steel–polypropylene hybrid concrete

Trottier and Banthia [54] investigated the toughness characterization of steel fibers at lower fiber dosage. At lower fiber dosage of  $40 \text{ kg/m}^3$ , there was no significant increase in the strength or moduli. Deformed fibers bring about significant improvements in the toughness or energy-absorption capabilities of concrete. Based on the four fiber geometries investigated, fibers with deformations only at the ends appear to be more effective than those with deformations over the entire length. . At high-matrix strengths, there is usually a steeper and more sudden drop in the load-carrying capacity after the first crack. While improvements in the resistance to shrinkage cracking have been reported with the use of hybrid fibers by blending, measurements of fracture response have not been reported.

## 2.4 Standard Test Methods

The influence of fibers on overall improvements in ductility and toughness are often interpreted in terms of improvements to fracture behaviour and crack propagation. Quantitative measures which allow for comparison between fibers and assess

improvements involve standard test methods and data reduction procedure. The fracture behaviour of fiber reinforced concrete is also investigated using the test configurations and specimens of dimensions specified in standardized test procedures. A review of different standard test is presented first.

Standardized test methods for quantifying improvements in material behaviour and obtaining specific material properties have been developed. In these tests material parameters which quantify ductility and toughness of the material are obtained from measured load response. The quantities derived from these tests allow for comparison of material behaviour. Standard test procedures for evaluating the response of FRC are available in ASTM 1609, UNI 11039-2, ASTM 1018, EN 14651 and JSCE SF 24. Additionally, researchers have proposed methods for obtaining fracture or material parameters from the measured test response from the standardized test procedures. The test procedures and the different data reduction procedures are reviewed in this section.

#### 2.4.1 ASTM 1609 test procedure

In ASTM C1609/C1609M-10 a standardized test procedure is available to establish the flexural toughness, the flexural strength and the residual strength factors of the fiber reinforced concrete using beam specimens. The loading and support system capable of applying third point loading the specimen without eccentricity or torque in accordance with ASTM C78-02 is shown in Fig 2.9. ASTM test is performed measuring the applied load and the beam net deflection (i.e. the absolute mid-span deflection minus the support deflection) at a constant deflection rate. The beam midpoint deflection between the tension face of the beam is measured in relation to the neutral axis of the beam at its support.

First peak deflection, toughness and Equivalent flexural strength are derived from the measured response. The standard load-displacement behaviours of fiber reinforced concrete beams are shown in Fig 2.10. The peak load is determined as that value of load

corresponding to the point on the load-deflection curve that corresponds to the greatest value of load obtained prior to reaching the end-point deflection. The first-peak load ( $P_1$ ) is defined as that value of load corresponding to the first point on the load-deflection curve where the slope is zero, that is, the load is a local maximum value. In specimens, which exhibit an increase in load after the load drop produced by cracking, the first peak load is the distinctive point in the load response associated with load drop as shown in Fig 2.9.

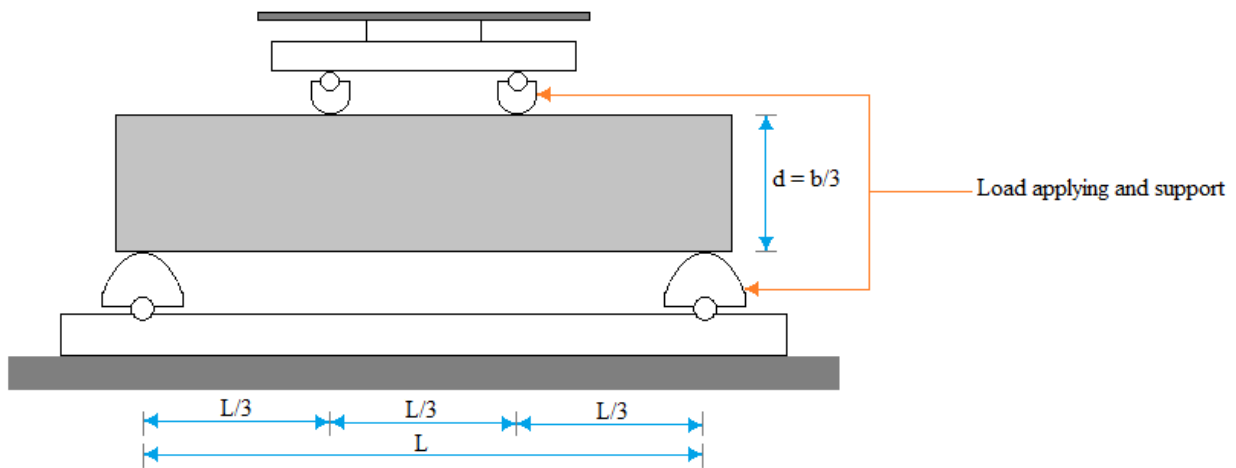


Figure 2.9: Diagrammatic View of a Suitable Apparatus for Flexure Test of Concrete by Third-Point Loading Method

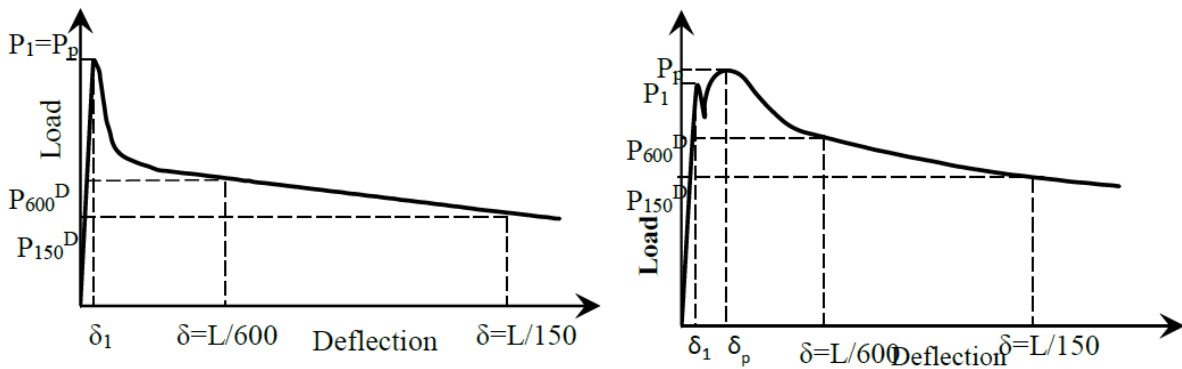


Figure 2.10: Example of Parameter Calculations

Strength corresponding to each peak load,  $f$  is determined following formula for modulus of rupture

$$f = \frac{PL}{bd^2}$$

First-peak deflection for third-point loading is estimated assuming linear-elastic behaviour up to first peak from the equation

$$\delta_1 = \frac{23 P_1 L^3}{1296 EI} \left[ 1 + \frac{216 d^2 (1 + \mu)}{115 L^2} \right]$$

The residual strengths,  $f_{600}^D$  and  $f_{150}^D$  are determined from the residual load values,  $P_{600}^D$  and  $P_{150}^D$  corresponding to net deflection values of 1/600 and 1/150 of the span length.

Toughness  $T_{150}^D$  is determined as the total area under the load-deflection curve up to a net deflection of 1/150 of the span length. The equivalent flexural strength ratio,  $RT_{150}^D$  is determined using the first-peak strength determined and the toughness determined. Record the number rounded to the nearest 0.5 % as equivalent flexural strength ratio, as appropriate for the specimen depth.

$$R_{T,150}^D = \frac{150 T_{150}^D}{f_1 b d^2} 100\%$$

#### 2.4.2 ASTM 1018 test procedure

In ASTM C1018, toughness indices are taken as the area under the load-deflection curve up to certain specified deflection to area under the load-deflection curve up to the first crack as shown in Fig 2.11. Three level of deflection  $3\delta$ ,  $5.5\delta$  and  $10.5\delta$ . Deflection value greater than  $10.5\delta$  can also be chosen for composite that can carry considerable loads at large deflection. The three suggested indices called  $I_5$ ,  $I_{10}$  and  $I_{20}$  are defined by following equations.

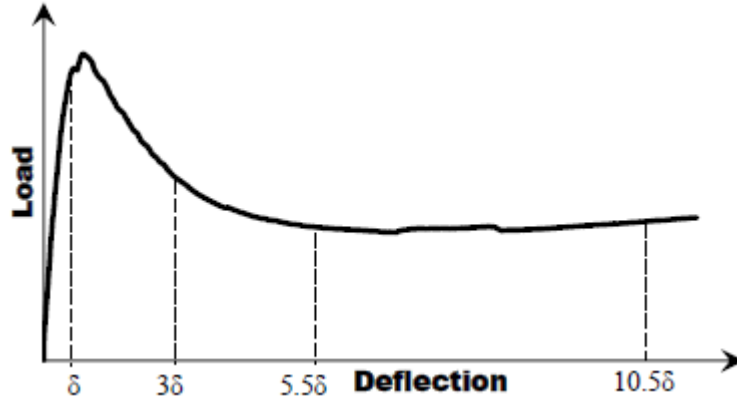


Figure 2.11: Important Characteristics of the Load-Deflection Curve

$$I_5 = \frac{\text{Area under the load-deflection curve up to } 3\delta}{\text{Area under the load-deflection curve up to } \delta}$$

$$I_{10} = \frac{\text{Area under the load-deflection curve up to } 5.5\delta}{\text{Area under the load-deflection curve up to } \delta}$$

$$I_{20} = \frac{\text{Area under the load-deflection curve up to } 10.5\delta}{\text{Area under the load-deflection curve up to } \delta}$$

The deflection values of  $3\delta$ ,  $5.5\delta$  and  $10.5\delta$  are chosen using elastic perfectly plastic behaviour as the datum as shown in Fig 2.12. Residual loads at specified deflections, the corresponding residual strengths and determination of specimen toughness based on the area under the load-deflection curve up to a prescribed deflection and the corresponding equivalent flexural strength ratio are also obtained.

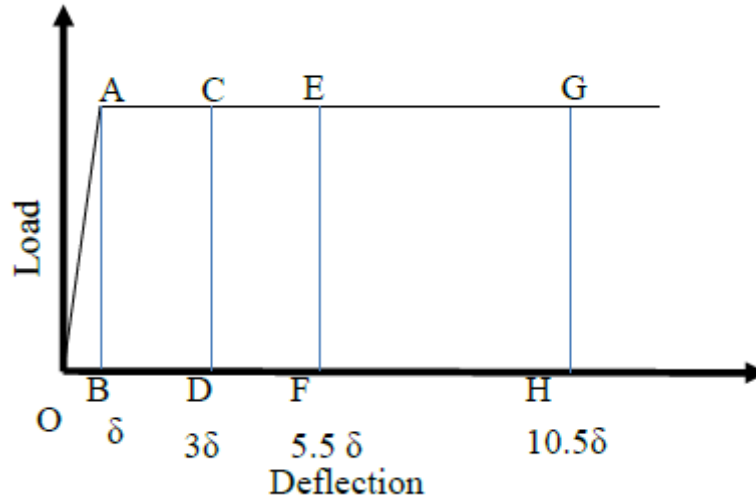


Figure 2.12: Definition of Toughness Indices for Elastic-Plastic Material Behaviour

$$I_5 = \frac{OACD}{OAB} \quad I_{10} = \frac{OAEF}{OAB} \quad I_5 = \frac{OAGH}{OAB}$$

#### 2.4.3 JSCE SF24

Ductility is commonly measured using the Japanese standard test method JSCE-SF4, which used beams in a third-point loading arrangements. The JSCE SF 24 provides a measure of flexural toughness from the measured load-deflection response as shown in Fig 2.13. The value of toughness,  $T_{JSCE}$  is determined as the area under the load-deflection curve up to a deflection equal to span/150. Toughness factor,  $F_{JSCE}$  is derived from the value of toughness.  $F_{JSCE}$  has the unit of stress such that its value indicates, in a way, the post-matrix cracking residual strength of the material when loaded to a deflection of span/150. The chosen deflection of span/150 for its calculation is purely arbitrary and is not based on serviceability considerations.

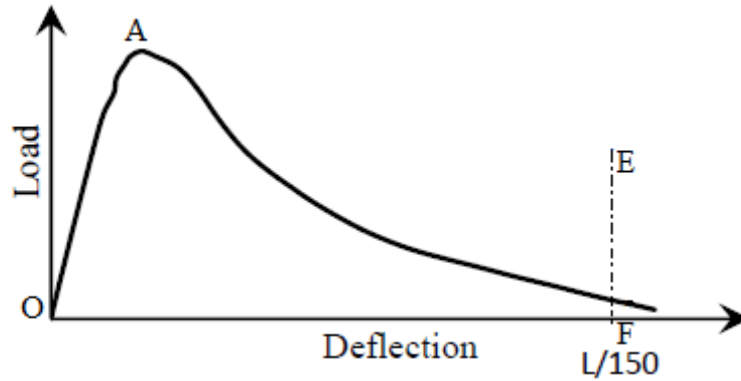


Figure 2.13: Definitions of JSCE Toughness and Toughness Factor

Toughness

$$T_{JSCE} = \text{AREA}_{OAEFO}$$

Toughness factor

$$F_{JSCE} = \frac{T_{JSCE}L}{BH^2wtb}$$

where,  $F_{JSCE}$  is Toughness factor or Equivalent flexural strength and  $wtb$  is averaged over the prescribed deflection.

The equivalent flexural strength as defined by the JSCE-SF4 for a deflection of 3 mm, the  $Re.3$  value, a measure of the ductility, is the average load applied as the beam defects to 3 mm expressed as a ratio of the load to first crack. This measure is also known as the equivalent flexural strength as denoted as  $f_{e,3}$  has been calculated as

$$f_{e,3} = \frac{P_{mean} \times l}{bd^2}$$

where  $P_{mean.150}$  is the area under the load-deflection curve divided by the limit deflection of 3 mm and  $l$ ,  $b$  and  $d$  are the span, width and depth of the prism, respectively (i.e. 450 mm, 150 mm and 150 mm, respectively).



#### 2.4.4 RILEM TC 162-Test Procedure

Centre point bend tests are performed on notched specimens with a nominal size (width and depth) of 150 mm and a minimum length of 550 mm. Net deflection at mid-span excluding extraneous deformations is increased at a constant rate of 0.2 mm/min. This test method is used to determine the limit of proportionality, equivalent flexural tensile strength, residual flexural strength which identify the material behaviour at selected deflection or CMOD.

##### *Limit of proportionality*

$$f_{ct,fl} = \frac{3F_L L}{2bh_{sp}^2}$$

where

$f_{ct,fl}$  is the LOP (N/mm<sup>2</sup>)

$F_L$  is the load corresponding to LOP (N)

$L$  is span of specimen (mm)

$b$  is the width of specimen (mm)

$h_{sp}$  is the distance between the tip of notch and top the specimen (mm)

##### *Residual flexural Tensile Strength*

$$f_{R,I} = \frac{3F_i L}{2bh_{sp}^2}$$

where

$f_{R,I}$  is the residual Tensile Strength corresponding with CMOD = CMOD<sub>j</sub> or  $\delta = \delta_i$  (i= 1, 2, 3, 4) (N) and  $F_i$  is the load corresponding to with CMOD = CMOD<sub>j</sub> or  $\delta = \delta_i$  (i = 1,2,3,4)

#### 2.4.5 UNI 11039-2 Test Procedure

UNI 11039-2 bending test is a four-point loading test on a prismatic beam. UNI test specifically prescribes the specimen absolute dimensions. The UNI [44] test employs a notched beam with a specimen which is 150 mm deep, 150 mm wide and the span length is 450 mm. It is sawed at mid-span with a depth equal to 0.3 times the overall specimen depth ( $0.3d$ ). The test is performed measuring the load  $P$  and the Crack Tip Opening Displacement (CTOD), at a rate of increase of the Crack Mouth Opening Displacement (CMOD), equal to  $0.05 \pm 0.01$  mm/min. A schematic diagram of the UNI test setup is shown in Fig 2.14.

The first-crack load which required subtracting the contribution due to matrix cracking is obtained by determining the value of CTOD corresponding to the peak load value obtained by performing four-point bending tests on plain concrete beams is determined ( $CTOD_0$ ). The value of  $CTOD_0$  can be assumed equal to  $25 \mu\text{m}$ .

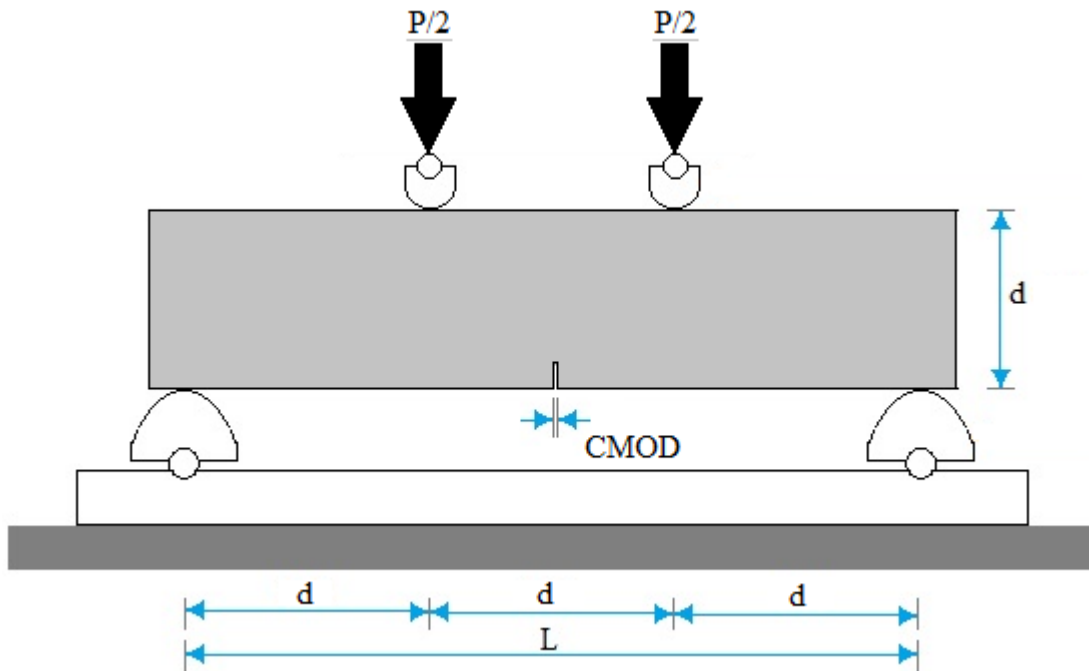


Figure 2.14: Schematic diagram of the UNI 11039 four-point bending test setup

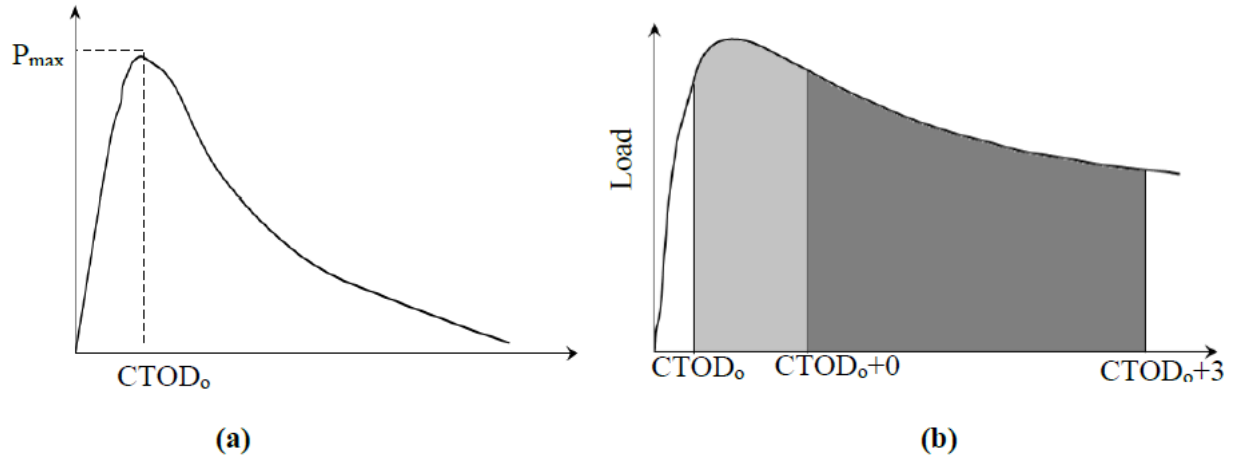


Figure 2.15: (a) Basic concrete load-CTOD, (b) Load-CTOD

The first-crack flexural strength is determined, according to UNI 11039, as follows:

$$f_{lf} = \frac{P_{lf}L}{b(h-a_0)^2}$$

where

$L$  (mm) = span between supports

$b$  (mm) = specimen width (equal  $d$ )

$h$  (mm) = specimen depth (equal  $d$ )

$a_0$  (mm) = notch depth

$P_{lf}$  (N) is the load value corresponding to  $CTOD_0$  for the FRC specimen.

The first and second Material's ductility indexes  $D_0$  and  $D_1$ , according to UNI 1039 [11] by means of the equivalent flexural strengths  $\hat{f}_{eq}(0-0.6)$  and  $\hat{f}_{eq}(0.6-3)$  (MPa), which denote SFRC ductility in a defined range of crack mean opening displacement. Ductility indexes  $D_0$  and  $D_1$  were derived by means of the following equations:

$$D_0 = \frac{f_{eq(0-0.6)}}{f_{If}} \quad D1 = \frac{f_{eq(0.6-3)}}{f_{eq(0-0.6)}}$$

where  $f_{eq(0-0.6)}$  is the equivalent strength (MPa) is calculated when the mean crack opening value is included between 0 and 0.6 mm,  $f_{eq(0.6-3)}$  is the equivalent strength (MPa) calculated when the mean crack opening value is included between (0.6 and 3) mm, derived from the following relationships:

$$f_{eq(0-0.6)} = \frac{l}{b(h-a_1)} \cdot \frac{U_1}{0.6} \quad f_{eq(0.6-3)} = \frac{l}{b(h-a_1)} \cdot \frac{U_2}{2.4}$$

where  $U_2$  and  $U_3$  (10.3 J) are the area under load -  $CTOD_m$  curve for  $CTOD_{net}$  intervals equal to 0-0.6 mm and 0.6-3 mm respectively. Such area are approximately proportional to the energy dissipated in the mean crack opening intervals considered.

#### 2.4.6 EN 14651 Test Procedure

Centre point bend tests are performed on notched specimens with a nominal size (width and depth) of 150 mm and a length  $L$  so that  $550 \text{ mm} < L < 700 \text{ mm}$ . Test is performed by increasing the  $CMOD$  at a constant rate of 0.05 mm/min up to a  $CMOD$  value of 0.1 mm and at a rate of 0.2 mm/min up to a  $CMOD$  value of 4 mm.

This European standard specifies a method of measuring a flexural tensile strength of metallic fibered concrete on moulded test specimen. The methods provided for the determination of the limit of proportionality (LOP) and of a set residual flexural tensile strength values. Arrangement as per EN14651 is shown in Fig 2.15

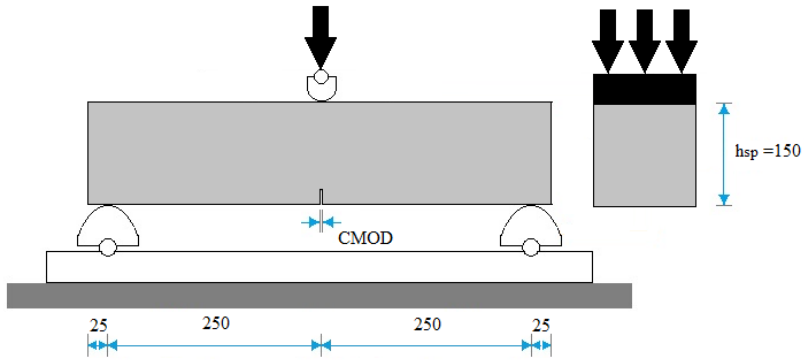


Figure2.16: Typical arrangement of measuring CMOD (EN 14651)

*Limit of proportionality*

$$f_{ct,fl} = \frac{3F_L L}{2bh_{sp}^2}$$

where

$f_{ct,fl}$  is the LOP (N/mm<sup>2</sup>)

$F_L$  is the load corresponding to LOP (N)

$L$  is span of specimen (mm)

$b$  is the width of specimen (mm)

$h_{sp}$  is the distance between the tip of notch and top the specimen (mm)

*Residual flexural Tensile Strength*

$$f_{R,i} = \frac{3F_i L}{2bh_{sp}^2}$$

where

$f_R$ , is Residual flexural Tensile Strength corresponding with  $CMOD = CMOD_j$  or  $\delta = \delta$  ( $i= 1.5, 2.5, 3.5, 4.5$  mm) (N) where  $CMOD_j$  corresponds to  $CMOD$  at  $j$  mm and  $F_i$  is the load corresponding to with  $CMOD_j$  as shown in Fig 2.17.

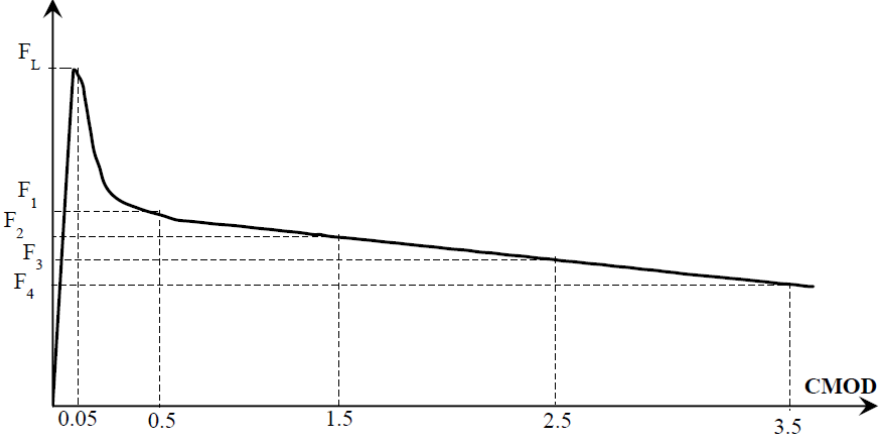


Figure 2.17: Load-CMOD and  $F_j$  ( $j=1.5, 2.5, 3.5, 4.5$ )

Toughness index is used to measure the energy absorbed in deflecting a beam at specified amount, being the area under a load–deflection curve in three-point bending. A measure of toughness index from the results of the EN 14651 test has been proposed as the ratio of the area under the force-CMOD curve up to CMOD of 4 mm for the FRC specimen over that for the plain-concrete specimen.

# Chapter 3

## Materials and Methods

### 3.1 Introduction

This section presents the details of materials and experimental methods used in the study. The types of specimens, mix proportions and test methods employed are presented.

#### 3.1.1 Cement

In the present investigation, commercially available 53 Grade ordinary Portland cement was supplied by ACC Cement with Specific Gravity of 3.1 and Fineness modulus of 325 m<sup>2</sup>/kg was used for all concrete mixtures.

#### 3.1.2 Fly Ash

Fly ash conforming to the requirements of IS 3812 and IS 1727 (1967) supplied by NTPC with Specific gravity of 2.5 and fineness modulus of 320 m<sup>2</sup>/kg was used as supplementary cementitious material in concrete mixtures.

#### 3.1.3 Aggregates

Crushed sand with a specific gravity of 2.67 and fineness modulus of 2.83 was used as fine aggregate and crushed granite of specific gravity of 2.63 was used as coarse aggregate. Two different classes of coarse aggregate fractions were used: 10-4.75 mm and 20-10 mm.

#### 3.1.4 Synthetic Fibers

FibreTuff™ Monofilament structural polypropylene fibers of 60 mm length manufactured by Bajaj Reinforcements were used in this study. The fibers are made of a

modified polyolefin and have a modulus of elasticity between 6 GPa to 10 GPa and tensile strength between 550 and 640MPa. The fibers are continually embossed surface anchorage mechanism to enhance bond. A photograph of the fibers used in this study is shown Fig 3.1.1.



Figure 3.1: Macro polypropylene fibers

### 3.1.5 Steel Fibers

3D Dramix Hooked End Steel fibers of 60 mm length, 0.75 mm diameter and of aspect ratio 80 manufactured by Baekart Pvt Ltd were used in this study. These fibers have Young's modulus of 210 N/mm<sup>2</sup> and tensile strength of 1225 N/mm<sup>2</sup>. These fibers are shown in figure.



Figure 3.2: 3D Dramix Steel fibers



### 3.1.6 Admixture

Super plasticizer (Glenium) was used to increase the workability of freshly prepared fiber reinforced concrete.

### 3.2 Experimental program and Mix Proportions

Concrete mix design for the mix design procedure given in IS: 10262 was followed with minor modification for M35 grade. For a target mean strength of 43 MPa, two different water/cement ratios equal to 0.48 was considered (from Fig 2, curve E IS 10262-1982 for 53G). Taking into considerations, the minimum requirements for cement content in kg/m<sup>3</sup> of concrete for M35 as per IS 456-2000 as 300 kg/m<sup>3</sup>, cementitious content was fixed at 340 kg/m<sup>3</sup>. Using this, the water content was determined. In the concrete mixture fine aggregate were taken as 45% of the total aggregate volume fraction. The weights of fine and coarse aggregate were then calculated considering the specific gravities of coarse and fine aggregate.

The Concrete mixtures were produced at a constant water/Cement ratio of 0.48 and one control mixture and three different mixtures with different dosage of fiber were prepared. The control mixture contained no fiber. Concrete mixtures labelled SF0.5 and PP0.94 were produced with dosage of steel and polypropylene fibers at 0.5% and 0.94% fiber volume fractions respectively. The final batch weights of the different mixes for one cubic meter of concrete are presented in Table 3.1. SF and PP represents steel and macro polypropylene respectively.

Table 3.1: Batch weights of the constituents

Materials (kg/m <sup>3</sup> )	Control	SF0.5	PP0.5	SF0.2+ PP0.3	SF0.94	PP0.94	SF0.5+ PP0.44
Steel fiber	-	39.2	-	15.6	73.7	-	39.5
Polypropylene fiber	-	-	4.55	2.7	-	8.5	4
OPC 53 Grade cement	200	200	200	200	200	200	200
Fly ash (Pozzocrete 60)	140	140	140	140	140	140	140
Water/Cement ratio	0.48	0.48	0.48	0.48	0.48	0.48	0.48
Admixture (%)	0.65	0.65	0.65	0.65	0.65	0.65	0.65
20 mm aggregates	508	508	508	508	508	508	508
10 mm aggregates	508	508	508	508	508	508	508
Fine aggregates (robo sand)	823	823	823	823	823	823	823
Water	163	163	163	163	163	163	163

### 3.2.1 Casting and Curing of Specimens

IS standard 150mm Cubes, 150mm X 300mm cylinder and 150 X 150 X 500 beams were cast from each mixture to evaluate compressive strength and toughness and ductility gain. Concrete was prepared using a drum mixer with a capacity of 0.25 m<sup>3</sup>. The ingredients were put into the mixer in the decreasing order of their sizes starting from 20mm aggregate to cement. Dry mixing of the aggregates and cement was done for two minutes and then water was added gradually in the rotating mixer and allowed to mix for 15 minutes. During the mixing process, the walls and bottom of mixer were scraped well to avoid sticking of mortar. After mixing, the slump was checked and noted down to

ascertain the effects of differently proportioned blends on workability of concrete. Finally the fresh concrete was placed in oiled moulds and compacted properly in three layers, each layer being tamped 35 times using a tamping rod. After the initial setting of concrete, the surface of the specimen was finished smooth using a trowel. Immediately after casting, all specimens were covered with plastic covers to minimize moisture loss. The specimens were stored at room temperature about 25°C. Specimens were demoulded 24 hours after casting and kept in curing water tank.

### 3.3 Test Methods

An experimental program was designed to study the influence of fiber on the toughness and ductility. Each concrete mixture was evaluated with respect to Slump, compressive strength, and flexural tensile Strength of fiber reinforced concrete.

#### 3.3.1 Slump

Slump was used to find the Workability of fresh concrete where the nominal maximum size of aggregate does not exceed 38 mm. slump cone was used to find the slump of the concrete as per the requirements of IS 1199-1959. Oil was applied on the base plate and interior surface of the slump cone. After that, Slump cone was attached to a base plate with screws and finally kept on the levelled surface. Immediately slump cone was filled with fresh concrete approximately one-quarter of height of the cone, each layer was tampered with the tampered rod 25 times. After compacting the top layer, mould and the base plate was cleaned with the clothes. Slump cone was Unscrewed from the base plate and removed immediately from the concrete by raising it slowly and carefully in a vertical direction. Finally slump cone of the base plate kept reverse position, height between the top of the mould and highest point of the concrete was measured with the scale. This height indicated the slump of the concrete.

#### 3.3.2 Compression Strength Testing

A 2000kN digital compressive testing machine was used for determine the compressive strength of hardened concrete using 150 mm cubes as per the requirements of IS 516-1959. Before starting the test the weight of the sample was recorded. The plates of the machine were cleaned and the specimen was kept centrally between the two plates. Load was applied gradually on the specimen at a load rate of 5.2 kN/s up to failure. Once the sample was failed, the failure pattern was recorded and the compressive strength was calculated from the maximum load recorded in the test.

Cylinders were tested using a servo-hydraulic testing machine to obtain the stress-strain response. The displacements were increased at a rate of 0.05 mm/min. Two LVDTs with a gauge length of 60 mm were used to measure the displacement on the cylindrical specimens. The LVDTs were attached to rings which were mounted 120 mm from the top and the bottom of the specimen. These aluminum ties were able to support the measuring devices, to allow lateral deformations when they occurred, and did not confine the specimens. The data acquisition and signal control were carried out using control unit.

### 3.3.3 Four-point-bending test

Flexural testing machine with servo hydraulic closed-loop test machine was used to determine the toughness and ductility as per ASTM C1609-M10 and EN 14651.

#### *3.3.3.1 ASTM C 1609 Procedure*

This test method utilizes 150 x 150 x 500 mm beams tested on a 450 mm span. The testing was done using a servo-controlled test machine where the net deflection of the centre of the beam is measured and used to control the rate of increase of deflection. Testing was done as per ASTM C1609 to capture the portion of the load-deflection curve immediately after the first-peak. The loading and specimen support system applied third-point loading to the specimen without any eccentricity or torque. The fixtures used in the testing allowed free rotation on their axes. Linear variable displacement transducers

(LVDT) were used to ensure accurate determination of the net deflection at the mid-span. Rectangular jig, surrounding the specimen was clamped to it at mid-depth directly over the supports. Two displacement transducers were mounted on the jig at mid-span, one on each side, to measure deflection through contact with appropriate brackets attached to the specimen. The average of the measurements represented the net deflection of the specimen exclusive of the effects of seating or twisting of the specimen on its supports. The loading was applied such that the net deflection of the specimen increased at a constant rate of 0.04 mm/ min up to a net deflection of  $L/900$ . Thereafter, i.e., beyond  $L/900$  and up to a deflection of  $L/150$ , loading rate was kept constant at 0.08 mm/min. Beyond  $L/150$  and up to the end point deflection, the rate of loading was kept constant at 0.16 mm/min. The testing was continued till the specimen failed.

### *3.3.4 Three-point-bending test (For notch beam)*

The test procedure adopted was consistent with the guidelines given by EN 14651:2005 and 150 X 150 X 500 (height X width X length) mm<sup>3</sup> prismatic specimens were tested in the three-point bending configuration. A notch of 25mm depth was introduced at the mid-span using a circular saw as per the guidelines given in EN 14651:2005. The flexure test was conducted in crack mouth opening displacement control by increasing the CMOD at a prescribed rate. The corresponding deflection of the beam was measured using the rectangular jig clamped to the specimen at mid-depth directly over the supports. The testing machine had sufficient stiffness to avoid unstable unloading phenomena in the softening branch of the load-CMOD curve. The notched beam was tested with a span equal to 450 mm during the tests, the rate of increase of the CMOD was controlled in two stages, at 0.05 mm/min for CMOD less than 0.1 mm and at 0.2 mm/min for CMOD greater than 0.1 mm. All the tests were ended when the CMOD reached a value of 4 mm.

## 3.4 Test Matrix

The test matrix used in this study showing the combinations of fibers evaluated and the ages of testing are given in Table 3.2.

Table 3.2 Test matrix of the experimental program

Sl no	Proportion	Total Volume Fraction (%)	Volume fraction of Steel fibers (%)	Volume fraction of Polypropylene fibers (%)
1	Control	-	-	-
2	0.5% SF	0.5	0.5	-
3	0.5% PP	0.5	-	0.5
4	0.3% SF+ 0.2% PP	0.94	0.3	0.2
5	0.94% SF	0.94	0.94	-
6	0.94% PP	0.94	-	0.94
7	0.5% SF+ 0.44% PP	0.94	0.5	0.44

The properties of each mix are investigated at 3 day, 7 day and 28 days.

# Chapter 4

## Experimental Results

### 4.1 Introduction

The evaluation of the properties of FRC composites is of prime importance for these composites to be used effectively and economically in practice. Fibers are known to contribute to improvements in properties such as toughness, ductility, load carrying capacity, crack control. Improvements in the properties of concrete are primarily attributed to the ability of the fibers to function as discrete reinforcement bridging cracks. Improvements in mechanical properties on using fibers are a result of crack closing stresses provided by fibers and the improvements depend upon the crack closing stresses generated by the fibers as a function of crack opening. The efficiency of fibers depend on its ability to contribute during localization and propagation of a crack. For a given fiber type, fiber volume fraction is a primary variable which controls the properties of the composite. Standard test procedures, which provide measures of specific properties derived from the mechanical response of specimens tested in flexure have been developed. These test measures allow for comparing different fiber types and for assessing the improvement provided by fibers as a function of volume fraction.

The results of an investigation into the early age fraction response of hybrid fiber reinforced concrete using macro steel and polypropylene fibers are presented in this chapter. The results of compression tests of cube and beam flexural tests at 3, 7 and 28 days are presented. The results of the flexural response are interpreted in terms of the influence of fibers on crack propagation in fiber reinforced concrete.

## 4.2 Compressive Strength

The mean compressive strength obtained from standard 150 mm cubes for control, steel, polypropylene and Hybrid FRC for 0.5% and 0.94% volume fraction at 3, 7 and 28 days of age are shown in Figure 4.1 and Figure 4.2, respectively. On comparing the compressive strengths, all the fiber FRCs exhibit an improvement over the control specimen at early age, i.e. at 3 days and 7 days. Among various fiber combinations at 0.5% volume fraction, polypropylene shows the highest strength at both 3 and 7 days. At the age of 28 days, all the specimens show comparable results. The same trend is seen at the higher volume fraction of 0.94%.

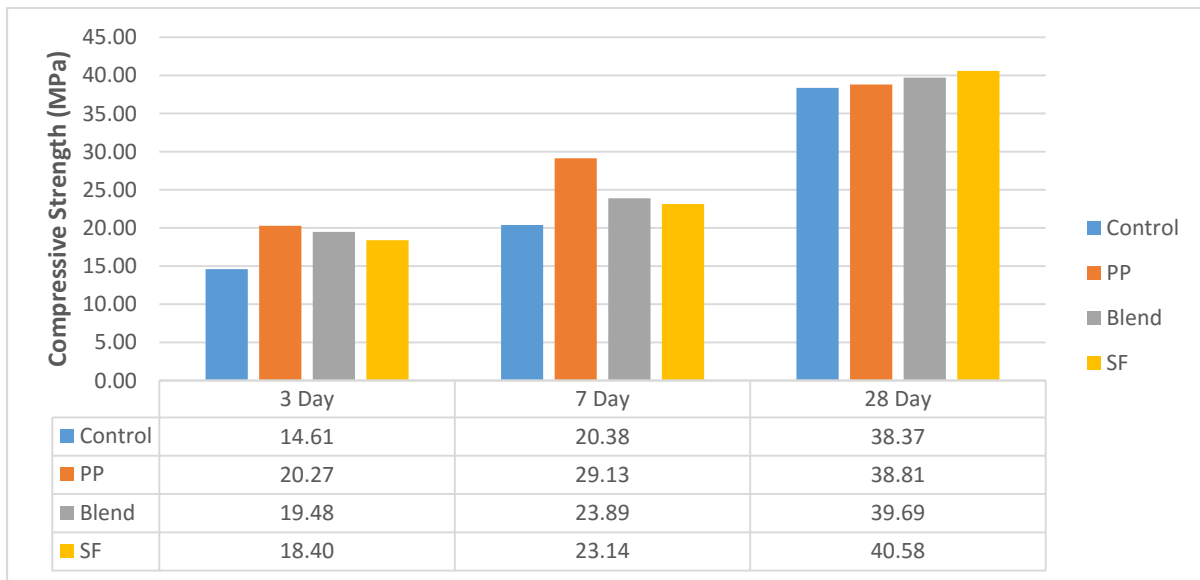


Figure 4.1 Compressive Strength Results for 0.5% Volume fraction at 3, 7 and 28 days



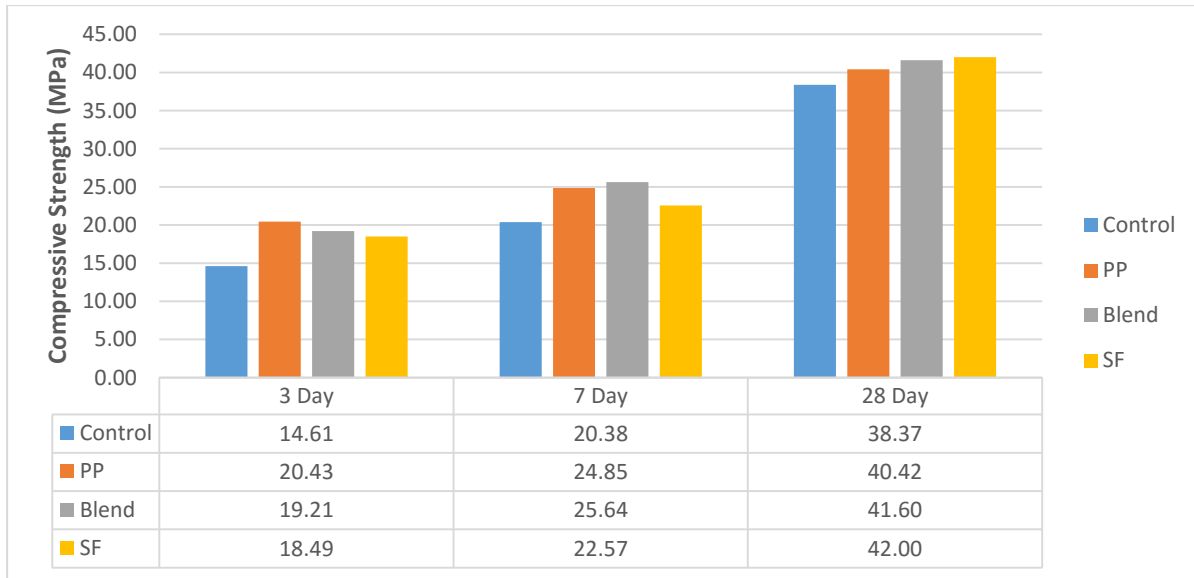


Figure 4.2 Compressive Strength Results for 0.94% Volume fraction at 3, 7 and 28 days

#### 4.3 Flexural Testing as per ASTM C1609 (Unnotched Beams)

The three point flexural testing of steel, polypropylene and hybrid FRC beams are conducted for a volume fraction of 0.5% and 0.94% at 3 day, 7 day and 28 day. Failure in both control and macro polypropylene FRC beams at 0.5% volume fraction was due to a single crack in the constant moment region. In hybrid and steel FRC beams with a higher volume fraction of 0.94%, multiple cracks were observed in the constant moment region.

The load deflection response of the control specimen is shown in Figure 4.3. All beams exhibit nonlinearity in the load response before peak load following the initial linear response. Following the peak load, which is associated with the localization of a single crack, the control beams show a monotonic and rapid decrease in the load with increasing deflection.

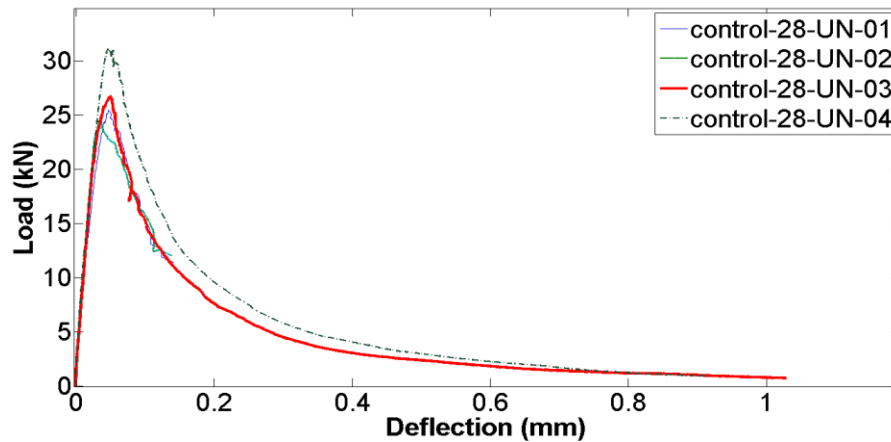


Figure 4.3 Load deflection response of control specimen

### Polypropylene FRC

The averaged load deflection plots for polypropylene FRC with volume fractions equal to 0.5% and 0.94 % at 3, 7 and 28 days are shown in Figure 4.4 and Figure 4.5, respectively. Polypropylene FRC beams both at 0.5% and 0.94% volume fraction exhibit similar response. In both the beams, there is a decrease in the load upon increasing the deflection immediately after the first peak. After the first peak the load drop ceases at a particular load which depends on the volume fraction of fibers. The beams exhibit a load recovery, where the residual load carrying capacity increases with increasing deflection. There is clear increase in the modulus of rupture (MOR) which is obtained from the peak load in the load response as the FRC ages. The increase in the MOR is shown in the Figure 4.6. It is also observed that the initial load drop also increases as the FRC ages. At 0.5% volume fraction, all the specimens exhibit a nominal increase in load with increasing deflection. At 0.94% volume fraction, there is a noticeable increase in the load carrying capacity with increasing deflection after the initial load decrease in the post-peak.

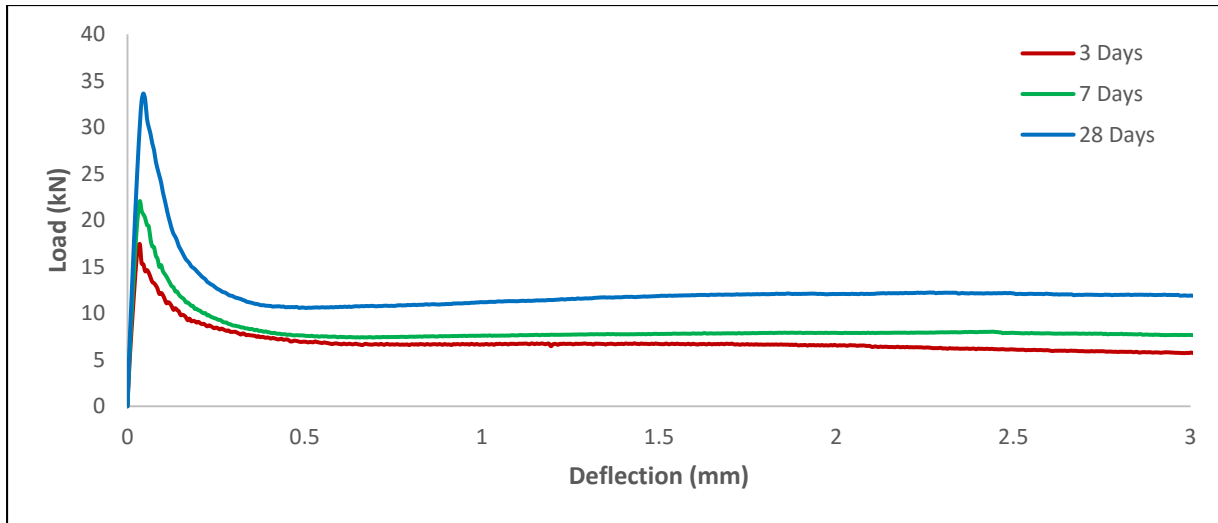


Figure 4.4 Load Deflection response from flexure test for 0.5% Polypropylene FRC at 3, 7 and 28 days

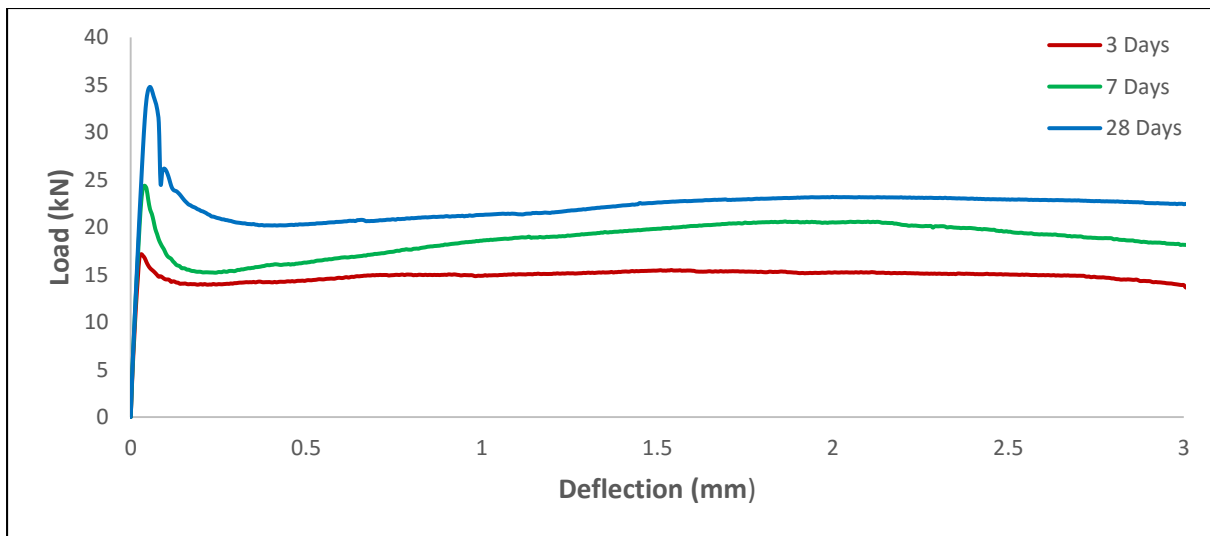


Figure 4.5 Load Deflection response from flexure test for 0.94% volume fraction of Polypropylene FRC at 3, 7 and 28 days

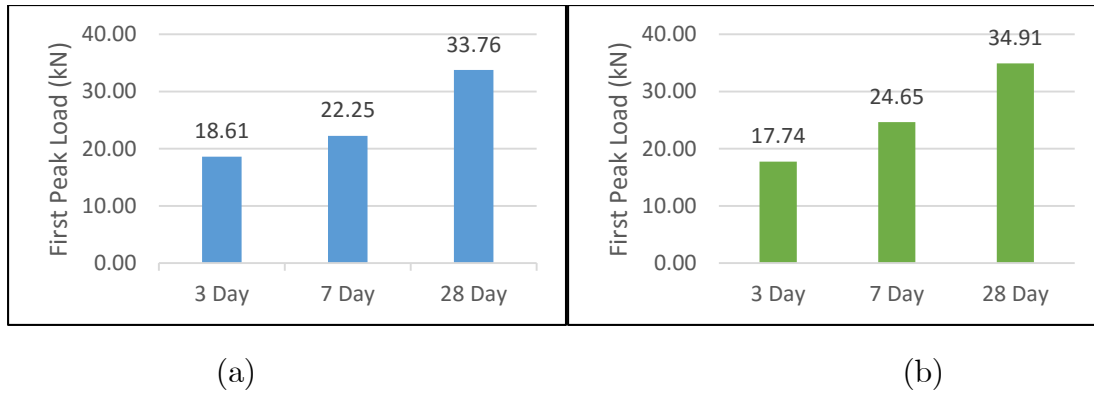


Figure 4.6 Variation of MOR as the age of Polypropylene FRC increases. (a) 0.5% VF (b) 0.94% VF

### Steel FRC (SFRC)

The average load deflection plots from flexural testing as per ASTM C1609 for steel FRC with 0.5% and 0.94 % volume fraction at 3, 7 and 28 days are shown in Figure 4.7 and Figure 4.8, respectively. An increase in MOR is observed as the FRC ages. In case of SFRC with 0.5% volume fraction there is an initial load drop prior to the hardening response. The Steel FRC with 0.94% volume fraction gives hardening response even at early age and the initial load drop is absent.

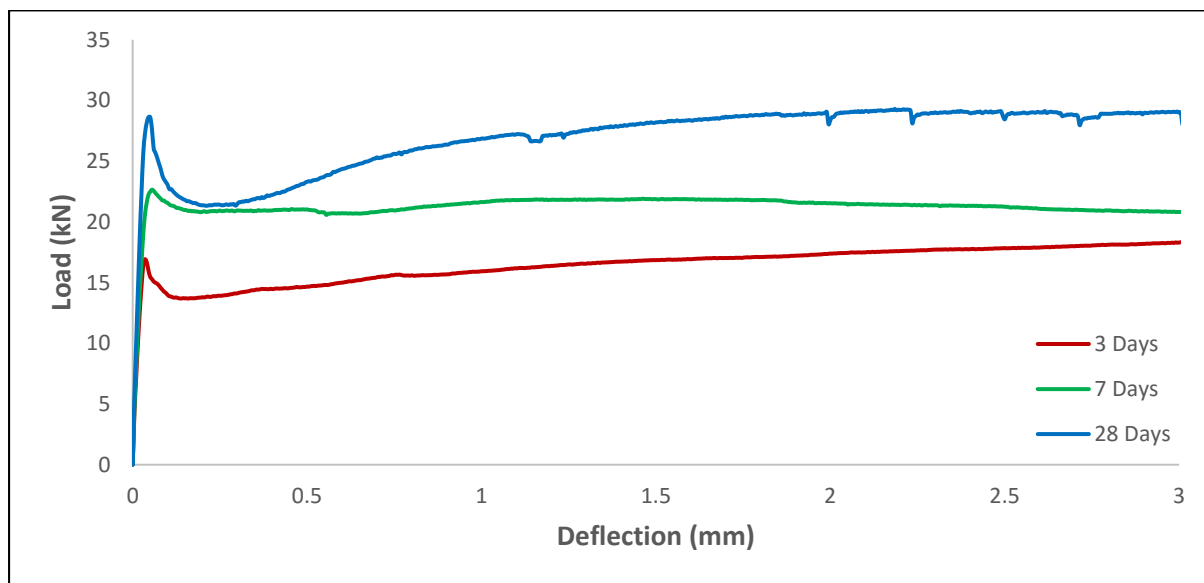


Figure 4.7 Load Deflection response from flexure test for 0.5% Steel FRC at 3, 7 and 28 days

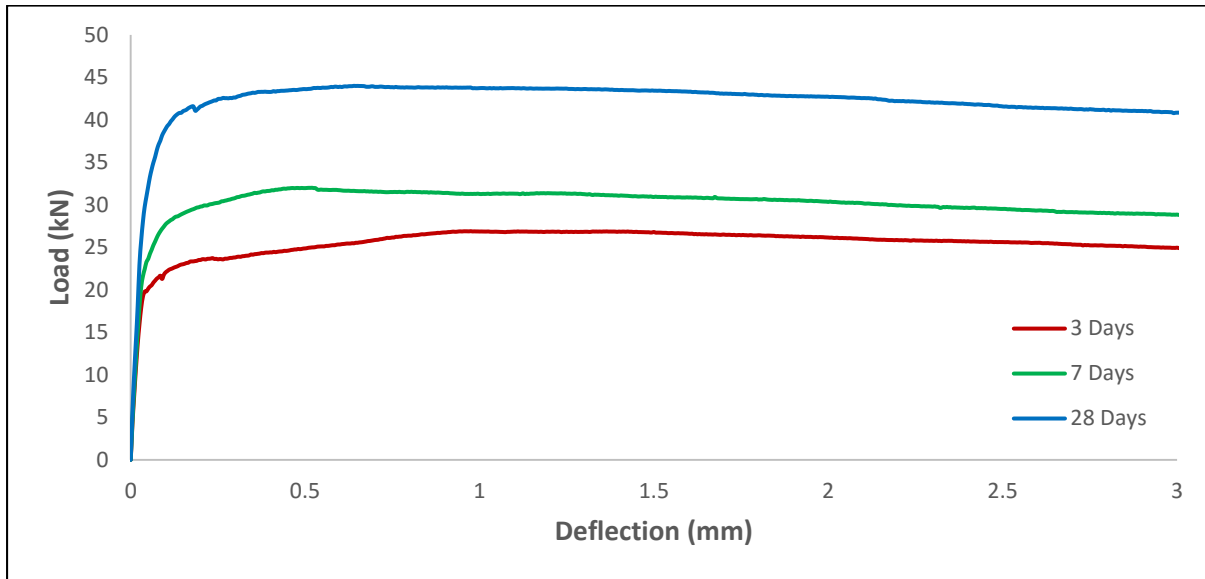


Figure 4.8 Load Deflection response from flexure test for 0.94% Steel FRC at 3, 7 and 28 days

#### Hybrid Fiber Reinforced Concrete

Considering the fiber blends, two fiber volume fractions were fixed at 0.5% and 0.94%. 0.5% Hybrid FRC is a combination of 0.3% Steel fibers and 0.2% Polypropylene fibers, and 0.94% Hybrid FRC is a combination of 0.5% Steel fibers and 0.44% Polypropylene fibers. The load deflection responses of both the volume fractions are shown in the Figure 4.9 and Figure 4.10, respectively. For 0.5% volume fraction, similar to the SFRC, there is an initial load decrease in the post-peak followed by a nominal increase in load carrying capacity with increasing deflection flattened response. For the 0.94% volume fraction, there is continued load increase and there is rapid load decrease with increasing deflection.

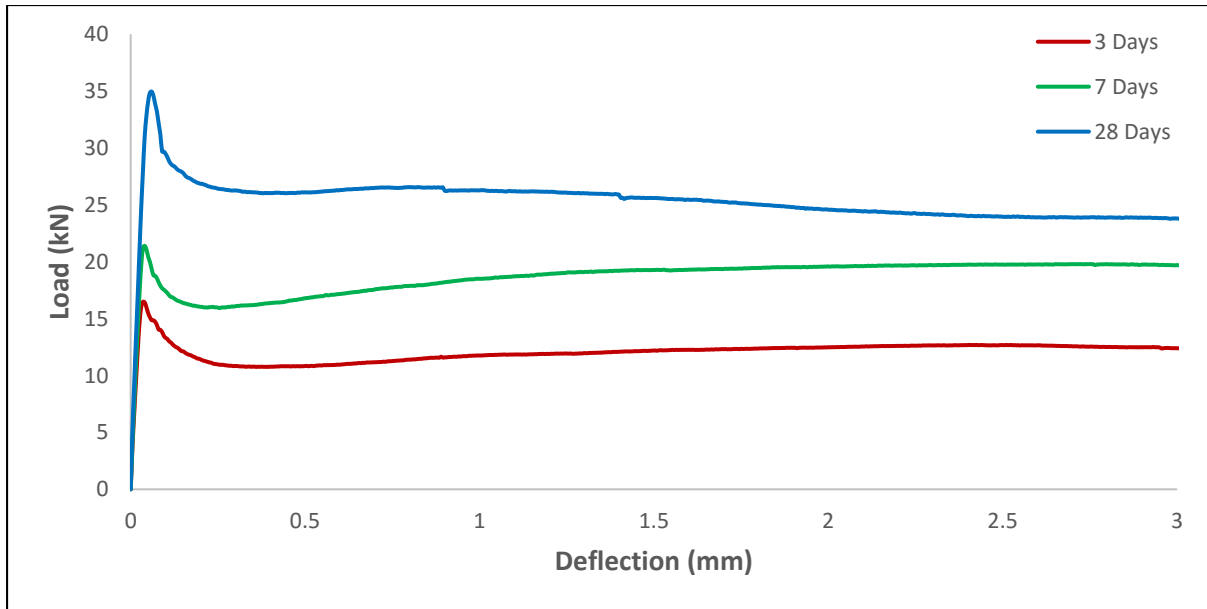


Figure 4.9 Load Deflection response from flexure test for 0.5% Hybrid FRC at 3, 7 and 28 days

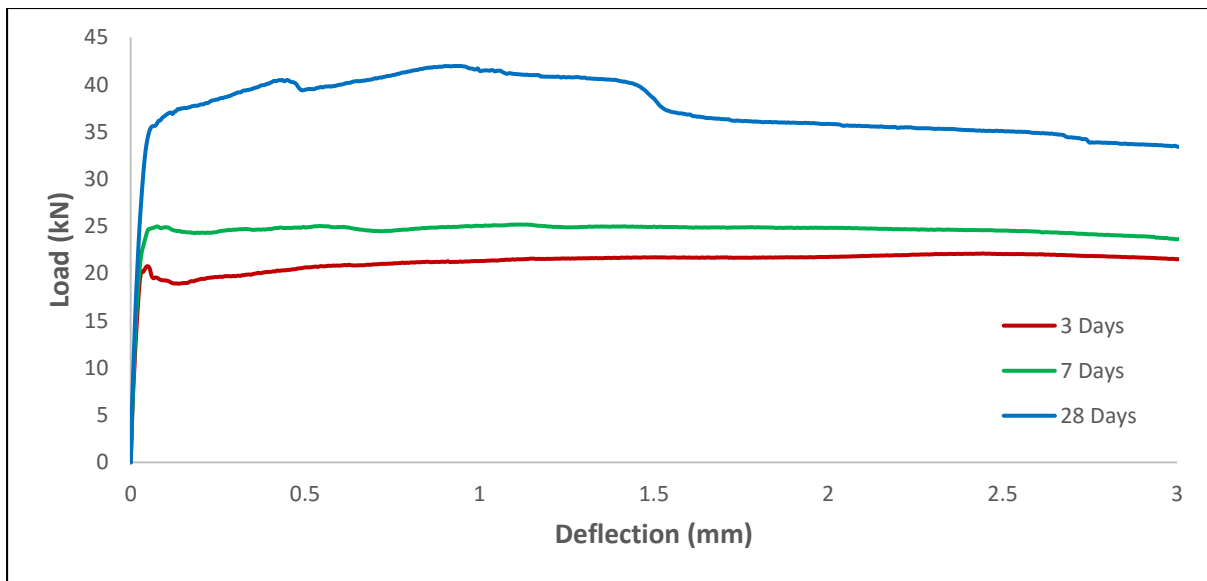
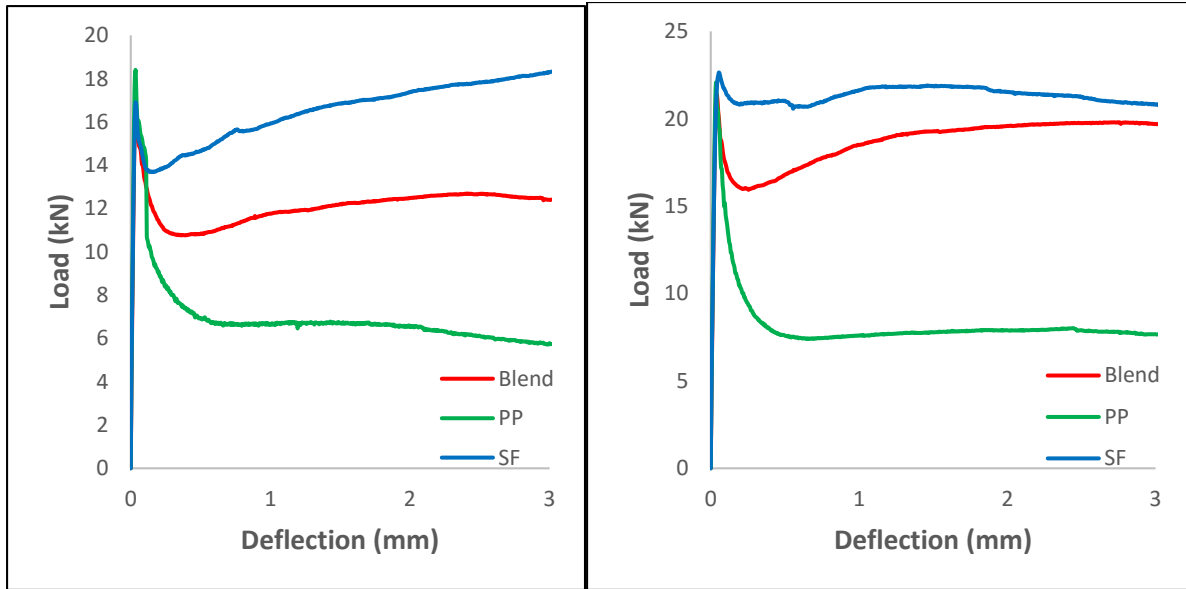


Figure 4.10 Load Deflection response from flexure test for 0.94% Hybrid FRC at 3, 7 and 28 days

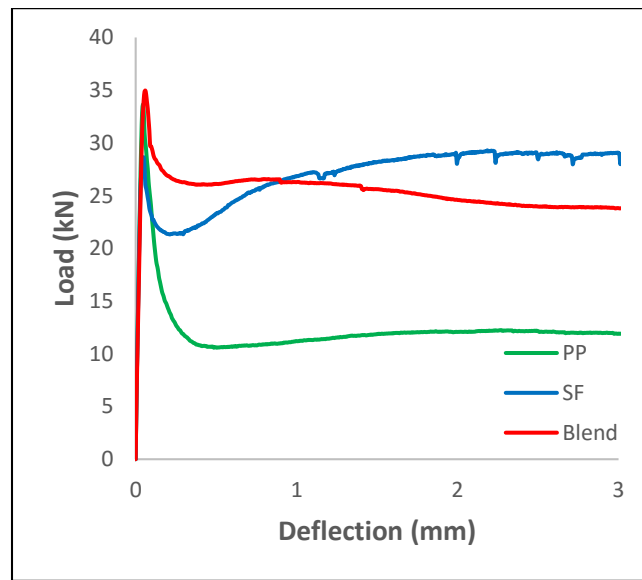
The load deflection responses of 0.5% and 0.94% volume fraction Polypropylene, Steel and Hybrid FRC beams at ages of 3 day, 7 day and 28 day are shown in Figure 4.11 and Figure 4.12. The variations in the peak load were found to be within the range of

experimental scatter for each fiber volume content suggesting that the fibers do not influence the peak load. The typical load deflection response indicates that at all ages, the FRC with steel fibers provides a superior response than the blend and polypropylene FRC, except for the lower fiber content at 28 days. For 0.5% volume fraction, it is observed that the hybrid FRC provides higher load carrying capacity in the descending part of the post-peak softening response and up to a deflection of about 0.9 mm when compared with steel and polypropylene FRC. Also the toughness values calculated using deflection up to 3 mm are comparable for both steel and hybrid FRC. The results indicate that, while in the early age steel provides higher load carrying capacity with increasing deflection in the post-peak load response when compared with Polypropylene and hybrid FRC, at a later age the hybrid blend gives a higher load carrying capacity in the immediate post-peak softening response at low volume fraction. Also, the response of the 0.5% hybrid blend provides better post-peak response with age; at 7 days of age the load response of hybrid blend approaches that of steel FRC at higher deflection. At higher volume fraction of 0.94%, the steel FRC gives a better response at all ages. The hybrid blend gives a comparable 28-day response when compared with steel FRC at lower deflection.



(a)

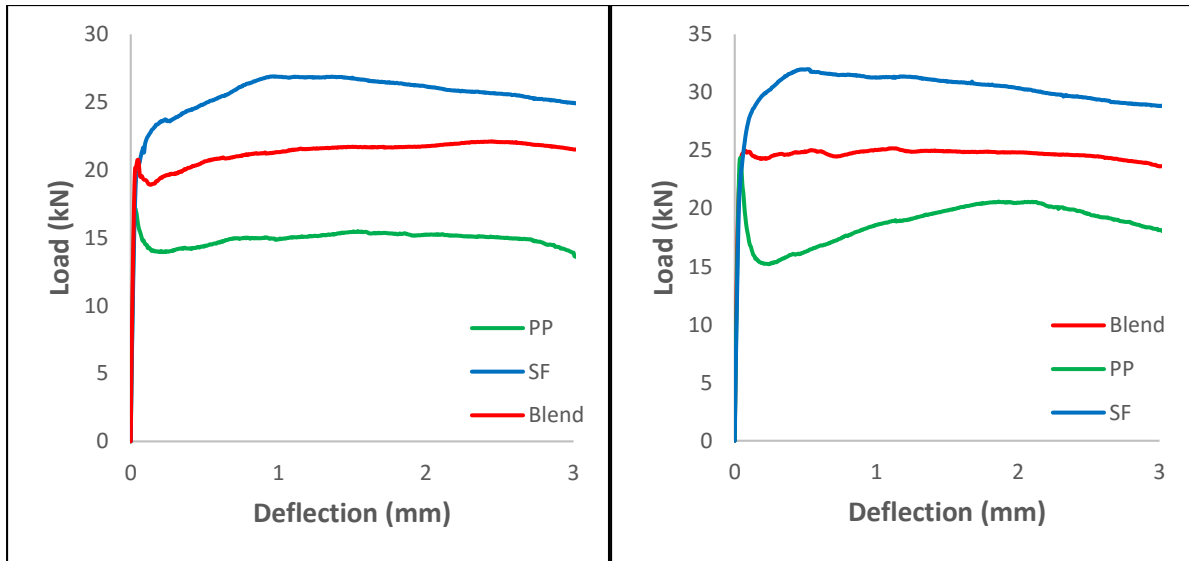
(b)



(c)

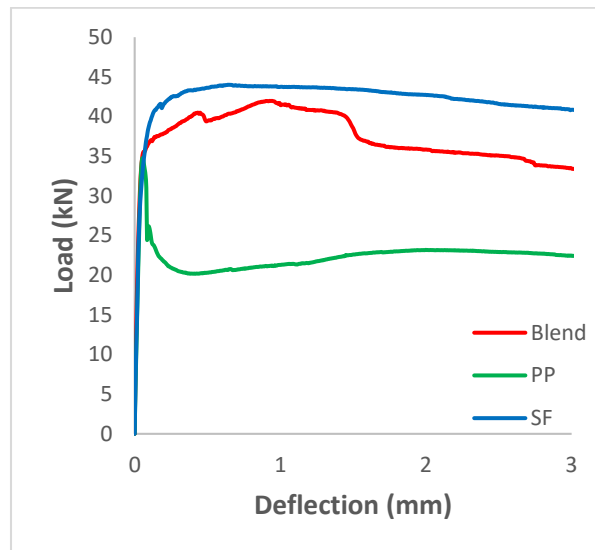
Figure 4.11 Load Deflection response of Polypropylene, Steel and Hybrid FRC beams at 0.5% Volume fraction on (a) 3 Day, (b) 7 Day and (c) 28 Day





(a)

(b)



(c)

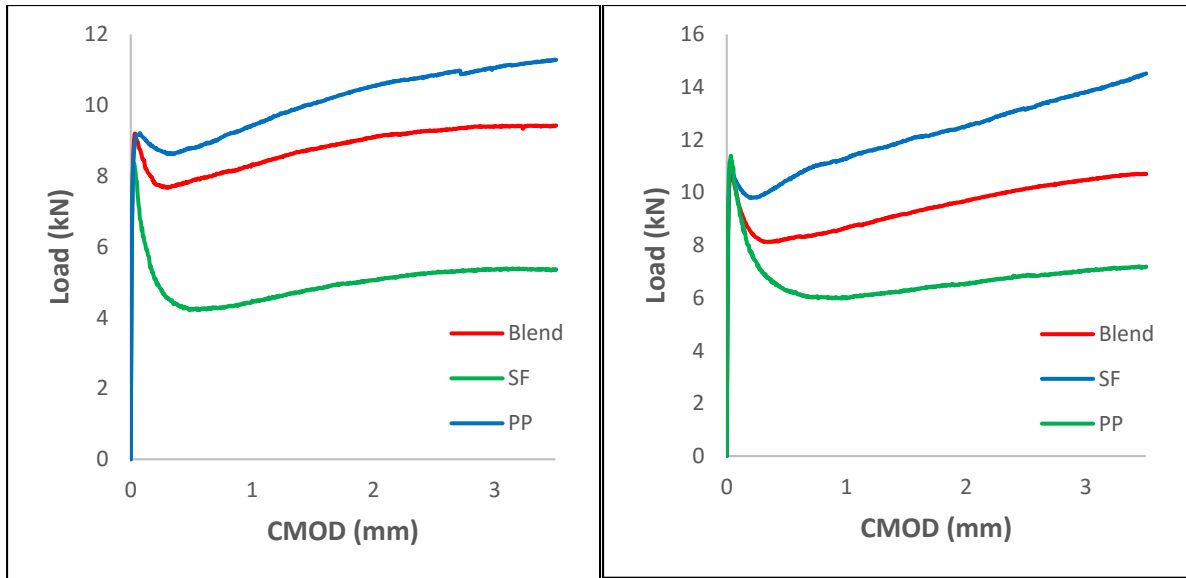
Figure 4.12 Load Deflection response of Polypropylene, Steel and Hybrid FRC beams at 0.94% Volume fraction on (a) 3 Day, (b) 7 Day and (c) 28 Day

#### 4.4 Flexure Testing on Notched Specimens (EN 14651).

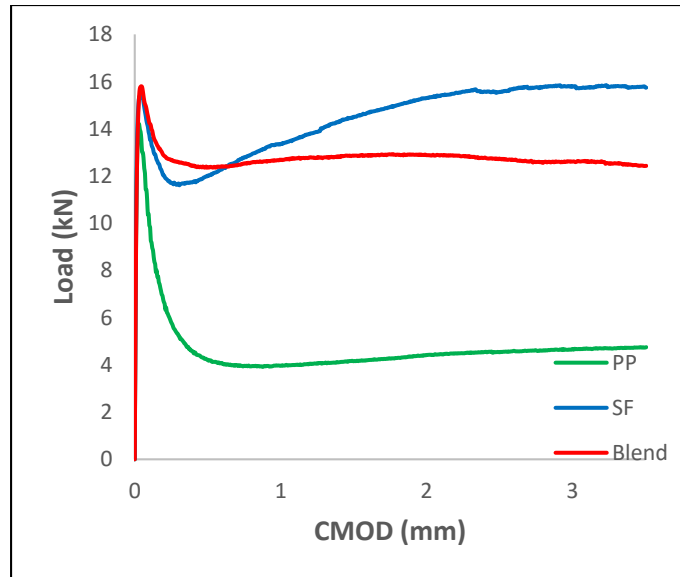
The load-CMOD response of response for polypropylene, steel and hybrid FRC with 0.5% and 0.94% volume fraction at 3, 7 and 28 days are shown in Figure 4.13 and Figure 4.14. The variations in the peak load were found to be within the range of

experimental scatter for each fiber volume content suggesting that the fibers do not influence the peak load. Similar to the load deflection response, the steel FRC provides higher load carrying capacity at any value of CMOD in the early ages.

The load CMOD response exhibits a hardening response following a decrease in the immediate post-peak for FRC with 0.5% volume fraction of steel, hybrid and polypropylene fibers. At 28 days the hybrid blend gives a better response than the steel FRC at smaller crack opening up to 0.6 mm. At 0.94% volume fraction, a common trend is observed at 3, 7 and 28 days; steel exhibits a better response followed by hybrid blend and polypropylene.



(a) (b)



(c)

Figure 4.13 Load CMOD response of Polypropylene, Steel and Hybrid FRC of 0.5% Volume Fraction at (a) 3 Day, (b) 7 Day and (c) 28 Day

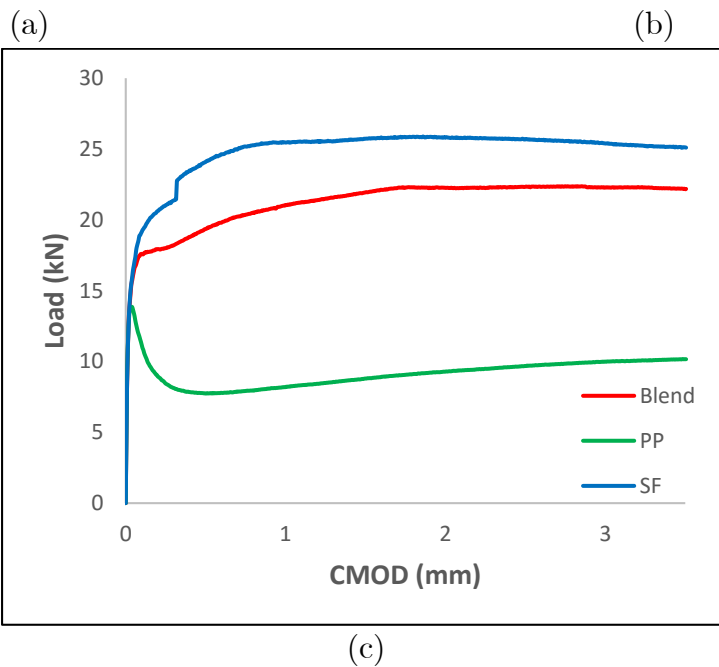
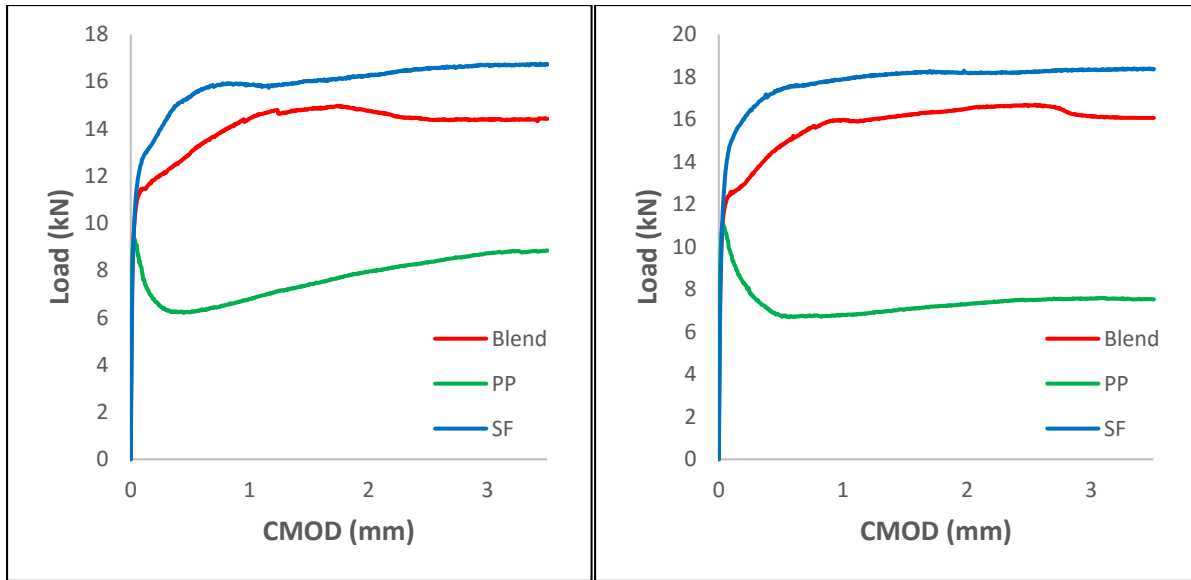


Figure 4.14 Load CMOD response of Polypropylene, Steel and Hybrid FRC of 0.94% Volume Fraction at 3 Day

#### 4.5 Analysis of Data

The response of the steel, polypropylene and hybrid FRC beams under flexure was analyzed in compliance with ASTM C1609, ASTM C1018, and JSCE SF4 for unnotched

beams and EN14651 for notched beams. The residual strength as per ASTM C1609 is graphically shown in Figure 4.15 and Figure 4.16. The residual Strength at span/600 (0.75 mm deflection) is observed to increase with increase in fiber volume at all ages. While there is a nominal increase in residual strength with fiber content in polypropylene FRC beams, the increase is significant in steel FRC and hybrid FRC beams. At 0.5% volume fraction the hybrid FRC exhibits comparable residual strength as the steel FRC at 7 and 28 days. For the higher volume content of 0.94%, 28 day residual strength is comparable for steel and hybrid FRC. For residual strength at L/150 deflection there is a considerable improvement in the residual strength with fiber content for steel, polypropylene and hybrid FRC. Equivalent flexural strength ratio also increases with an increase in the fiber volume indicating that more energy is required to break the specimen with higher fiber volume, Figure 4.17. This trend is observed at all ages.

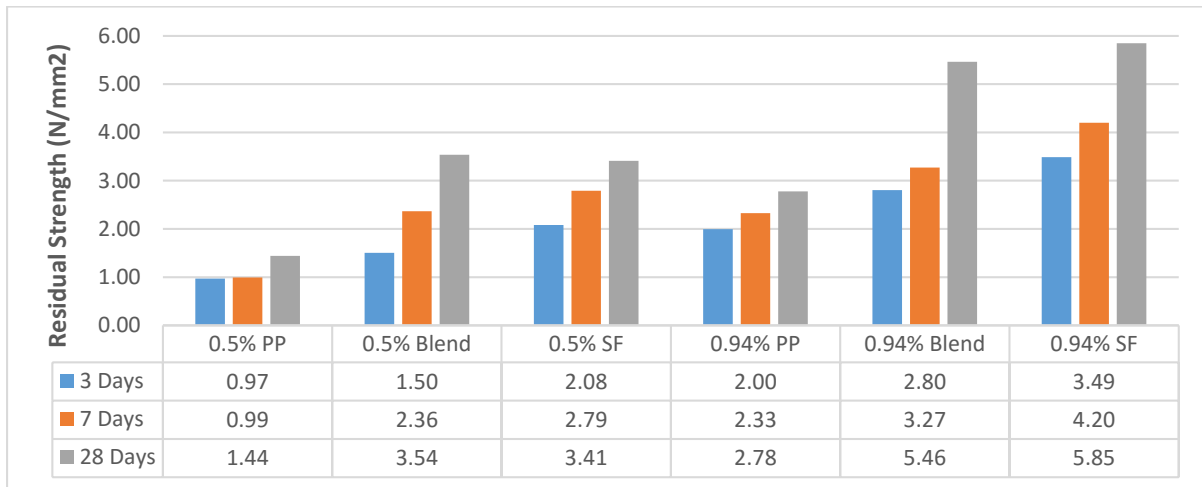


Figure 4.15 Residual Strength at L/600 as per ASTM C1609

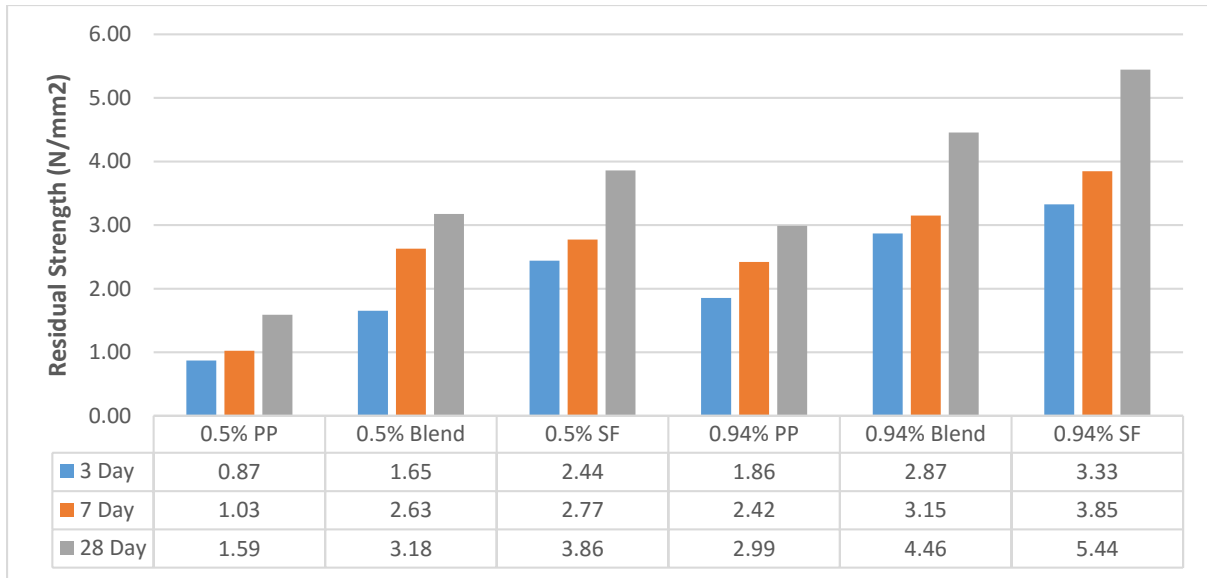
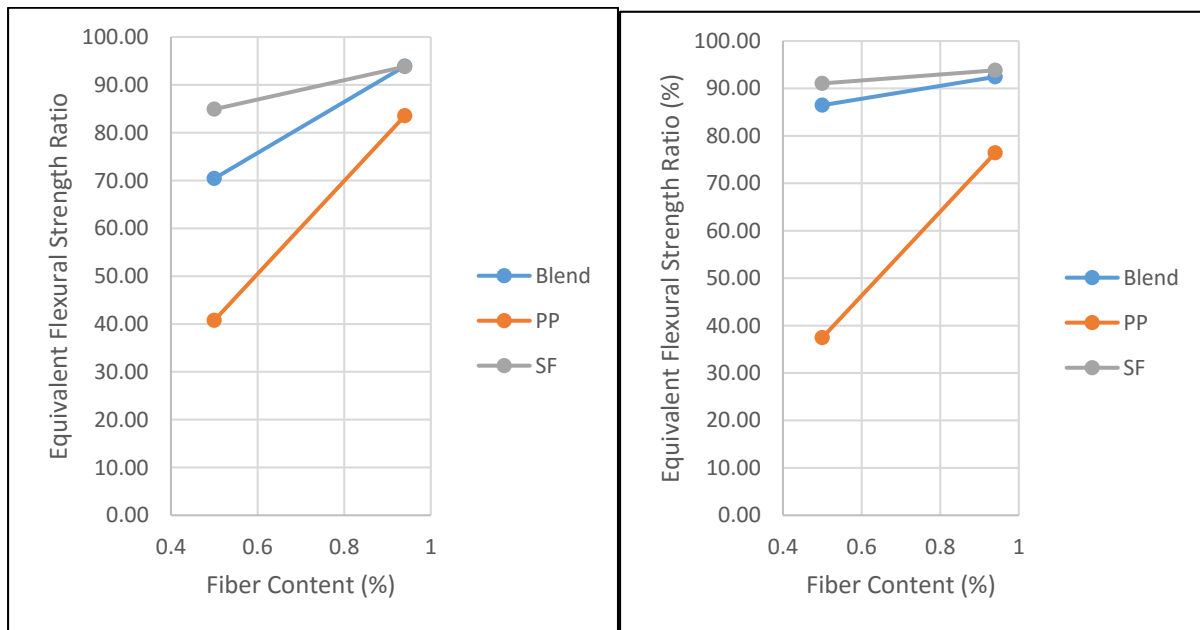
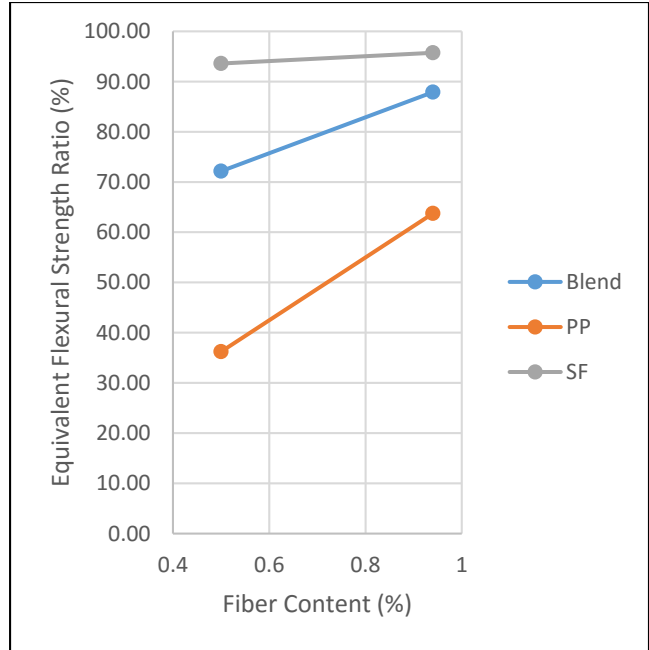


Figure 4.16 Residual Strength at L/150 as per ASTM C1609





(c)

Figure 4.17 Equivalent Flexural Strength Ratio as per ASTM C 1609 at (a) 3 day (b) 7day and (c) 28 day

Toughness factor for steel, polypropylene and hybrid FRC calculated as per JSCE standard 4 is shown in Figure 4.18 for 3, 7 and 28 days. The toughness factor is observed to increase with fiber volume indicating the enhancement in energy absorption capacity of beam.

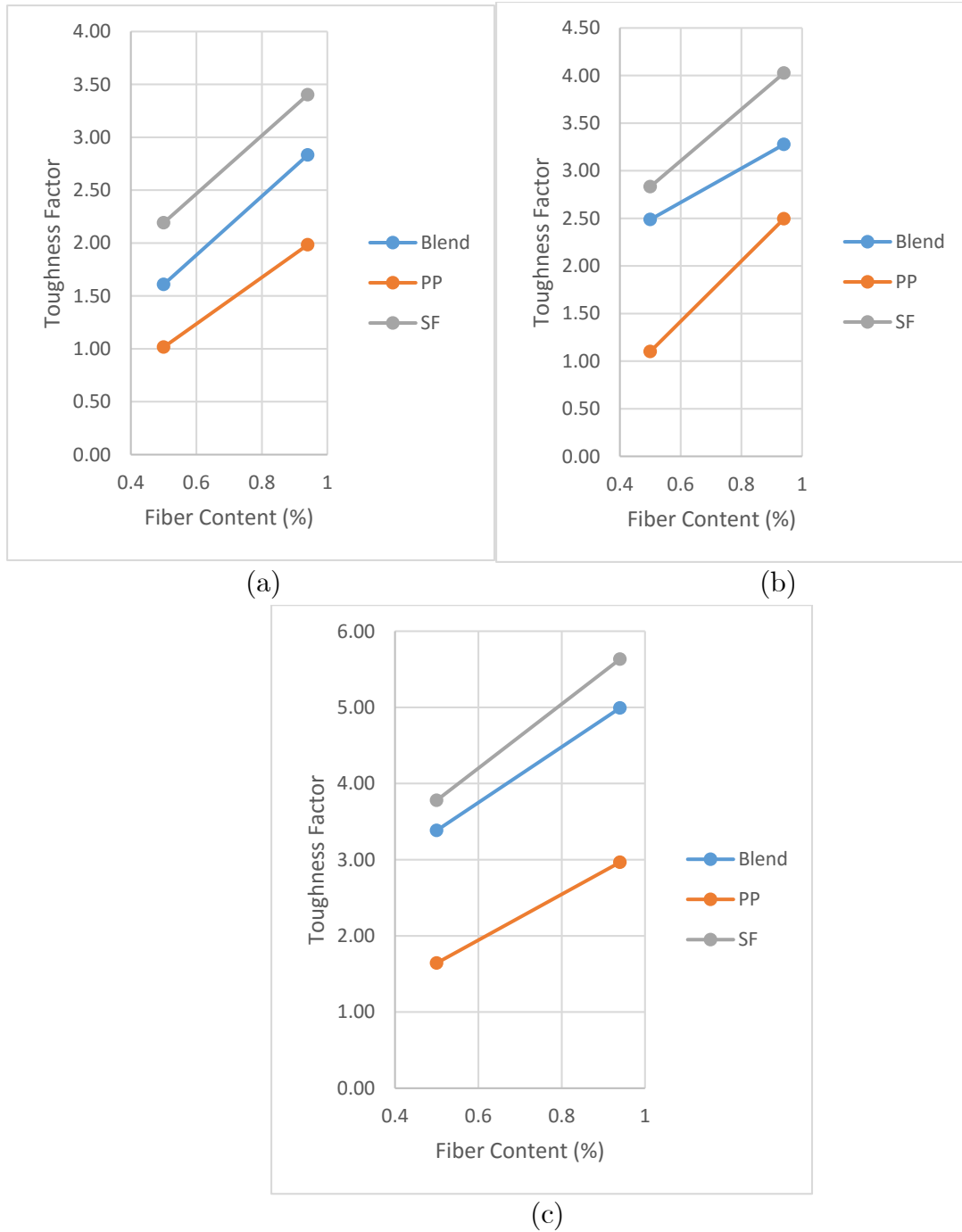
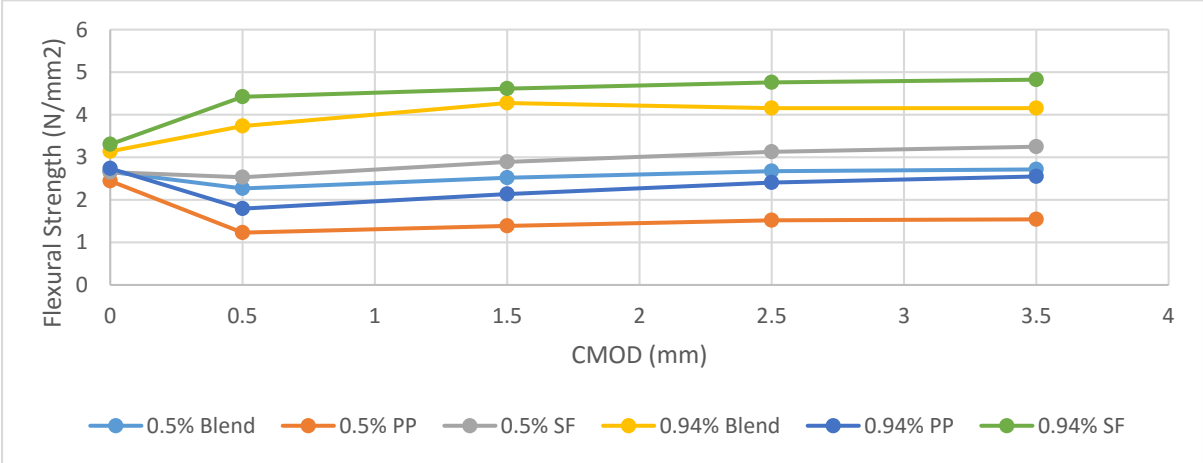


Figure 4.18 Toughness Factor as per JSCE SF4 at (a) 3 day (b) 7day and (c) 28 day

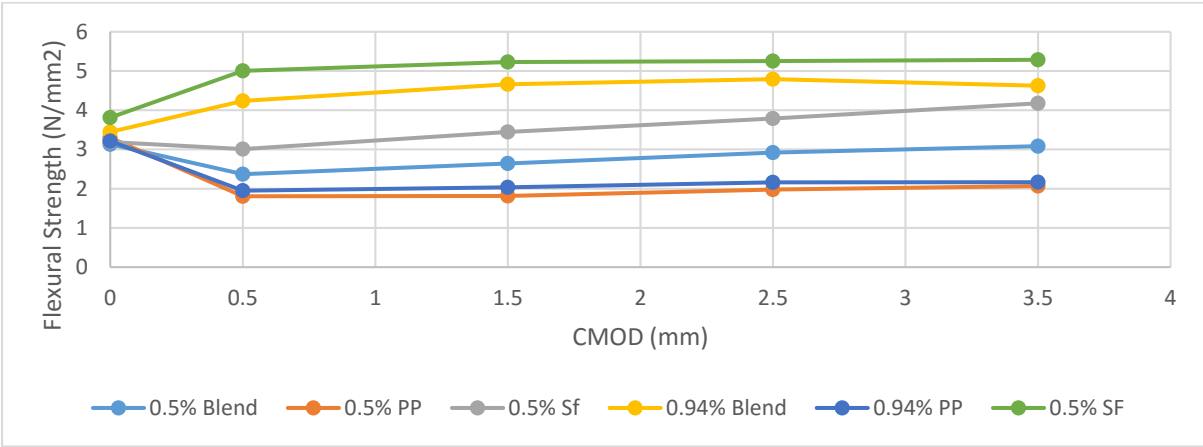
The residual flexural strength calculated as per EN14651 from the test response of notched specimens tested in CMOD control are shown in Figure 4.19 for steel, polypropylene and hybrid FRC at 3, 7 and 28 days, respectively. The residual flexural strength provides a measure of effectiveness in providing crack closure. Flexural strength



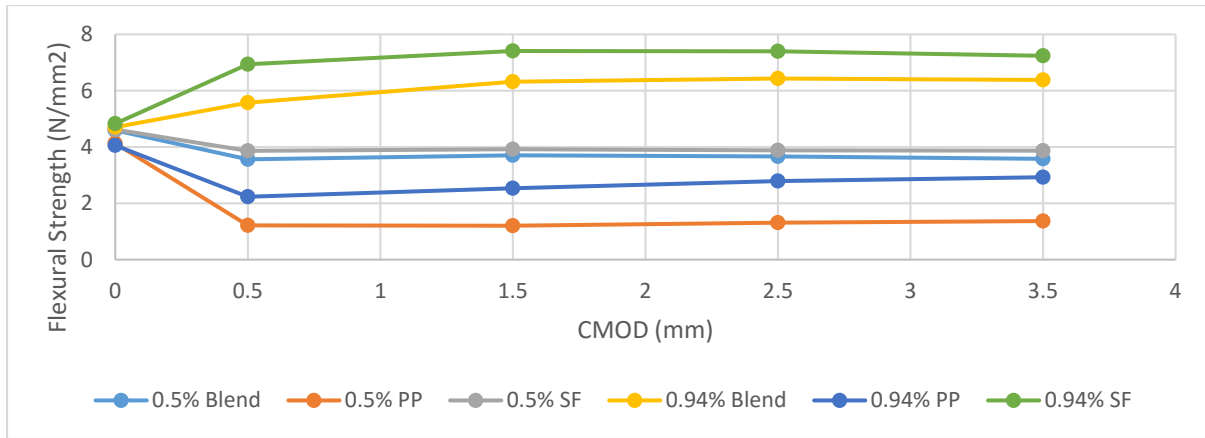
remaining constant implies as the crack opens as the load carrying capacity of the beam remains constant. For 0.94% steel and hybrid FRC, the flexural strength tends to increase till a crack opening of 0.5 mm. This shows the load carrying capacity increases even when the crack opens.



(a)



(b)



(c)

Figure 4.19 Residual Flexural Strength as per EN 14651

#### 4.6 Summary of Findings

From the response of both the notched and unnotched specimens, it is observed that at a lower volume fraction of 0.5% the hybrid FRC improves as it ages. At 28 days, the hybrid FRC showed a better response at a lower deflection about 0.9 mm and crack opening of about 0.6 mm. From the early age studies, it is observed that polypropylene FRC alone couldn't make comparable response with steel FRC.

For polypropylene FRC, the load drop in the post peak is accompanied with an increasing deflection, which is indicative of increasing compliance produced by the crack propagating along the height of the beam. Also load drop was found to increase as the concrete ages. For polypropylene FRC, the failure was observed to be produced by a single crack in the constant moment region. But multiple cracks were visible for specimens in both hybrid and steel FRC of higher volume content.

The compressive strength showed an improvement on adding fibers. The polypropylene FRC showed a good performance in the early ages.

# Chapter 5

## Digital Image Correlation Results

### 5.1 Introduction

Digital image correlation (DIC) is a full-field optical technique which provides spatially continuous measurement of displacements across the surface of the specimen. Compared with other optical techniques, DIC is a very robust measurement technique which does not require the use of lasers. It provides reliable measurements without the requirement of any special vibration isolation, which allows the use of this technique during a mechanical test. The technique relies on a random sprayed-on speckle and a digital camera for image acquisition. With the advent of digital cameras, which provide increased resolution, the accuracy obtained from the technique has increased allowing for the use of the technique in applications which required measurements at a higher resolution. DIC has been used to determine the stress concentration produced by a stress riser such as a crack and for stress distribution due to damage. Application of the technique have included determining the stress concentration for evaluating fracture parameters in composite and metallic specimens [45] [46] [47]. Successful application of DIC in concrete specimens include determination of the strain profile associated with cohesive stress transfer produced with debonding of FRP composite laminates and to derive the cohesive stress-crack separation relationship [48].

DIC measurements were performed on notched specimens tested as per EN 14651. A speckle pattern was created in a region close to the notch. While the available resolution from the technique considering the area of measurement does not allow for determining fracture parameters, the information from the surface displacements and strains obtained using DIC are used for evaluating the crack propagation. The surface displacements and

strains were analysed for evaluating the crack growth in concrete in relation to the observed load response in flexure and to compare with measurements obtained from other instrumentation.

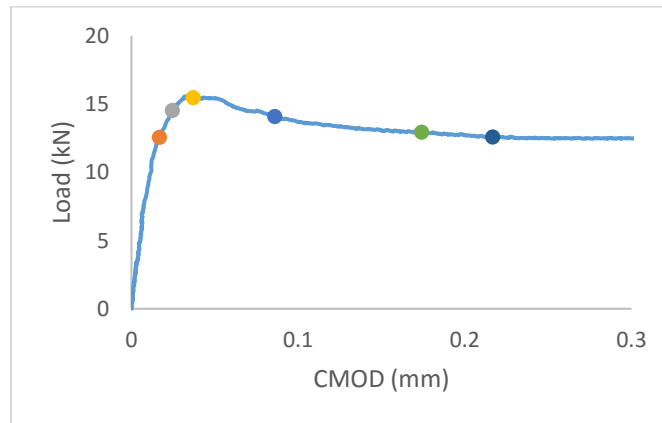
## 5.2 Background

DIC relies on correlation of the random pattern of speckles between images of the deformed and reference (undeformed) configurations of the specimen within small neighbourhoods called subsets [Sutton et al. (1983,1988)]. The speckle pattern represents a random pattern, which gives a unique distribution of pixel grey level values in each subset. A two-dimensional displacement field was obtained for all points on the surface from cross-correlating the image of the deformed specimen with the image of the specimen in the reference configuration. A subset size equal to 35x35 pixels was used for the correlation. In a given image, the pixel grey value in each subset associated with the random sprayed-on pattern forms a unique grey-level distribution, which differs from grey-level distribution of another subset. In the analysis, positions within the deformed image were mapped on to positions within the reference subsets using second-order, two-dimensional shape functions. Spatial domain cross-correlation was performed to establish correspondence between matching subsets in images of the reference and deformed states. Quintic B-spline interpolation of the grey values was used to achieve sub-pixel accuracy. The cross correlation analysis of the digital images was performed using the VIC-2D<sup>TM</sup> software, which maximizes the correlation coefficient between grey levels in the subsets in the reference and deformed images. Surface displacements and displacement gradients at each loading stage were calculated at each subset centre, by evaluating the shape functions and their partial derivatives at the subset centre. For the setup used in this study, the random error in the measured displacement is in the range of 0.002 pixels. Strains were computed from the gradients of the displacements. A conservative estimate of the

resolution in strain obtained from the digital correlation was 10[Bruck et al (1989), Schreier (2002)].

### 5.3 Results

Typical load-CMOD response of a polypropylene FRC beam with 0.5% volume fraction is Figure 5.1. The strain in the X-direction ( $\epsilon_{xx}$ ) at distinct point on the load response of the specimen (shown marked on the load response) are also plotted. It can be observed that strain localization is initiated close to the peak load and leads to the formation of single crack emanating from the notch. The growth of the crack can clearly be identified with softening in the post peak load response. Correspondingly there is also an increase in the CMOD. The results indicate that the localization close to the peak load, results in an increase in the crack opening. As the crack propagates, there is a steady increase in the crack opening and an associated drop in the load.



(a)

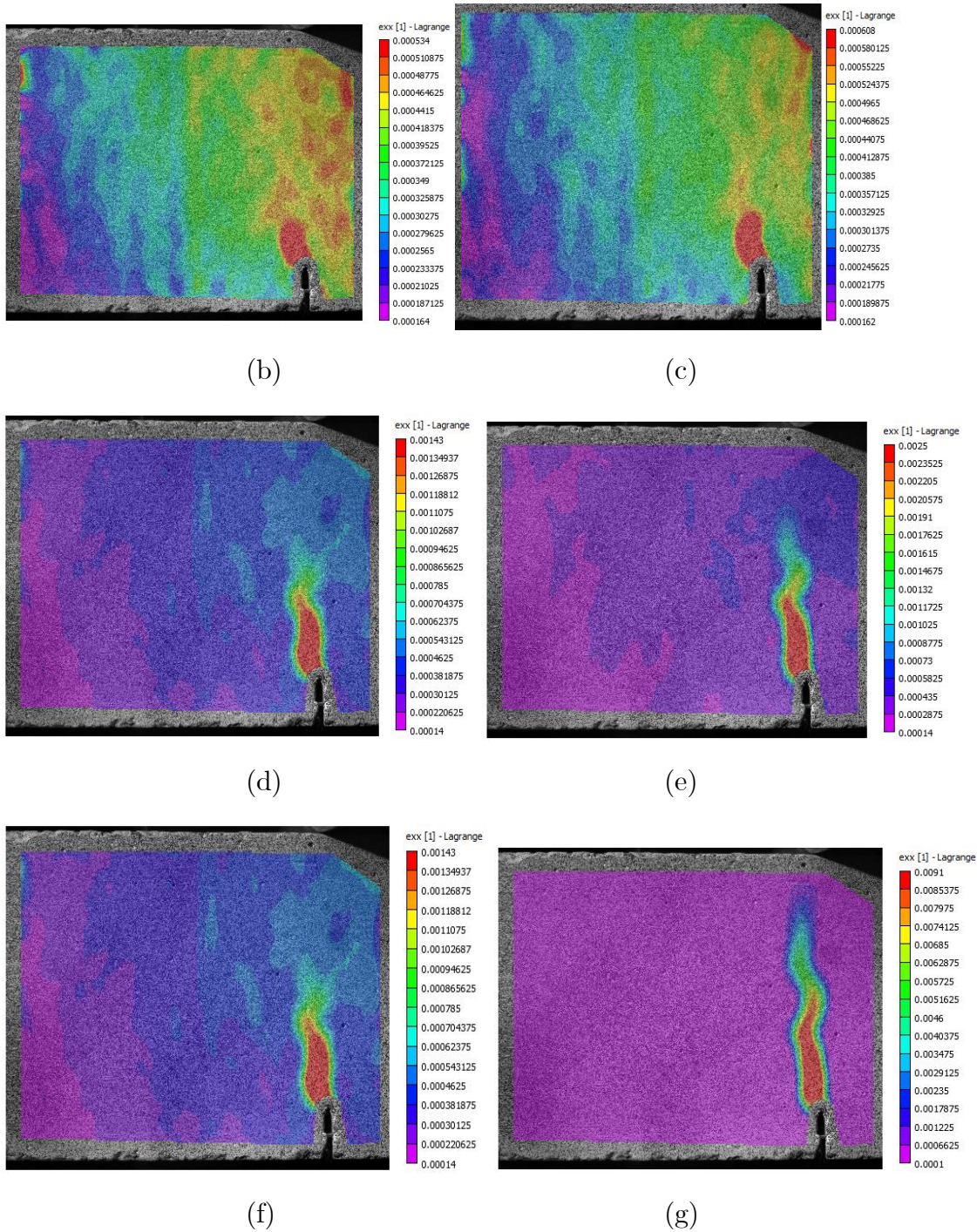
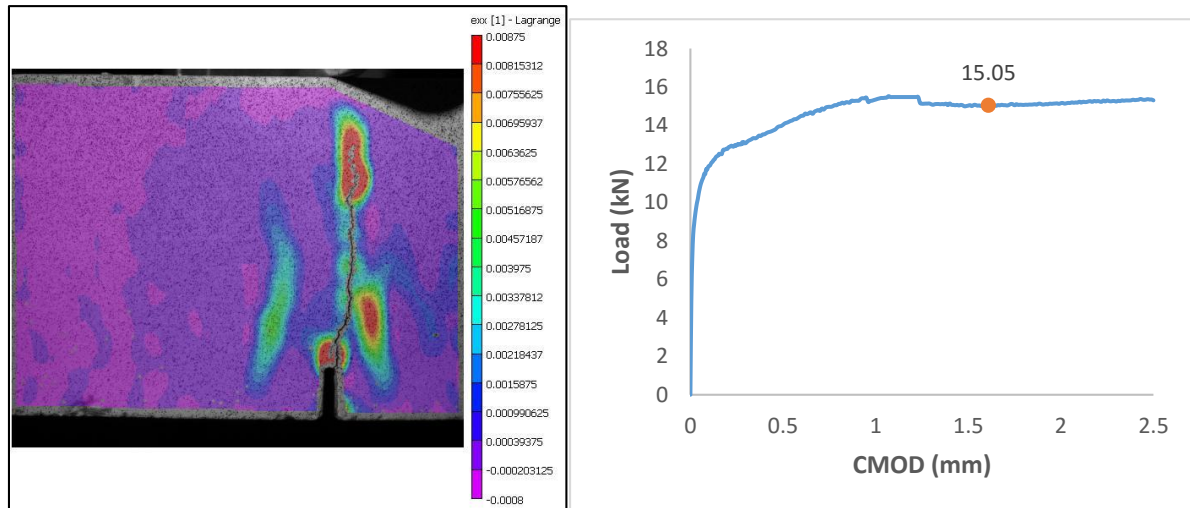


Fig 5.1: (a) Load-CMOD of plot of Hybrid specimen with 0.5% volume fraction (b)  $\epsilon_{xx}$  at 12.54 kN (pre-peak); (c)  $\epsilon_{xx}$  at 14.51 kN (pre-peak); (d)  $\epsilon_{xx}$  at 15.45 (peak); (e)  $\epsilon_{xx}$  at 14.06 kN (post-peak); (f)  $\epsilon_{xx}$  at 12.92 kN (post-peak); and (g)  $\epsilon_{xx}$  at 12.56 kN (post-peak)

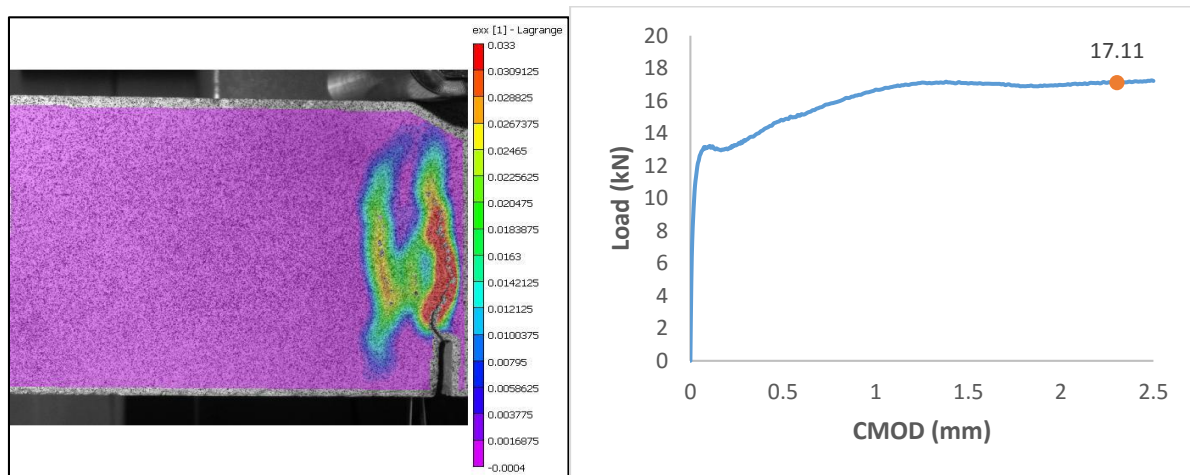
From the DIC analysis it is observed that there is formation of multiple cracks in case of Hybrid FRC and Steel FRC at higher volume fraction of 0.94%. The strain



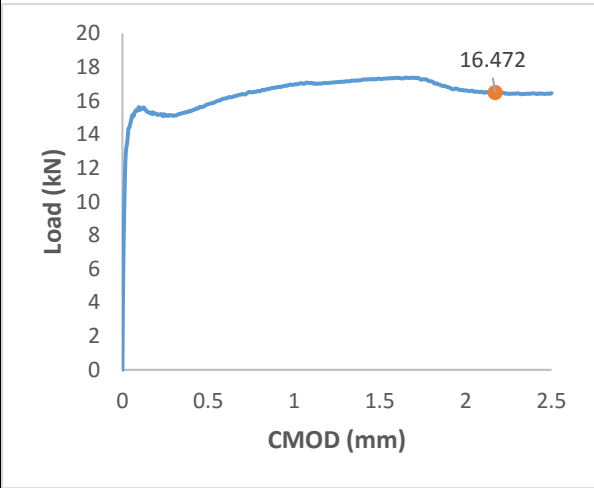
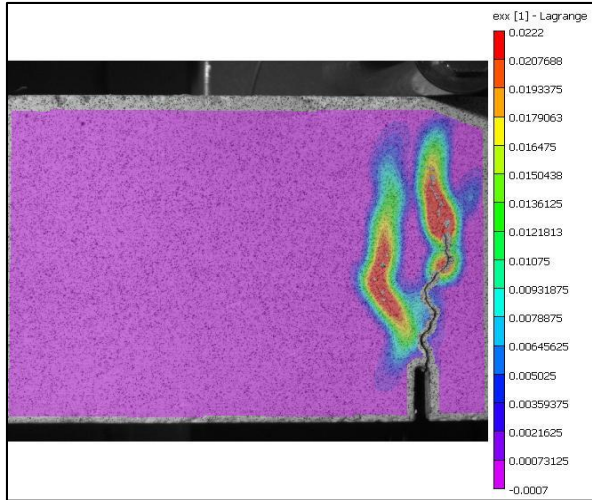
profile showing the multiple cracks are shown in Figure 5.2. The multiple cracking is observed at all ages. Multiple cracking was absent in case of polypropylene.



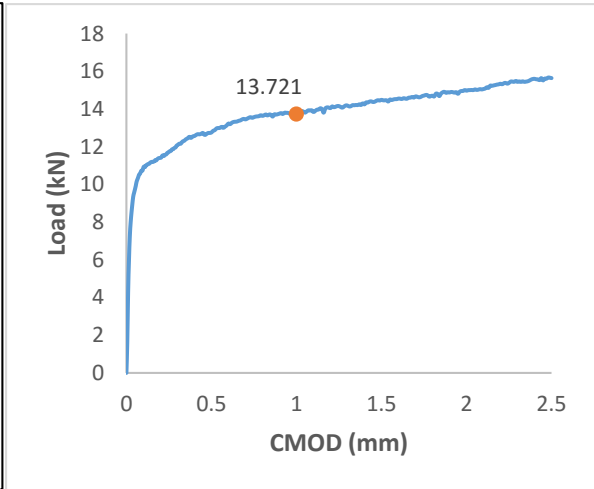
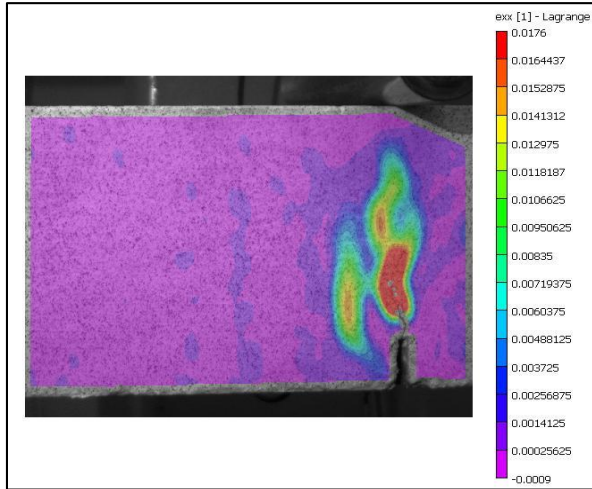
(a)



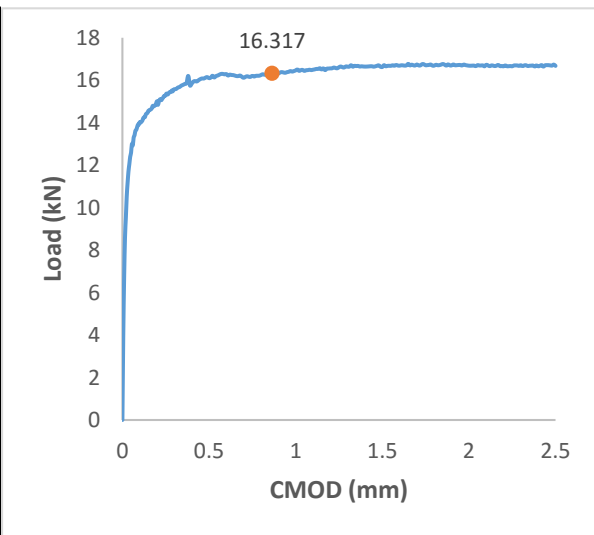
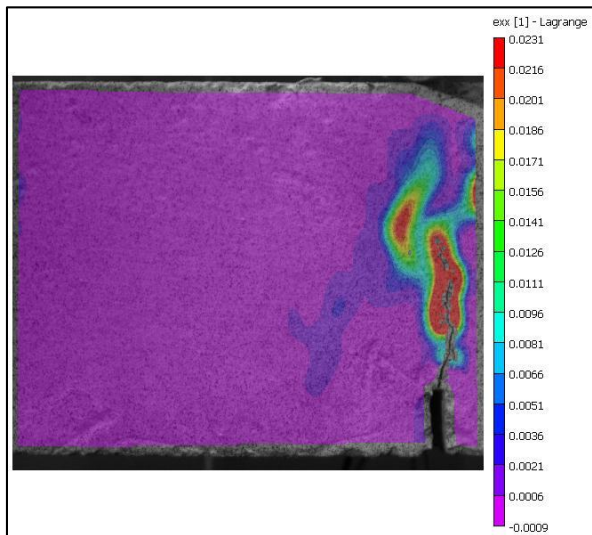
(b)



(c)



(d)





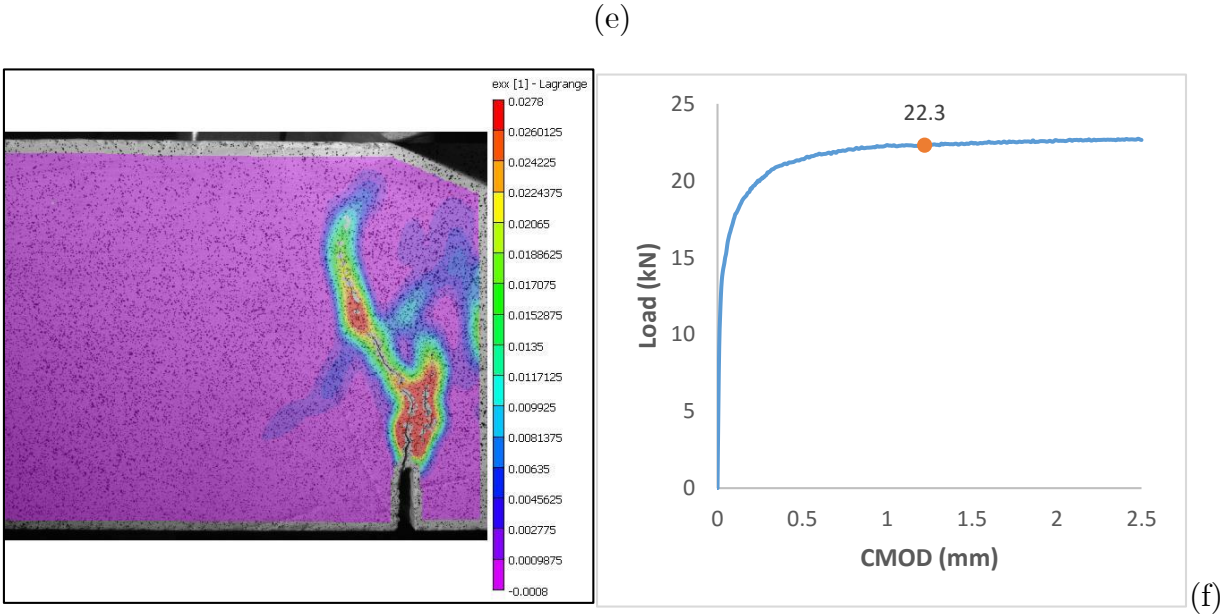


Fig 5. 2: The strain profile showing the multiple cracking of hybrid and steel FRC at 0.94% volume fraction and the load CMOD response; (a) Blend at 3 day (b) Blend at 7 day (c) Blend at 28 day (d) Steel FRC at 3 day (e) Steel FRC at 7 day (f) Steel FRC at 28 day

The variation in  $\epsilon_{xx}$  (strain) at different heights along the depth of the beam are analysed at distinct points in the load response for both control and various fiber reinforced concrete are analysed. Five locations at fixed heights above the notch were selected for evaluating the variation in the strains due to crack propagation. At each location the displacement and strain relative the centreline of the notch was evaluated to determine the variation as a function of depth. The location of the lines are given in Table 5.1 and shown in Figure 5.3. The variation in displacement,  $u$  and strain  $\epsilon_{xx}$  along line 1, located just above the notch at distinct point in the load response for control, steel, polypropylene and hybrid FRC at 0.5% and 0.94% volume fraction at 3, 7 and 28 days are shown in Figure 5.4 to Figure 5.22.

A region of finite length associated with very rapid increase in displacement is observed in the displacement profile along line 1. The region associated with the rapid gradient in displacement is broadly centred on the notch. Within this region, the displacements sharply rise above the linear trend with a gradual slope away from the

notch. The size of the region associated with the rapid increase in displacement remains relatively constant with increasing deflection of the beam.

Table 5.1 Location of Lines

Line No	Depth From Crack Tip (mm)
1	12.5
2	25
3	37.5
4	50
5	62.5

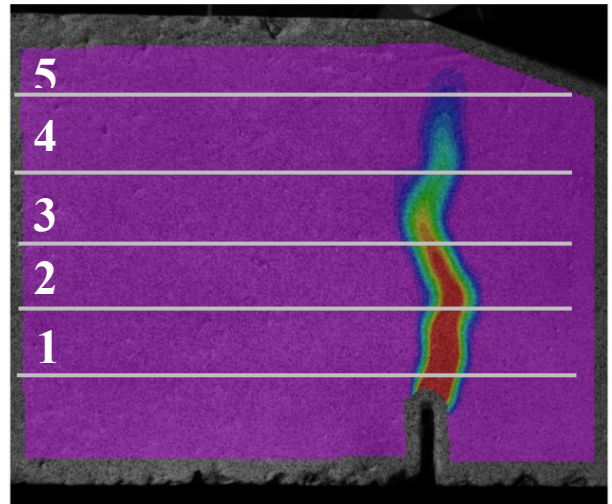


**Figure 5.3 Horizontal strips for strain computations**

The increase in strain along line 1 close to the notch is indicative of strain localization, which is centred over the notch. The strain localization is noticed over a finite width, along the line. The width associated with localization appears to remain constant during the immediate post peak softening load response following the peak load. This indicates that strains in a finite region close to the crack plane are influenced by the crack.

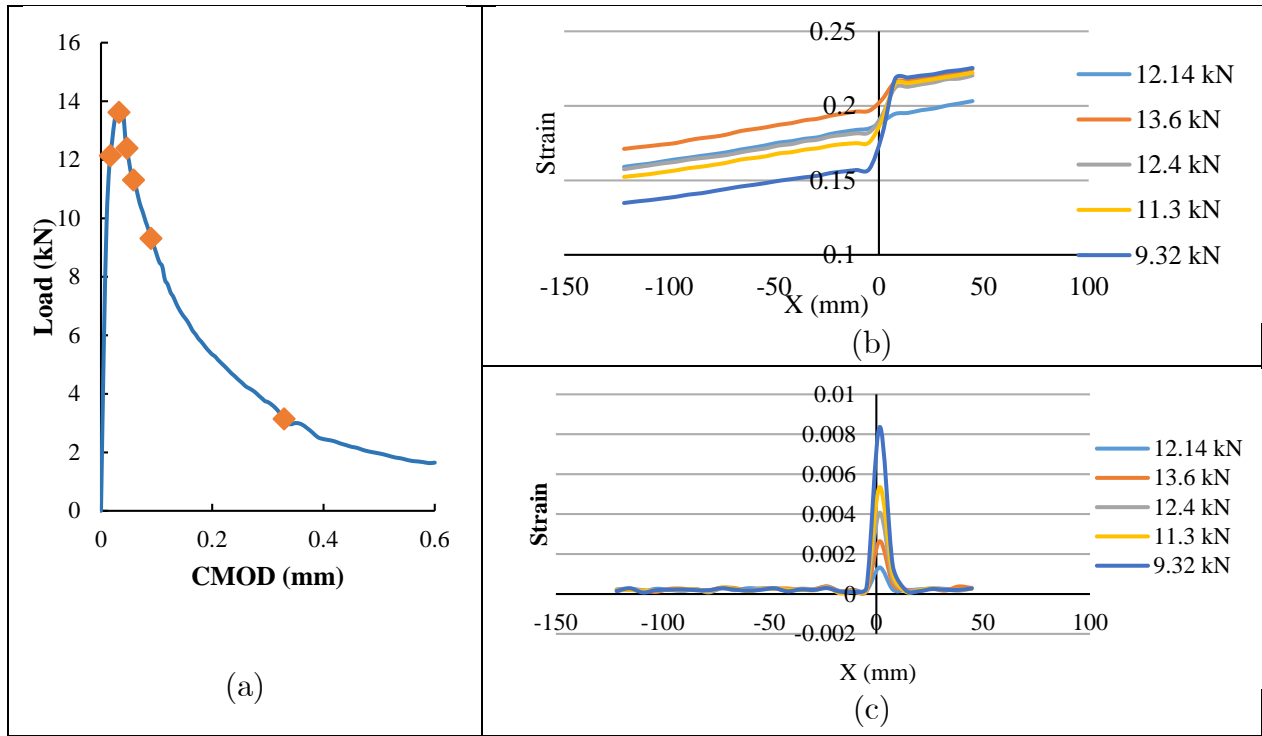


Fig 5.4: (a) Typical load response of control; (b) Displacement profile at line 1; (c) Strain profile at line 1 at distinct load points

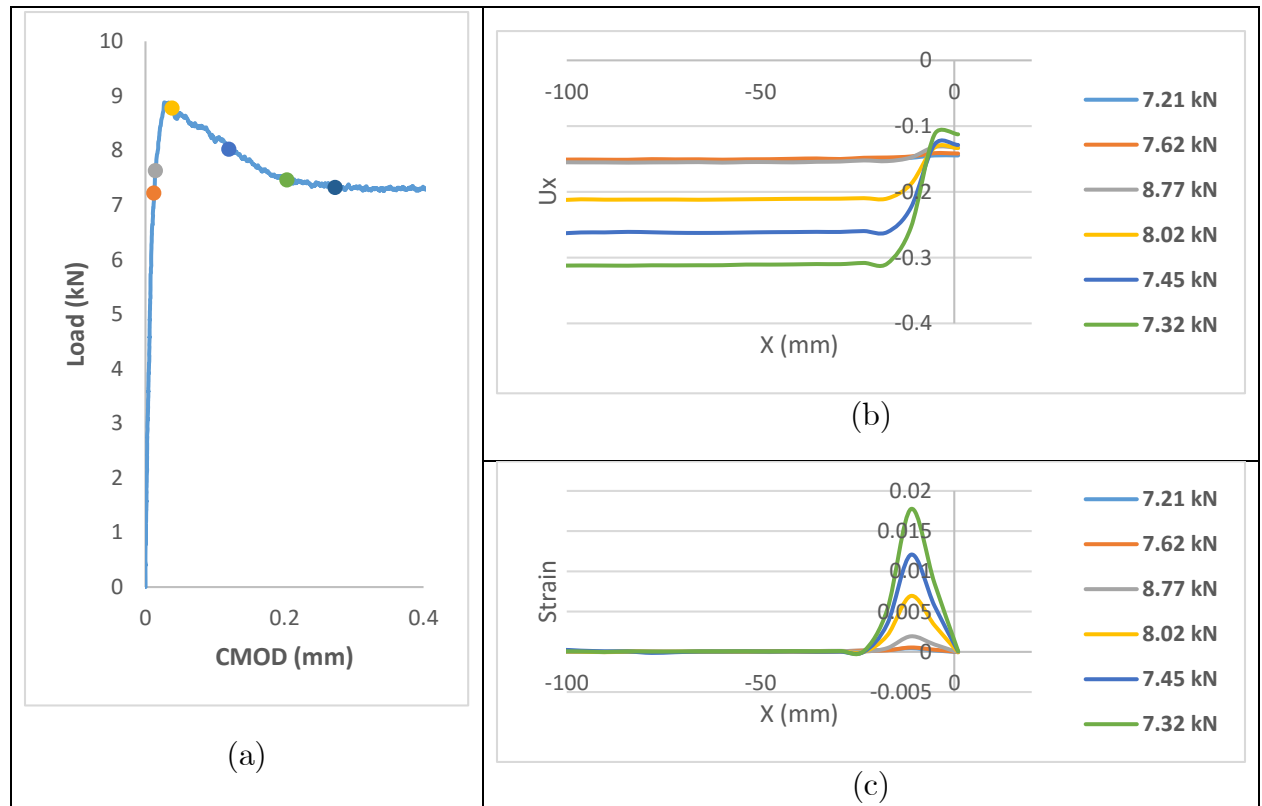


Fig 5.5: (a) Typical load response of 0.5% Hybrid FRC at 3 days; (b) Displacement profile at line 1; (c) Strain profile at line 1 at distinct load points

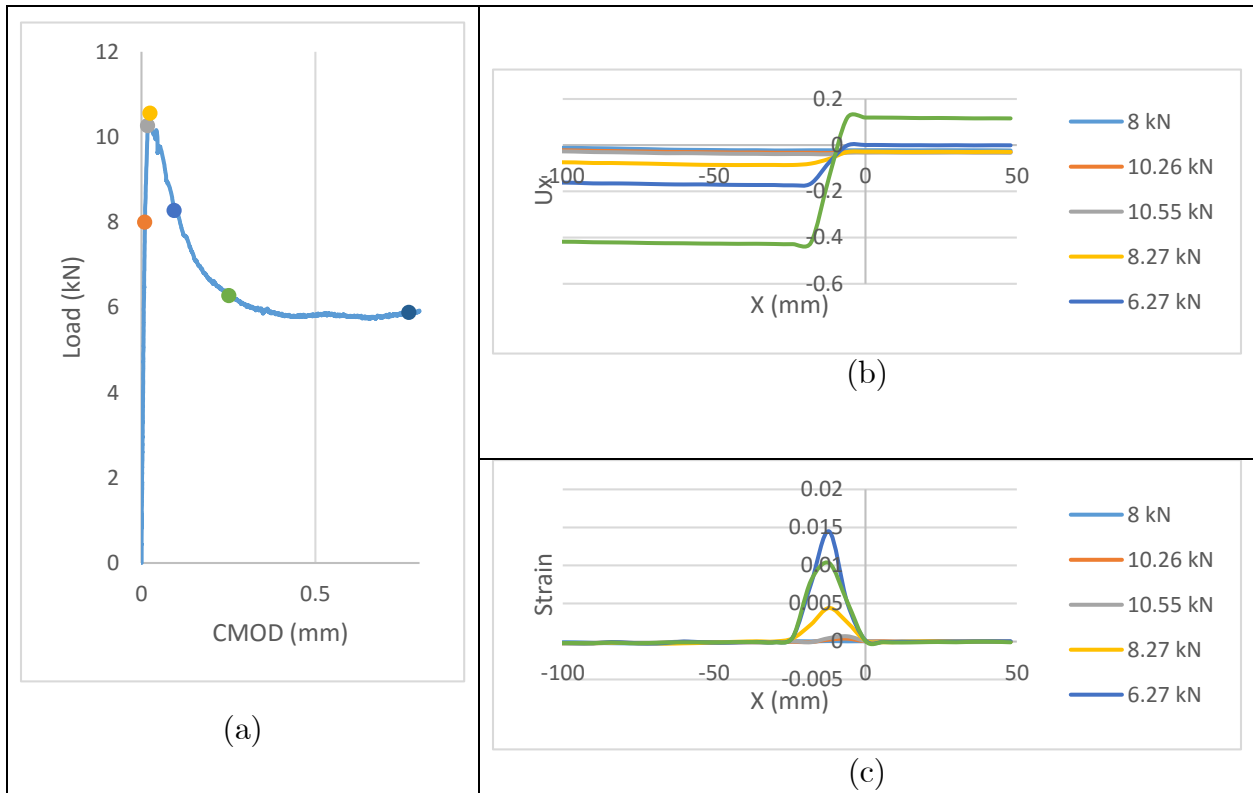


Fig 5.6: (a) Typical load response of 0.5% Hybrid FRC at 7 days; (b) Displacement profile at line 1; (c) Strain profile at line 1 at distinct load points

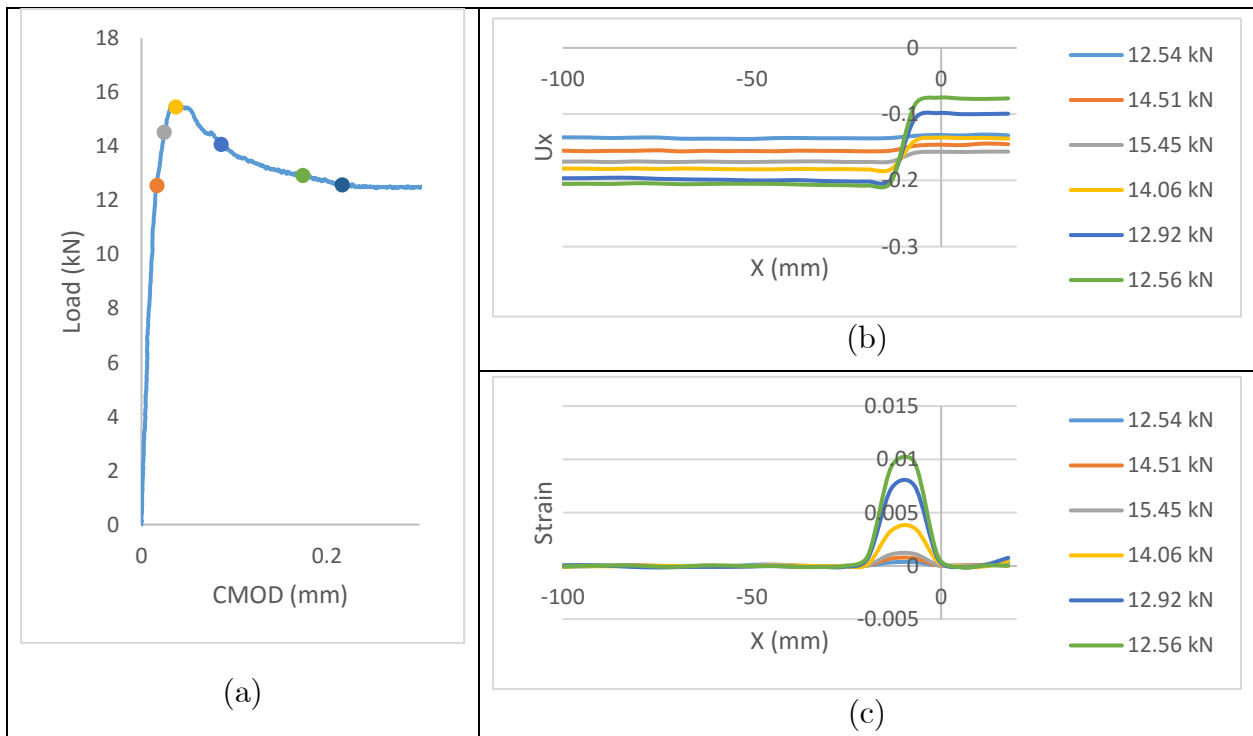


Fig 5.7: (a) Typical load response of 0.5% Hybrid FRC at 28 days; (b) Displacement profile at line 1; (c) Strain profile at line 1 at distinct load points

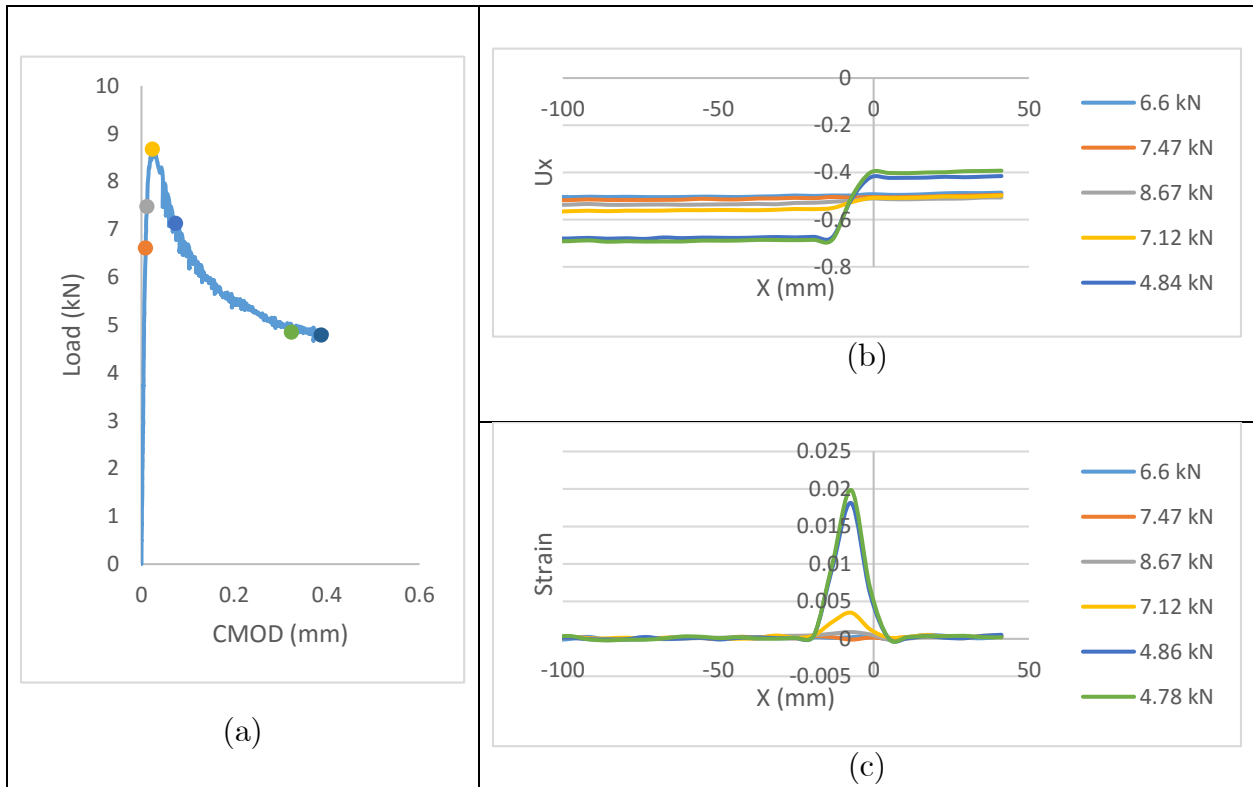


Fig 5.8: (a) Typical load response of 0.5% Polypropylene FRC at 3 days; (b) Displacement profile at line 1; (c) Strain profile at line 1 at distinct load points

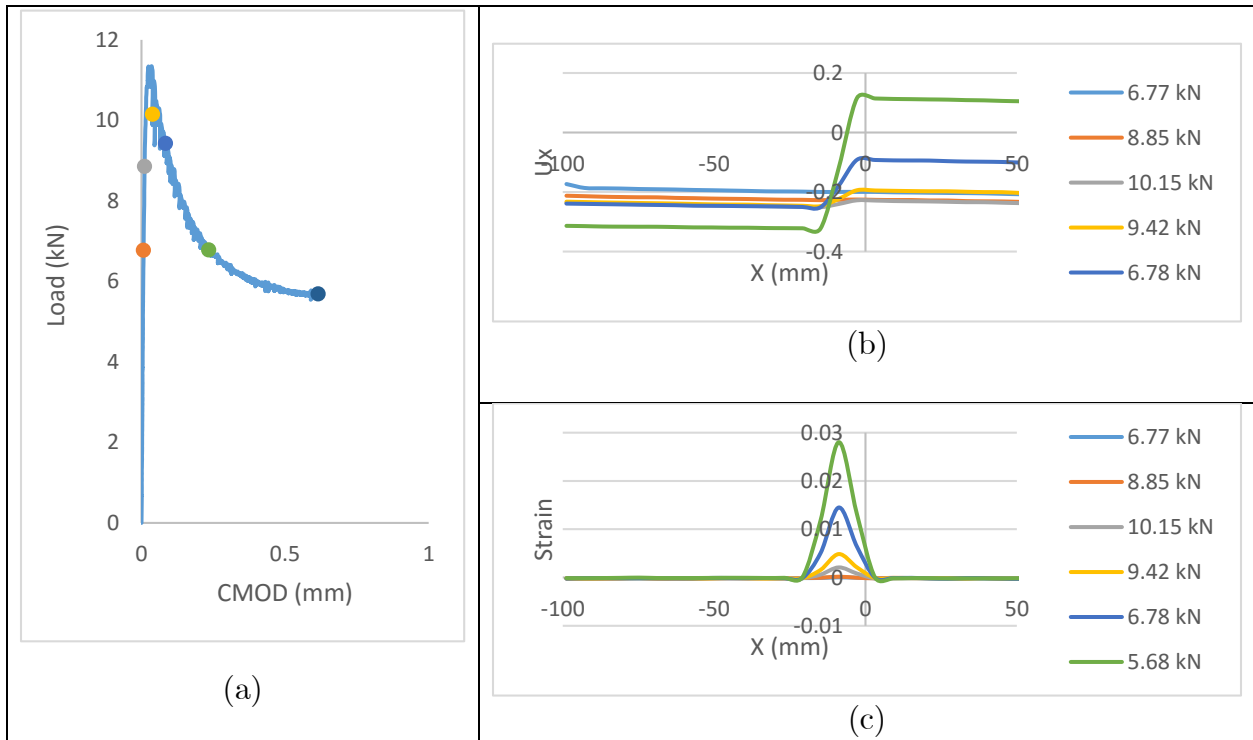


Fig 5.9: (a) Typical load response of 0.5% Polypropylene FRC at 7 days; (b) Displacement profile at line 1; (c) Strain profile at line 1 at distinct load points

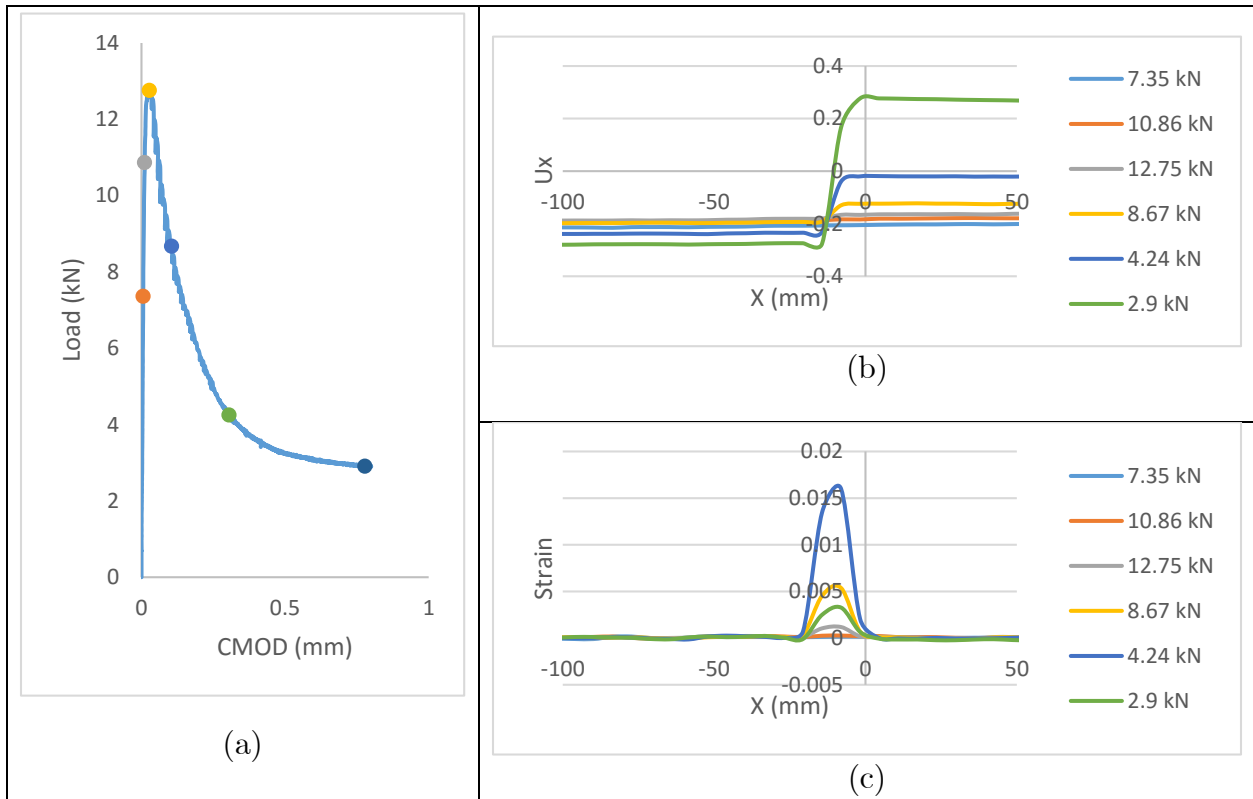


Fig 5.10: (a) Typical load response of 0.5% Polypropylene FRC at 28 days; (b) Displacement profile at line 1; (c) Strain profile at line 1 at distinct load points

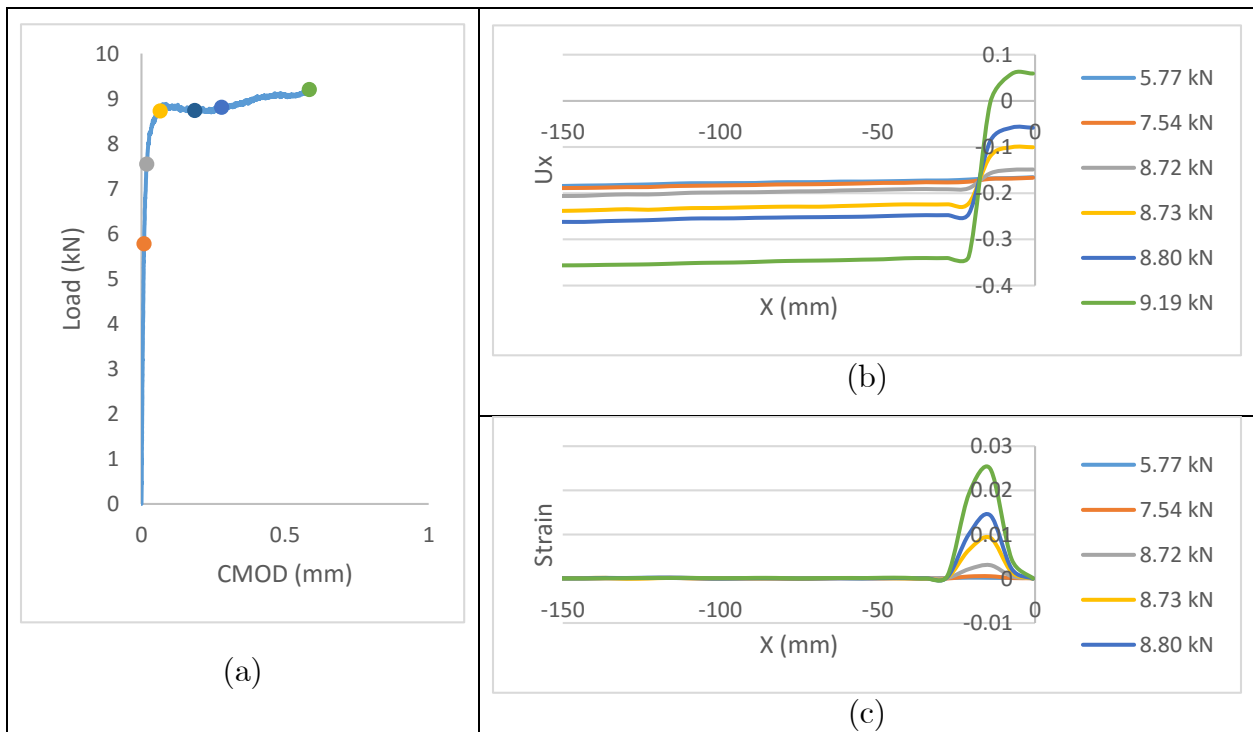


Fig 5.11: (a) Typical load response of 0.5% Steel FRC at 3 days; (b) Displacement profile at line 1; (c) Strain profile at line 1 at distinct load points

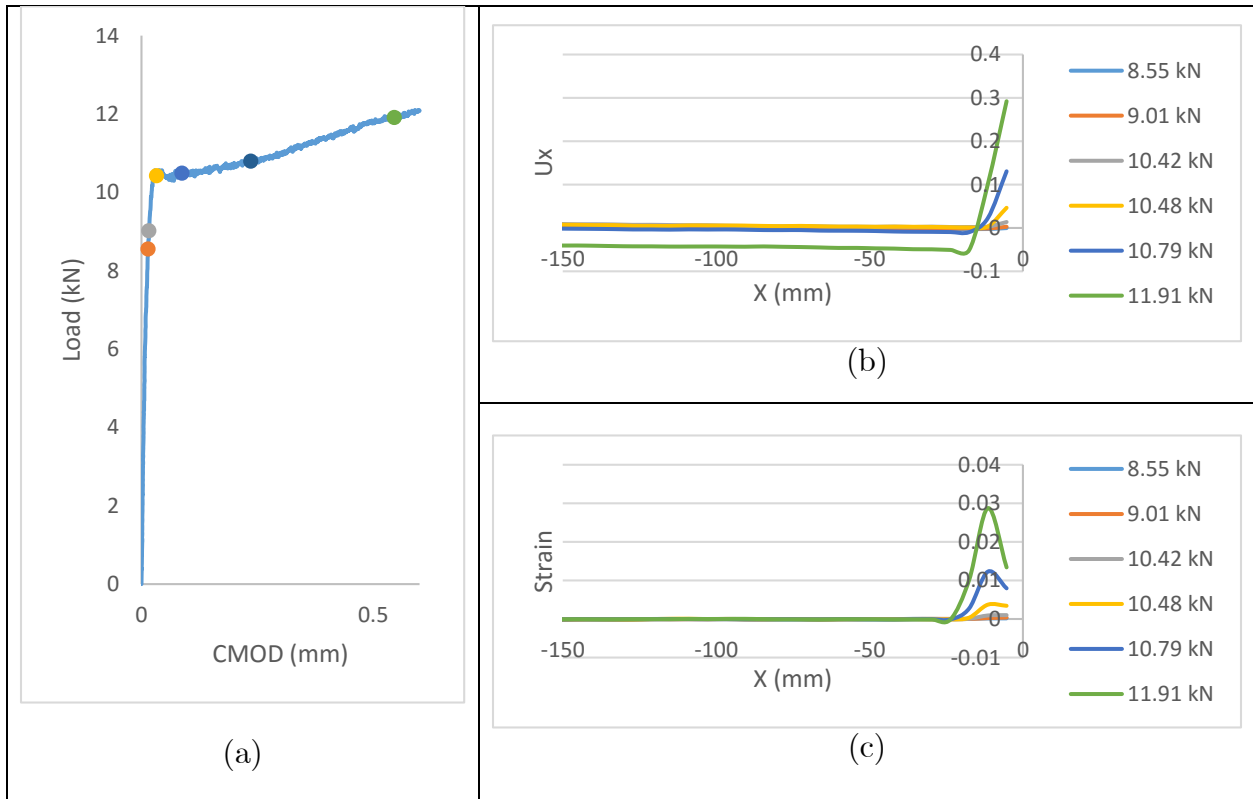


Fig 5.12: (a) Typical load response of 0.5% Steel FRC at 7 days; (b) Displacement profile at line 1; (c) Strain profile at line 1 at distinct load points

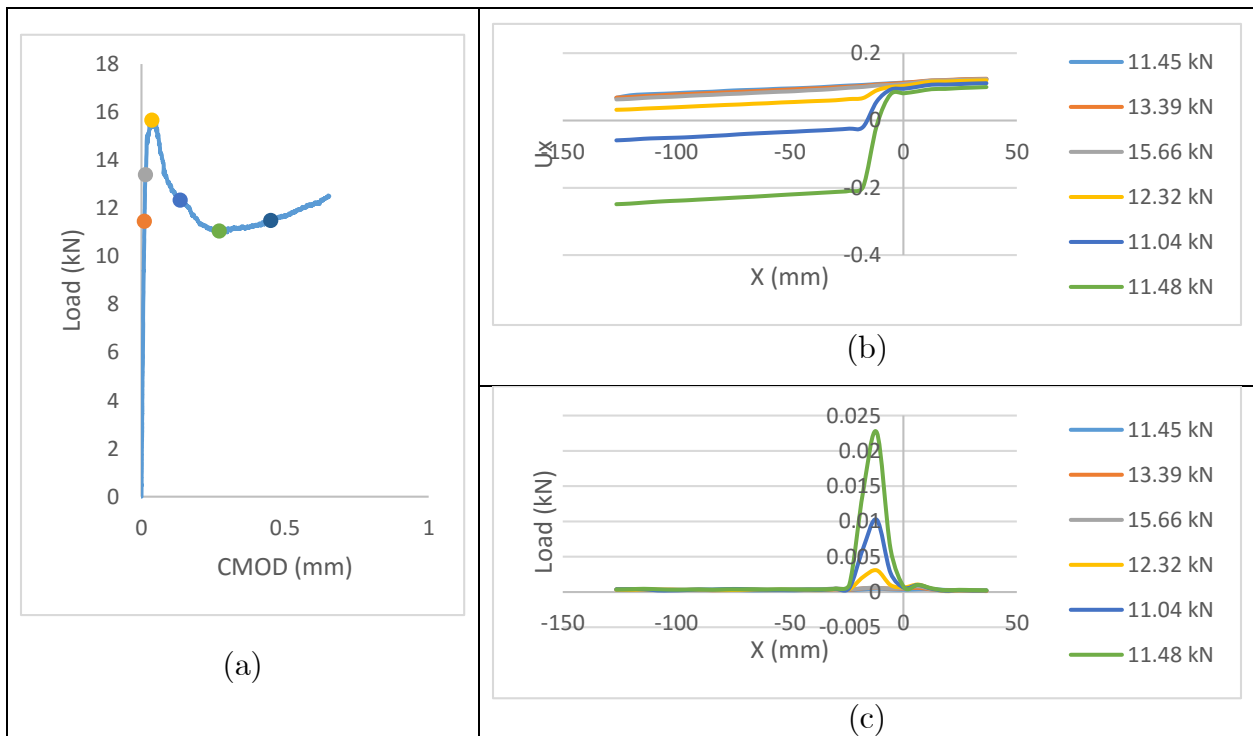


Fig 5.13: (a) Typical load response of 0.5% Steel FRC at 28 days; (b) Displacement profile at line 1; (c) Strain profile at line 1 at distinct load points

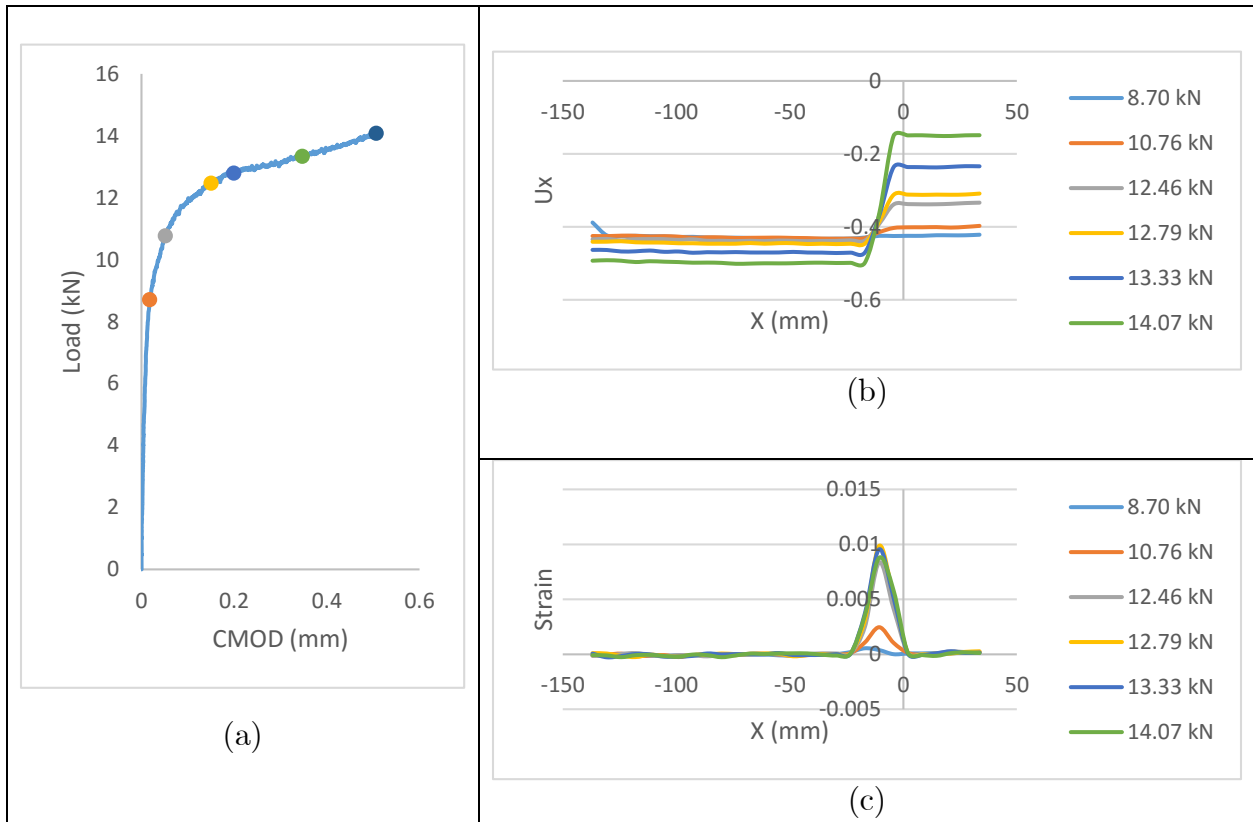


Fig 5.14: (a) Typical load response of 0.94% Hybrid FRC at 3 days; (b) Displacement profile at line 1; (c) Strain profile at line 1 at distinct load points

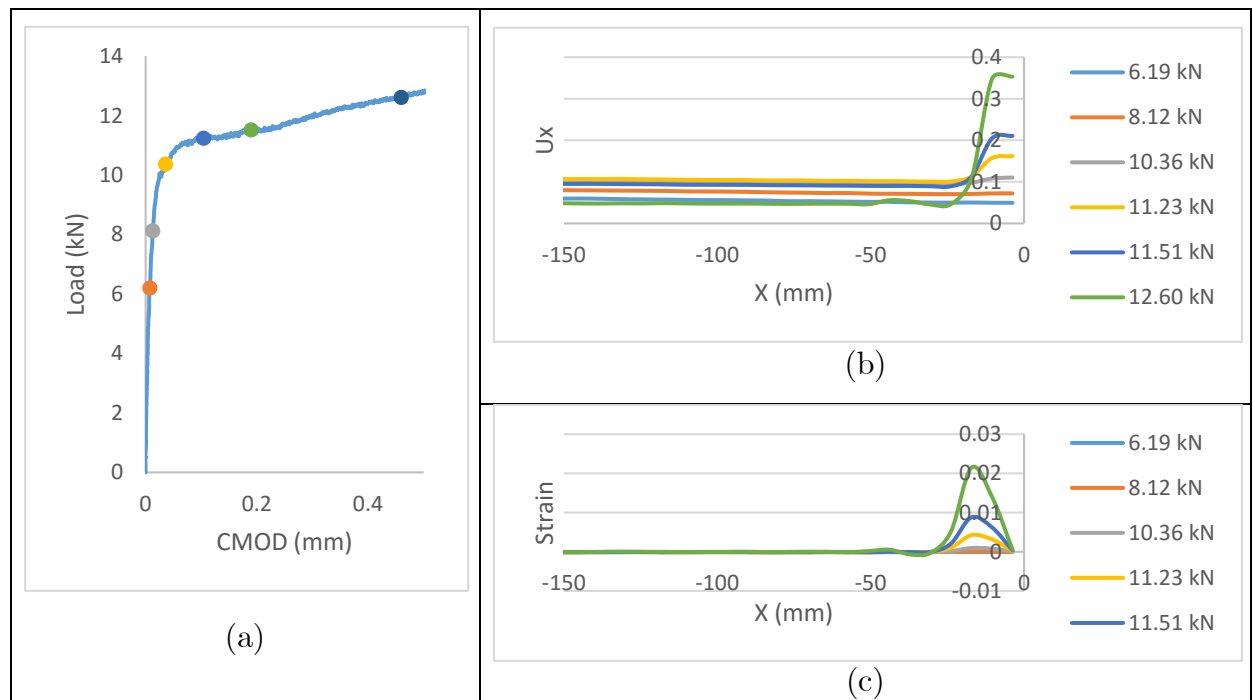


Fig 5.15: (a) Typical load response of 0.94% Hybrid FRC at 7 days; (b) Displacement profile at line 1; (c) Strain profile at line 1 at distinct load points



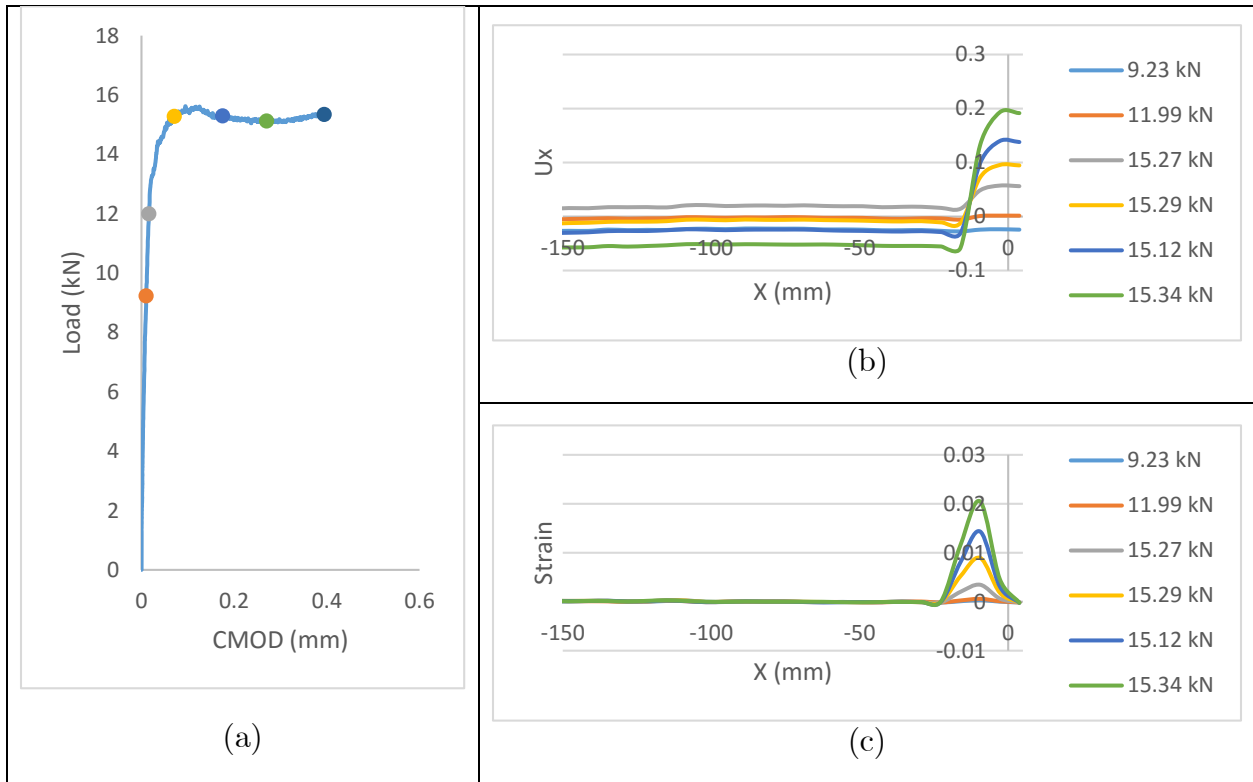


Fig 5.16: (a) Typical load response of 0.94% Hybrid FRC at 28 days; (b) Displacement profile at line 1; (c) Strain profile at line 1 at distinct load points

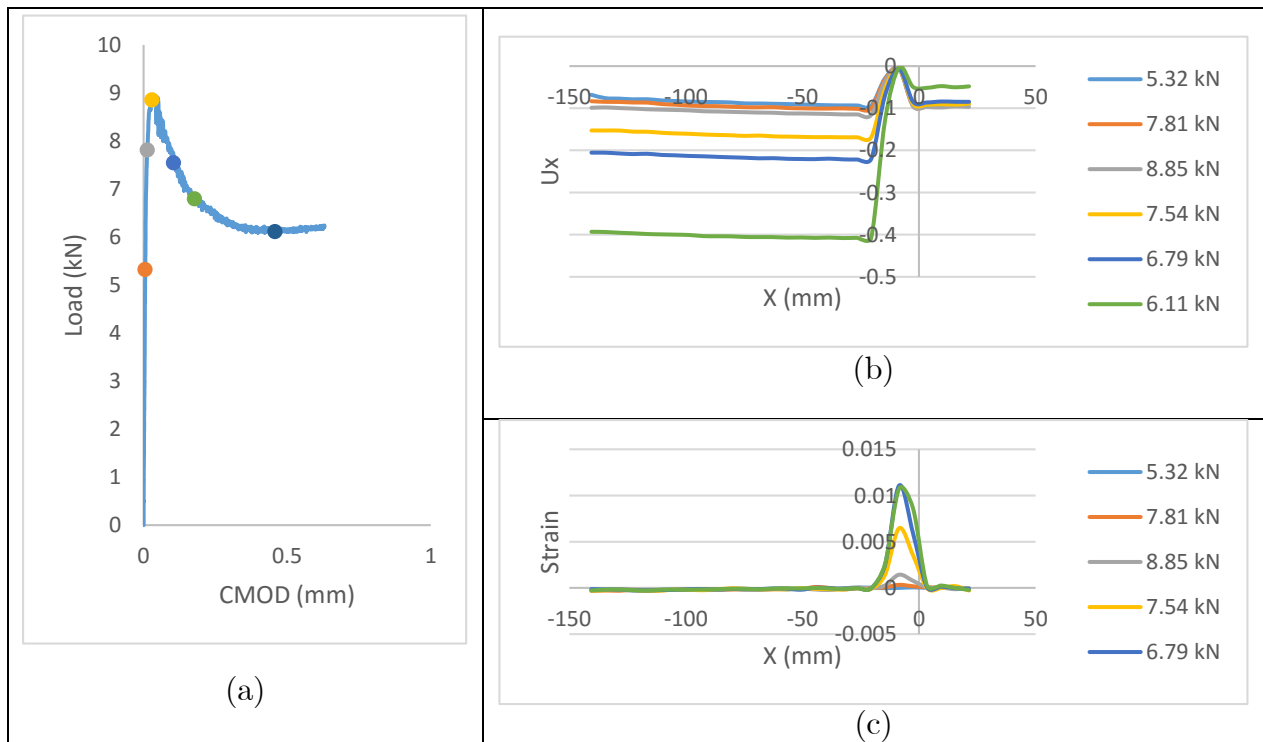


Fig 5.17: (a) Typical load response of 0.94% Polypropylene FRC at 3 days; (b) Displacement profile at line 1; (c) Strain profile at line 1 at distinct load points

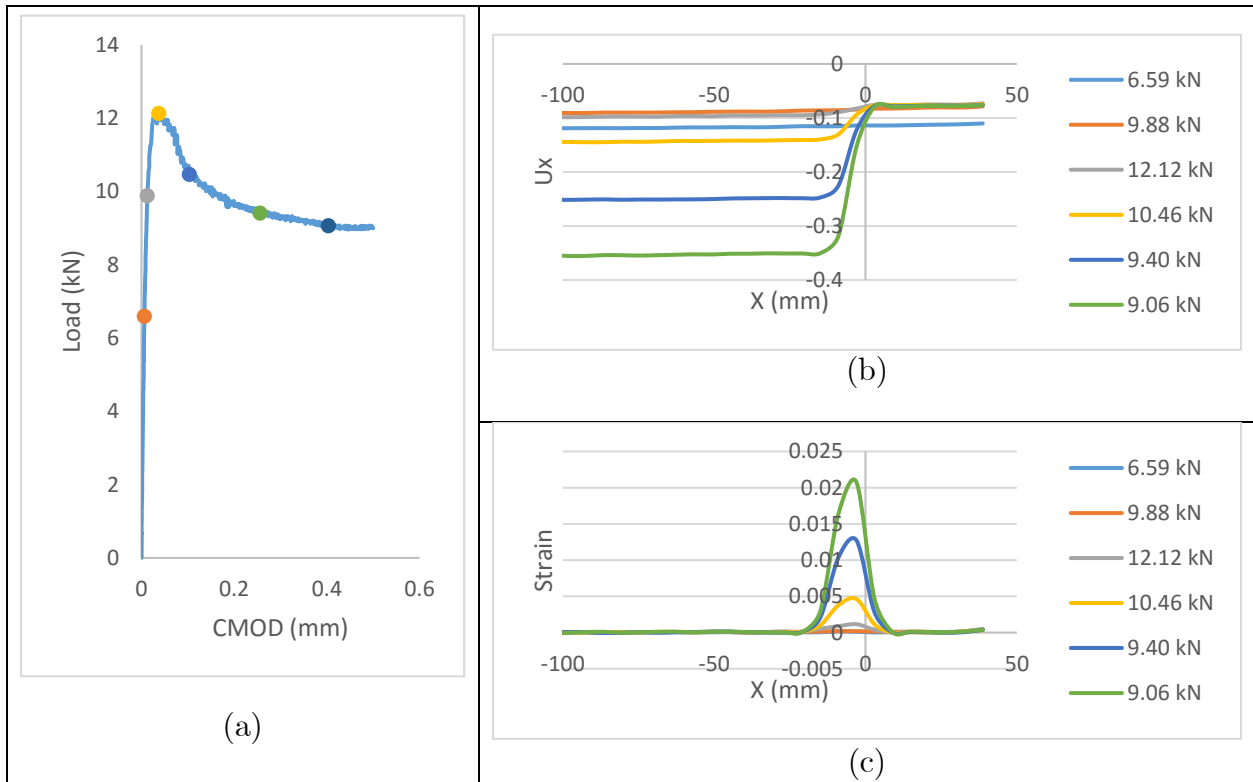


Fig 5.18: (a) Typical load response of 0.94% Polypropylene FRC at 7 days; (b) Displacement profile at line 1; (c) Strain profile at line 1 at distinct load points

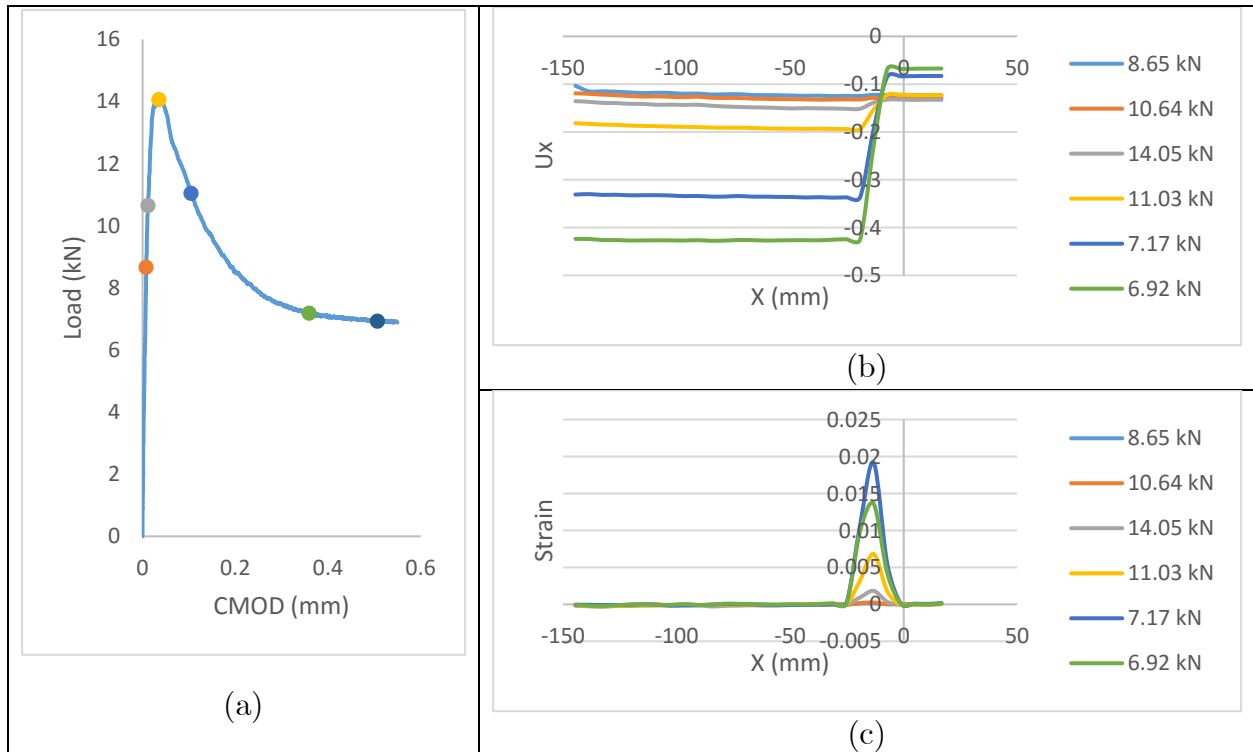


Fig 5.19: (a) Typical load response of 0.94% Polypropylene FRC at 28 days; (b) Displacement profile at line 1; (c) Strain profile at line 1 at distinct load points

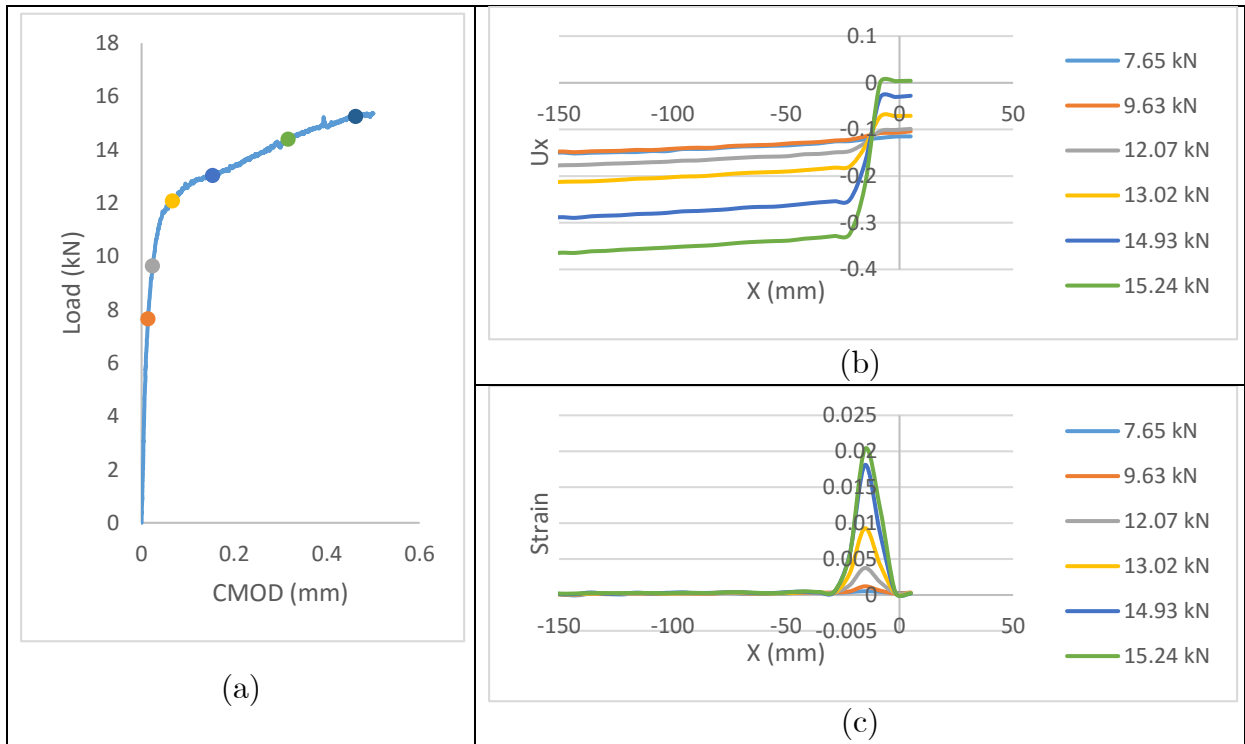


Fig 5.20: (a) Typical load response of 0.94% Steel FRC at 3 days; (b) Displacement profile at line 1; (c) Strain profile at line 1 at distinct load points

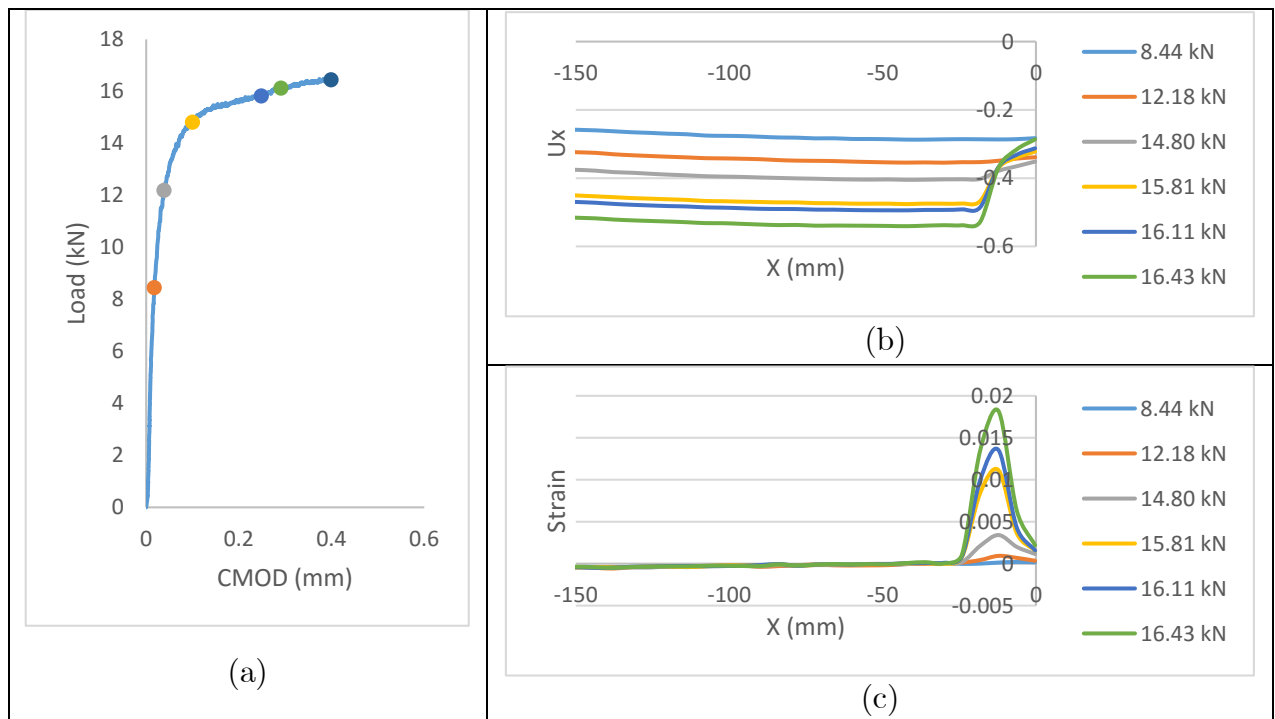


Fig 5.21: (a) Typical load response of 0.94% Steel FRC at 7 days; (b) Displacement profile at line 1; (c) Strain profile at line 1 at distinct load points

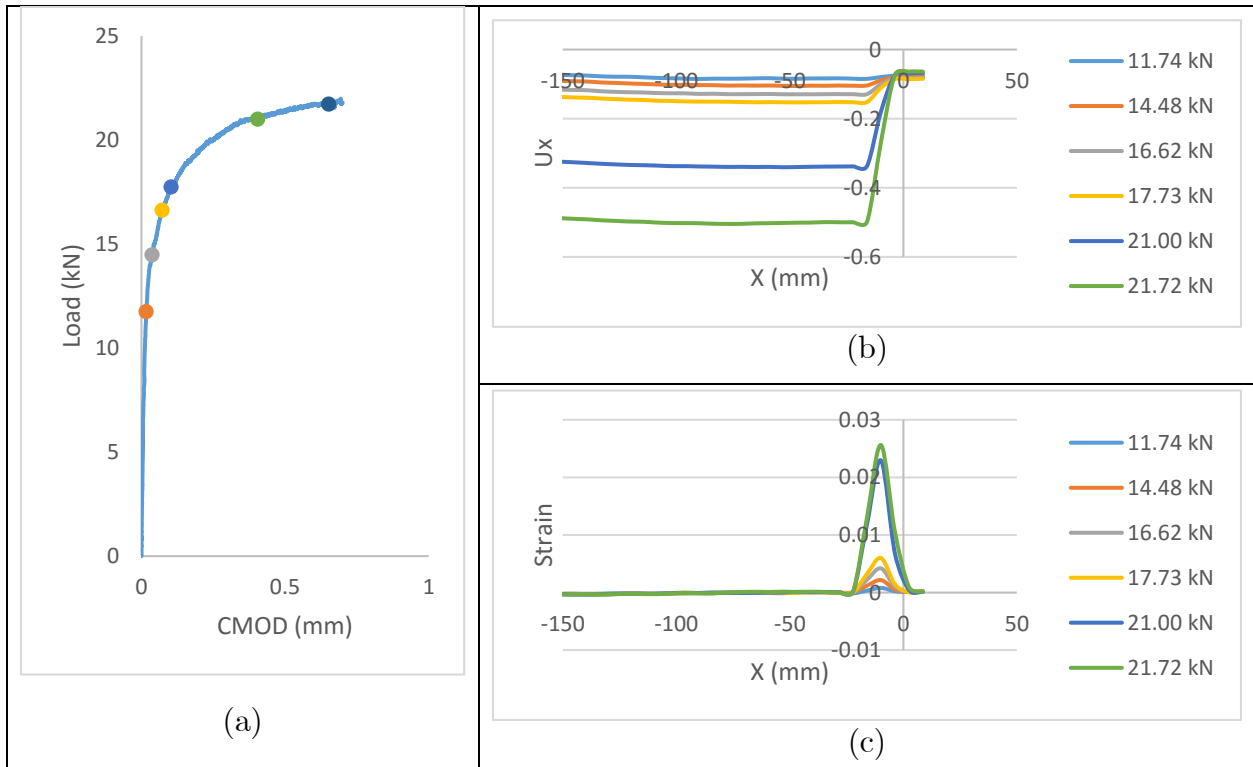
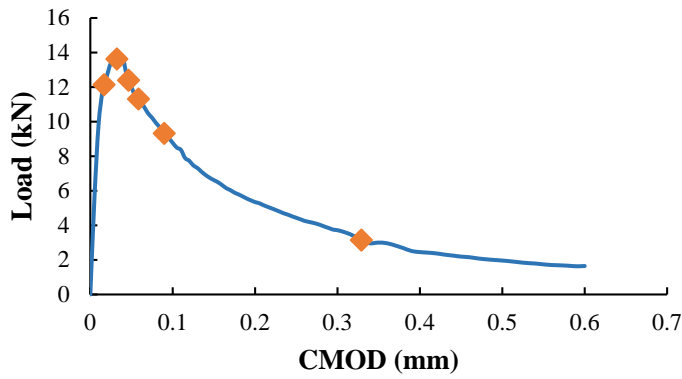


Fig 5.22: (a) Typical load response of 0.94% Steel FRC at 28 days; (b) Displacement profile at line 1; (c) Strain profile at line 1 at distinct load points

Typical result showing strain in the x direction ( $\epsilon_{xx}$ ) at five distinct point on the load response of specimen in the pre peak, close to the peak and in the post peak are shown in Figure 5.23 and 5.24 for 5 lines located at different depths relative to the notch. The respective loads are given in figure for control and hybrid FRC specimens with 0.5% volume fraction at 28 days. The distances of the lines above the bottom face of the beam are tabulated in the figure.

The extent of crack propagation and the strain profiles associated with the crack are nominally identical for the control and fiber reinforced concrete. The strains at line 5 even at load 5 are very small in magnitude and there is no indication of strain localization along the line. This suggests that the crack propagation in control and fiber reinforced concrete is nominally identical in the immediate post-peak associated with load drop after peak load.



Line No	Depth from Crack Tip (mm)
1	12.5
2	25
37.5	62.5
4	50
5	62.5

(a) Load CMOD of Control at 28 days

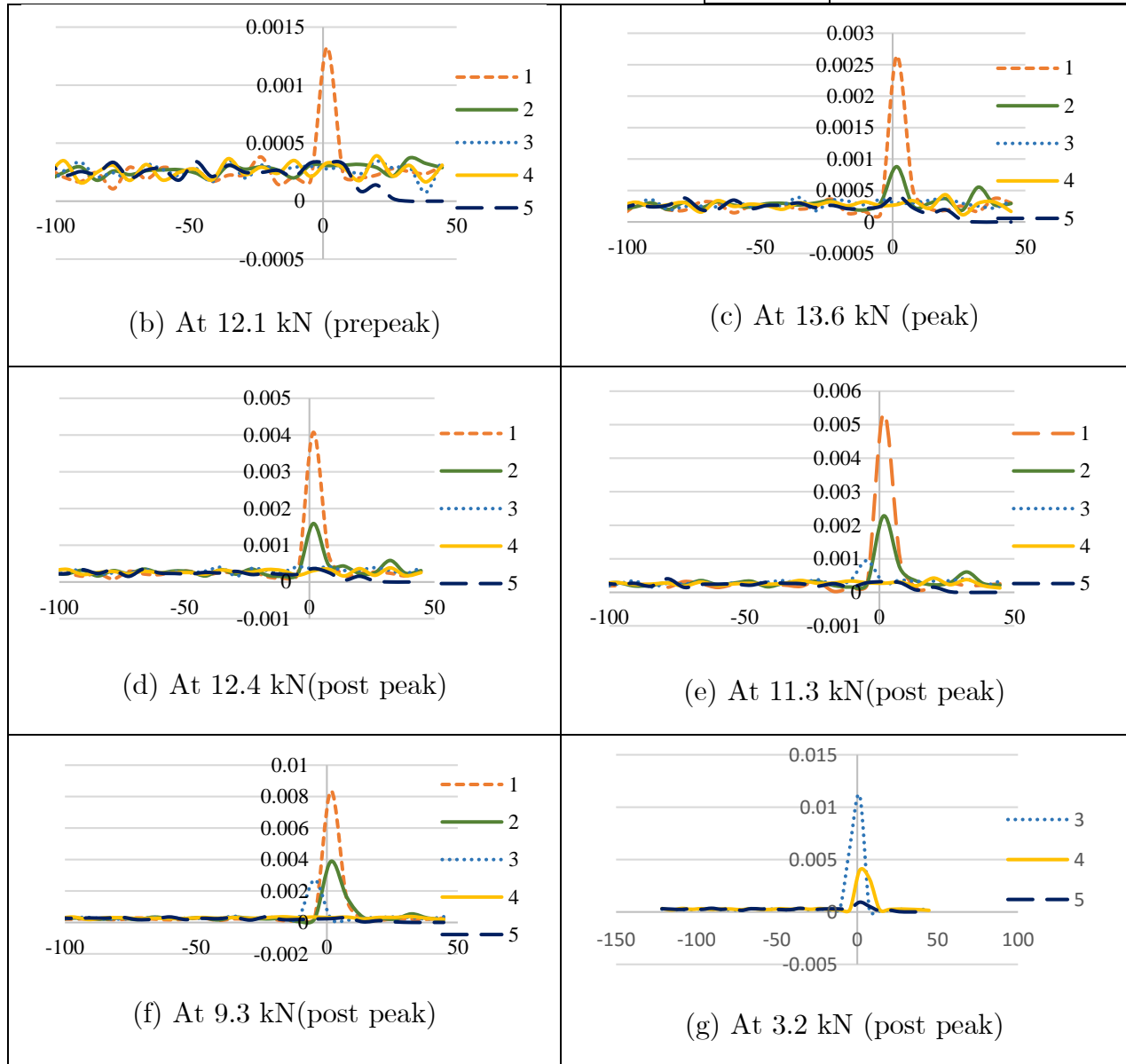
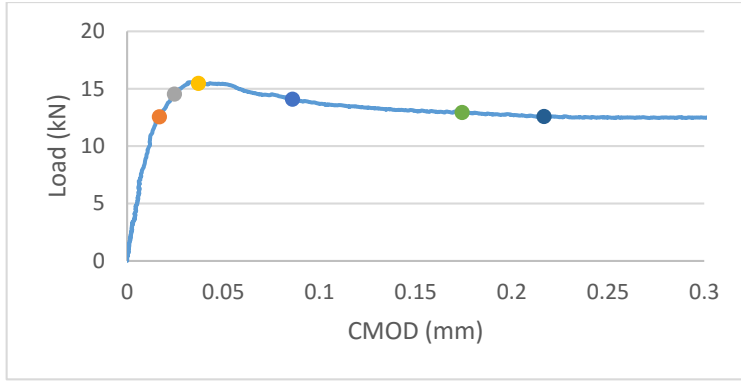
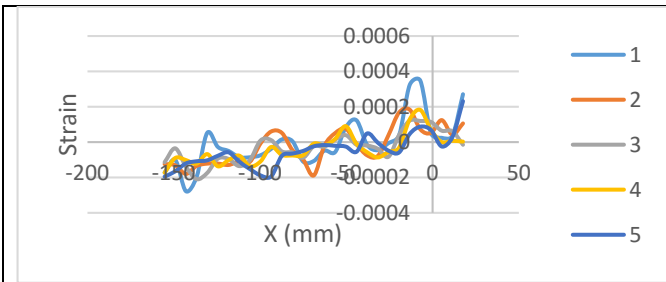


Fig 5.23 Variation of Strain value ( $\epsilon_{xx}$ ) on lines along the depth of section at distinct loads for control Specimen

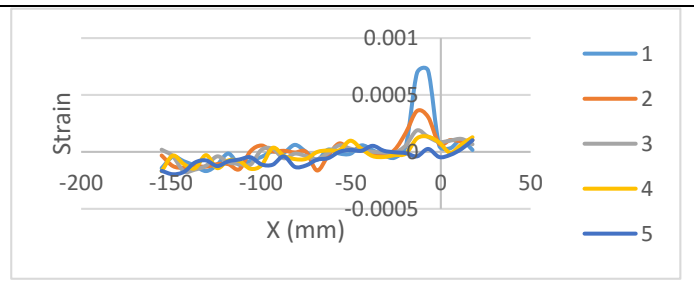


Line No	Depth from Crack Tip (mm)
1	12.5
2	25
3	37.5
4	50
5	62.5

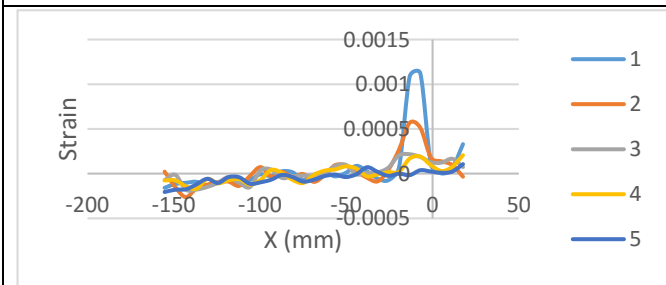
(a) Load CMOD of Hybrid FRC at 0.5% at 28 days.



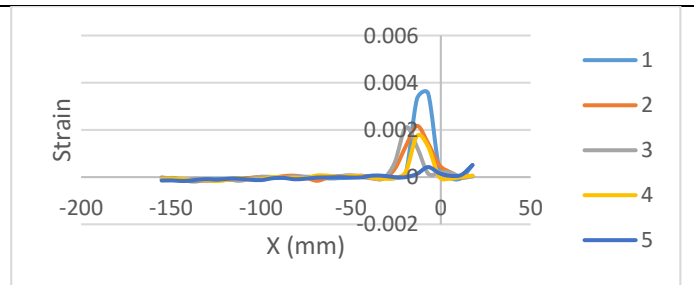
(b) At 12.54 kN (Pre peak)



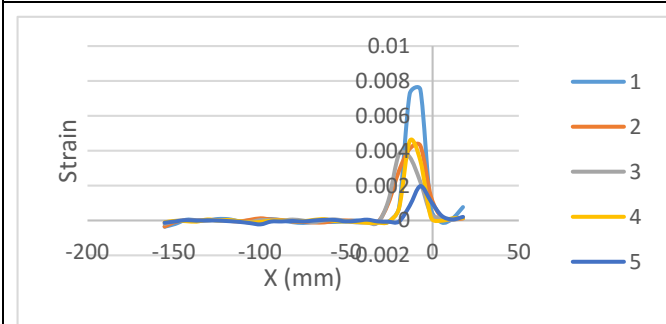
(c) At 14.51 kN (Pre peak)



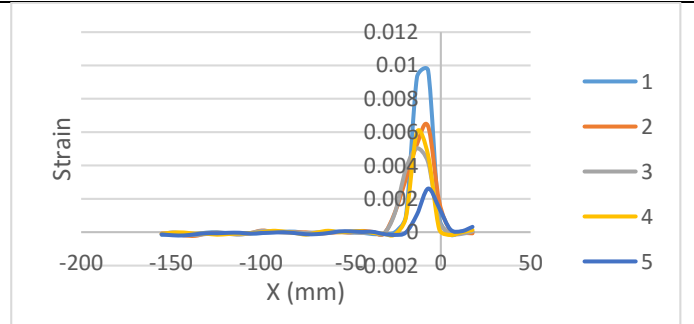
(d) At 15.45 kN (Peak)



(e) At 14.06 kN (Post peak)



(f) At 12.92 kN (Post peak)



(g) At 12.56 kN (Post peak)

Fig 5.23 Variation of Strain value ( $\epsilon_{xx}$ ) on lines along the depth of section at distinct loads for Hybrid FRC with 0.5% volume fraction at 28 days.

#### 5.4 Analysis of results

An analysis of the influence of fibers on providing control of crack opening as the crack propagates into the matrix was performed by combining the results from DIC with the measured crack tip opening displacement (CTOD) obtained from a surface mounted gage at the tip of the notch. The depth of crack at any load was established from an analysis of  $\epsilon_{xx}$  along horizontal lines located at different heights above the notch. The contribution of fibers result in the load arrest after an initial load drop in the immediate post-peak response. The increase in the total tensile resistance can be attributed to the increased resistance provided by additional fibers across the crack face with an increase in crack length and the additional stress due to increased resistance to crack opening displacement. The resistance to crack opening comes from either pull out of the fiber from the matrix or fiber extension which could ultimately lead to fiber fracture.

Examination of the failed surface revealed polypropylene fibers exhibited breakage in addition to fibers pulled out from the matrix while the steel fibers generally exhibited pull out from the matrix. The post-peak load response at the different volume fractions is associated with both breakage and pullout response of fibers from the concrete matrix averaged over the crack. During crack propagation, debonding and sliding contribute significantly to the pull out resistance of the fibers and hence to the total energy consumption when a large crack develops in the matrix. Fiber breakage is also observed to contribute to the energy dissipated during crack propagation.

#### 5.5 Summary and Findings

The results of the experimental investigation reveals once the matrix has cracked, initial part of the load response is controlled by crack propagation. Multiple cracking was

observed in case of hybrid and steel FRC at a higher volume fraction of 0.94%. And this behaviour at observed at all ages i.e. 3, 7 and 28 days.



# Chapter 6

## Analytical Model

### 6.1 Introduction

The bending failure of concrete beams may be modeled by the development of a fictitious crack in an elastic layer with a thickness proportional to the beam depth. A brief review about use of various types of stress crack opening ( $\sigma$ - $w$ ) relationship was presented in section 2.2. The cracked hinge model proposed by Olesen [57] was used for development of analytical model. The basic idea of the cracked hinge is to model a part of the beam close to the propagating crack as a layer of independent spring elements. These spring elements are formed by incremental horizontal strips, and are attached at each end to a rigid boundary (Figure 6.1). In this way the disturbance of the strain field, caused by the presence of the crack, is confined to take place between the rigid boundaries. Each rigid boundary may translate and rotate such that it may be joined with an uncracked beam modeled according to the classical beam theory. The constitutive relation of the spring layer is the same as that of the FRC, and according to the fictitious crack method, given by

$$\sigma = \begin{cases} E\varepsilon & \text{Precrack State } (w = 0) \\ \sigma_w(w) = g(w) * f_t & \text{cracked State } (w > 0) \end{cases}$$

where  $E$  = elastic modulus;  $\varepsilon$  = elastic strain;  $\sigma_w(w)$  denotes the stress-crack opening relationship; and  $f_t$  = uniaxial tensile strength. The shape of the stress-crack opening relationship is defined by some function  $g(w)$  of the crack opening  $w$ , normalized such that  $g(0)=1$ .

For FRC materials the stress crack open relationship is rather complex. It depends on amount, type of fibers, and age of matrix and pullout of fibers. The hinge model by Olesen starts by adopting a nonlinear hinge with finite length ' $s$ ' usually a factor of depth as shown in Figure 6.1 within which the stress transfer through fibers is assumed to be taking place.

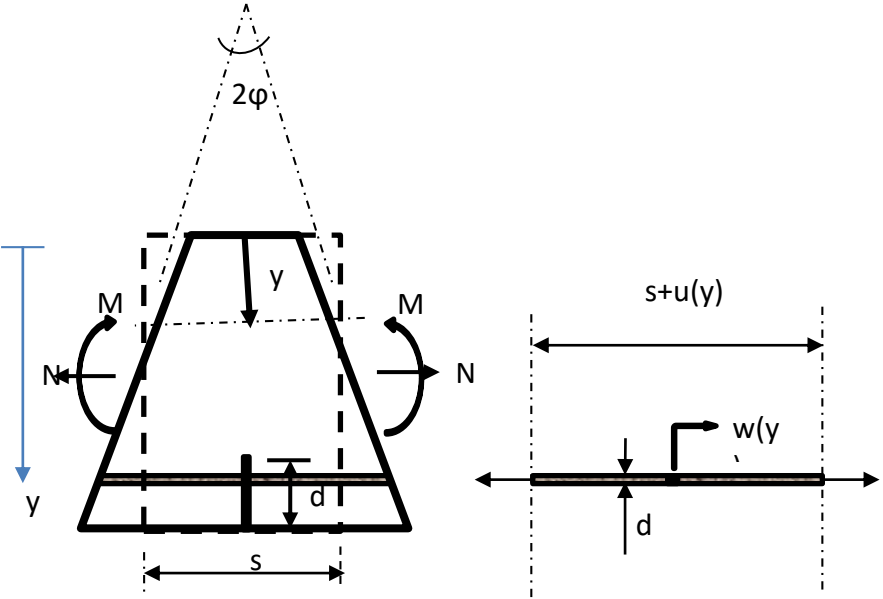


Fig 6.1 Geometry, Loading, and Deformation of Cracked Incremental Horizontal Strip of Hinge

The deformation of the hinge is described by half the angular deformation and the depth of the neutral incremental strip  $y_0$ . It proves convenient to introduce the mean

values of the curvature and the distribution of longitudinal strains  $\kappa^*$  and  $\varepsilon^*$ , respectively given by

$$\kappa^* = 2\phi/s \text{ and } \varepsilon^*(y) = (y-y_0) \kappa^*. \quad (5.1)$$

The deformation of an incremental strip is given by  $u(y) = s\varepsilon^*(y)$ , in the case where the strip has cracked the deformation,  $u(y)$  may also be obtained as the sum of the elastic deformation of the strip and the crack opening

$$u(y) = s\varepsilon^*(y) = s \frac{\sigma_w(w(y))}{E} + w(y) \quad (5.2)$$

From the equations 5.1 and 5.2 it can be written as

$$\sigma_w(w(y)) = (2(y - y_0)\phi - w(y)) \frac{E}{s} \quad (5.3)$$

The bilinear stress crack model assumed by Olesen is shown in Figure 6.2 and the shape of the stress-crack opening relationship is defined by some function  $g(w)$  of the crack opening  $w$  with slopes of lines and their offsets on ordinate axis which represent normalised tensile strength.

$$g(w) = b_i - a_i w = \begin{cases} b_1 - a_1 w & 0 \leq w < w_1 \\ b_2 - a_2 w & w_1 \leq w \leq w_2 \end{cases} \quad (5.4)$$

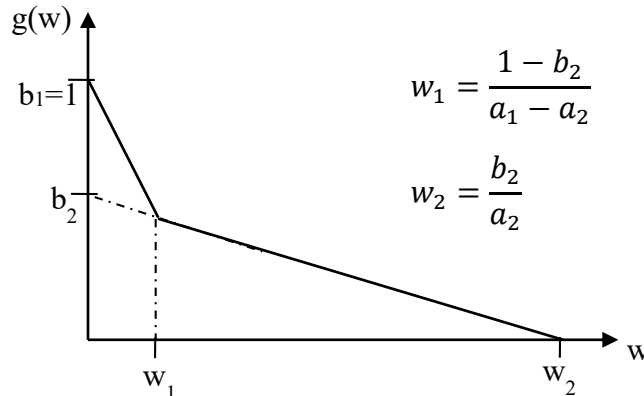


**Fig 6.2 Definition of Parameters of Bilinear Stress-Crack opening relationship**

From equation 5.3 and 5.4  $w(y)$  and  $\sigma_w(w(y))$  for each value of  $i$ , the following solutions are obtained:

$$w(y) = \frac{2(y-y_0)\varphi-\zeta_i}{1-\beta_i} \quad (5.5a)$$

$$\sigma_w(w(y)) = \frac{\zeta_i-2(y-y_0)\varphi\beta_i E}{1-\beta_i} \frac{1}{s} \quad (5.5b)$$

where

$$\beta_i = \frac{f_t a_i s}{E}; \quad \zeta_i = \frac{f_t b_i s}{E} \quad i \in 1,2$$

The solutions given in (5.5) establish in analytical form the crack opening profile  $w(y)$  and the stress distribution in the cracked part of the hinge  $\sigma_w(w(y))$  as functions of the hinge deformations  $w$  and  $y_0$ . As the crack propagates from the bottom of the hinge, the Stress distribution changes through three distinct phases (Figure 6.3). The crack-opening profile is divided into different intervals of  $i$ .

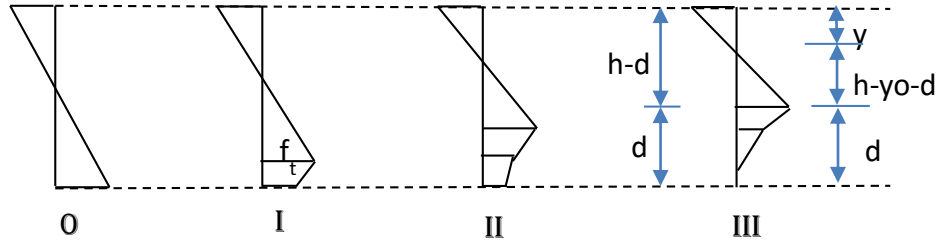


Fig 6.3 Distinct Phases of Stress Distribution during propagation of the crack in the section

Now complete stress distribution for all phases of pre and post cracking was established where phase 0 representing pre crack stress state and others post crack stress states. Now by equating sectional stresses with external applied force N, a relation between moment and curvature was established in the form of closed form equations. To make the derivation simple, following normalisation were introduced.

$$\mu = \frac{6M}{f_t h^2 t} \quad \rho = \frac{N}{f_t h t} \quad \theta = \frac{hE}{s f_t} \varphi \quad \alpha = \frac{d}{h} \quad (5.6 \text{ a-d})$$

The explicit equations for moment rotation with derivations are given in annexure I.

## 6.2 Load deflection curve from moment curvature analysis

Load-deflection curve can be calculated from given moment rotation relationship. Consider a beam with rectangular cross-section with depth h, width t and span L. The span of the beam is divided into three parts with a centre nonlinear hinge and elastic beam on the either side of the hinge as shown in Figure 6.4. The deflection  $v$  is calculated as a sum of elastic deflection and crack deflection (i.e.  $v = v_e + v_c$ .)

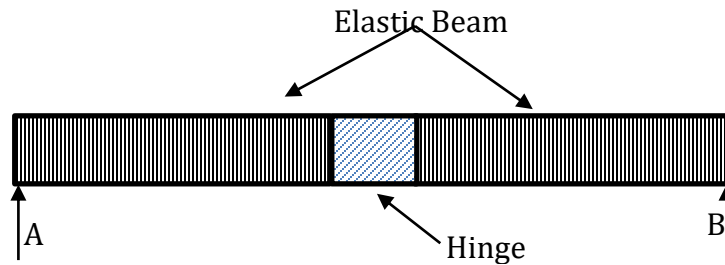


Fig 6.4 Model representation of simply supported beam after cracking

As per classical beam theory, the elastic deflection  $v_e$  is given by equation 5.7 (a) and deflection from the nonlinear hinge can be considered as rigid body rotation and is given by equation 5.7(b) but the hinge deflection is sum of deflection due to crack and elastic deformation of hinge, hence to get deflection from crack only elastic deformation should be subtracted from hinge deflection and is given by equation 5.7(c)

$$v_e = \begin{cases} \frac{ML^2}{12EI} & \text{for centre point loading} \\ \frac{ML^2}{9EI} & \text{for third point loading} \end{cases} \quad (5.7a)$$

$$v_h = \phi * L/2 \quad \text{and} \quad (5.7b)$$

$$\phi_c = \phi - \phi_e \text{ where} \quad (5.7c)$$

Equation (5.7) upon normalisation as shown in Eq (5.8a) the normalised elastic deflection and crack deflection is be given by equations 5.8b and 5.8c

$$\delta = \frac{2\nu hE}{L s f_t} = \frac{2\nu \theta}{L \phi} = \delta_e + \delta_c \quad (5.8a)$$

$$\delta_e = \begin{cases} \frac{L}{3s} \mu(\theta) & \text{for centre point loading} \\ \frac{4L}{9s} \mu(\theta) & \text{for third point loading} \end{cases} \quad (5.8b)$$

$$(5.8c)$$

$$\delta_c = \theta_c = \theta - \mu(\theta)$$

Total deflection is then given by

$$\delta = \delta_c + \delta_e = \begin{cases} \theta + \left(\frac{L}{3s} - 1\right) \mu(\theta) & \text{for centre point loading} \\ \theta + \left(\frac{4L}{9s} - 1\right) \mu(\theta) & \text{for third point loading} \end{cases} \quad (5.9)$$

Load is calculated for the given loading type from the known moment from equation

$$P(\theta) = \begin{cases} \frac{2}{3} \frac{f_t h^2 t}{L} \mu(\theta) & \text{Centre point loading} \\ \frac{f_t h^2 t}{L} \mu(\theta) & \text{Third point loading} \end{cases} \quad (5.10)$$

The load deflection curve obtained for a beam with adopted parameters (indicated in plot) is shown in figure 5.2.2.

### 6.3 Proposed Analytical Formulation for multi-linear softening

In order to capture the load recovery and a second peak (or subsequent peak points) after initial post-peak softening, a multi linear stress crack opening is required. Unlike the

bi-linear case, the multi-linear stress crack opening relationship may not be readily amenable to deriving closed form solutions. In order to simplify the algorithm, the formulation and definition of stress crack opening relationship has been modified keeping the background mechanism and assumptions identical to the Olesen model. Multi linear Stress crack opening relationship can be described with coordinates as shown in Figure 6.5, where  $b$  axis is described as a fraction of  $f_t$  (such that  $b$  values will be always less than 1) and corresponding stress will be  $b$  times  $f_t$ , the stress distribution for the given relationship is shown in Figure 6.6.

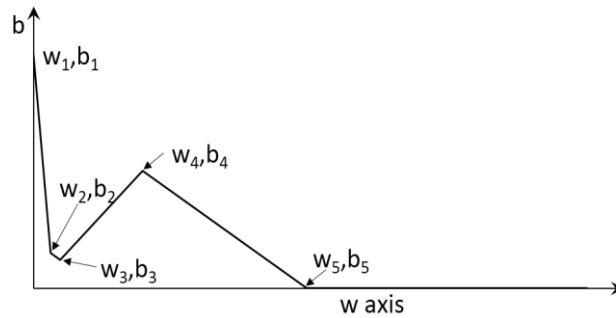


Fig 6.5 Definition of Parameters of Multi linear Stress-Crack relationship

A procedure for obtaining the moment-curvature relationship considering the multi-linear stress-crack opening relationship is presented below. The stress distribution in a section of height  $h$ , with crack tip located at a depth  $d$ , is shown in Figure 5.3.2. The stress distribution in the cracked portion reflects the multi-linear cohesive stress-crack opening relationship shown in Figure 5.3.1.

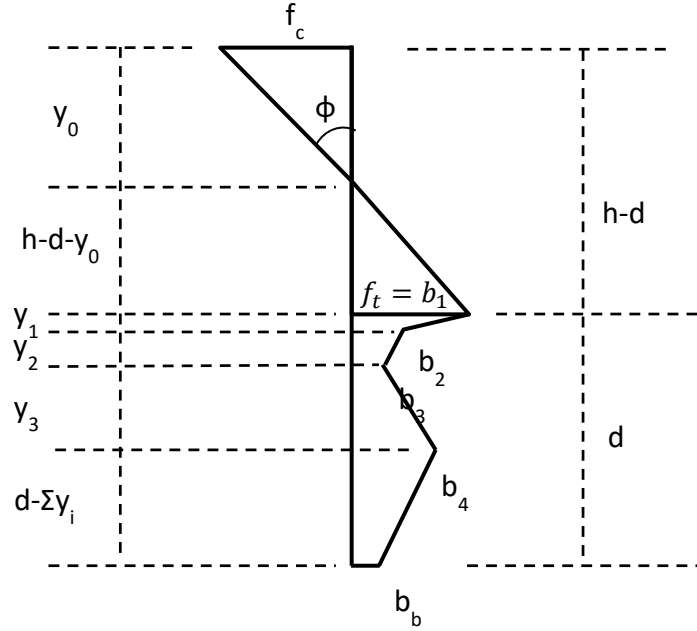


Fig 6.6 General Stress distribution for multi linear case

From compatibility relationship,

$$f_c = \frac{f_t \cdot y_0}{h-d-y_0} \quad (5.9)$$

At the crack tip, the response is elastic (the strain should be elastic) and stress will be equal to tensile strength (i.e.  $\sigma_w = f_t$ ). Therefore, keeping  $y$  as  $h-d$  and  $\sigma_w = f_t$  in equation 5.3 gives

$$d + y_0 = h - \frac{s \cdot f_t}{2\phi \cdot E} = h - \frac{h}{2\theta} \quad (5.10)$$

For a given stress crack opening relationship, using equation 5.3 at start point and end point of a line and their difference gives a relation between  $k_i$  and normalised rotation as follows. (See Annexure III for detailed derivation).

$$k_i = (b_{i+1} - b_i) + (w_{i+1} - w_i) \frac{E}{s f_t}, \quad (5.11)$$

$$\text{where } k_i = \frac{2\theta y_i}{\iota}$$



Slope of the lines are given by

$$m_i = \frac{b_{i+1} - b_i}{w_{i+1} - w_i} \in i = 1 \text{ to } n - 1 \quad (5.12)$$

where 'n' represents number of coordinates

In the Equation 5.11,  $k_i$  is normalised  $y_i$ , which is independent of rotation. Then all transitions rotations ( $\vartheta_i$ ) are found by force equilibrium as depth, now can be expressed as summation of  $y_i$  and is given as in equation 5.12 where transition rotation is rotation at which the slope of line changes.

$$\theta_i = \frac{1}{2} \left[ \left( 1 + \sum k_i \right) + \left( 1 + \sum (k_i (b_{i+1} + b_i)) \right)^{1/2} \right] \quad (5.13)$$

After evaluating transitions the normalized rotation is gradually increased, when  $\vartheta < 1$  (pre crack state),  $\mu = \vartheta$  and for  $\vartheta > 1$ , if we observe Figure 6.6 for a given rotation, stresses distribution above the crack can be expressed in terms of  $\alpha$  using equations 5.9 and 5.10. Stress distribution below the crack is known except in the bottom  $d - \sum y_i$  portion. Stress at bottom ( $b_b$ ) is expressed in terms of  $\alpha$  using equation 5.3 by substituting  $y=h$  and calculating width at bottom by using slope of the corresponding line given by equation 5.12. (5.14)

$$b_b = \frac{(1+2\alpha\theta)+j_i(b_i-m_iw_i)}{1+j_i} \quad \text{where } j_i = \frac{E}{m_i s f_t}$$

The requirement of force equilibrium (the total force on the section is zero) results in a quadratic equation in terms of  $\alpha$ , the depth of crack. The depth of neutral axis is obtained from equation 5.10. Moment of stresses is used to calculate the normalised moment. The moment curvature relationship is obtained by repeating the exercise for different values of curvature. (See Annexure II for detailed derivation).

## 6.4 Inverse analysis

The crack hinge model provides a conceptual framework to interpret the flexural response of a beam in terms of a propagating crack with the crack closing stresses provided by fibers bridging the crack. In the previous sections the forward analysis for predicting the flexural load response using the crack hinge model with known cohesive stress-crack opening relationship has been performed. The cohesive crack closing stresses on the load response has been shown to have a significant influence on the flexural load response, from the peak load to the shape of the post-peak load response. It is established that the tensile strength and the initial slope of the cohesive stress-crack opening relationship influence the peak strength in flexure. Further, the load recovery portion of the post-peak load response has been shown to be totally the contribution of fibers bridging the crack. The measured response in flexure therefore provides a means for determining the cohesive stress-crack opening relationship.

To determine the cohesive stress-crack opening relationship from the measured flexural response an inverse analysis algorithm has been developed in which the experimentally obtained load deflection response was given as input and the difference with the predicted load response using the hinged crack is minimized. The difference between the two responses was minimized in the least squares sense. An objective function of the normalized squares of residuals for the peak load and the load response was developed.

$$Norm = \frac{1}{n} \sqrt{\sum_{i=1}^n (P_i^{exp} - P_i^{theoretical})^2}$$

where  $P_u^{exp}$  and  $P_u^{theoretical}$  and the peak loads obtained from the experiment and from the numerical model, respectively and  $P_i^{exp}$  and  $P_i^{theoretical}$  are the  $i^{th}$  loads in the experimental and numerically predicted load responses at corresponding values of deflection, respectively.

A multilinear cohesive stress-crack opening relation of the form shown in Figure 6.7 was assumed. The parameters of the cohesive relationship were optimized to minimize the least square residual. A two-step inversion strategy was developed to separately optimize the tensile strength and the initial softening part of the cohesive behaviour. As the initial part of load deflection response is highly dependent on matrix properties, it was found to be highly sensitive to  $f_t$  and initial slope of stress crack relation and hence this part of load response was optimized separately by considering load deflection relationship up to a deflection of 0.3 mm. In first step the tensile strength ( $f_t$ ) and slope of initial line of stress crack opening relationship by changing  $b_2$  using the load response including the initial softening up to a displacement of 0.3 mm. In the next step, the value of  $f_t$  obtained in the previous step was kept fixed while the other cohesive values at predefined crack openings were optimized.

The inversion procedure was implemented numerically in Matlab®. In Matlab®, constrained function minimization algorithm was used in which, constraints were applied on crack opening parameters and tensile strength of concrete. In the first step of optimization, considering the load deflection response up to 0.3 mm, the value of  $w_2$  was fixed at 0.06 mm as it is observed that the peak is attained before an opening of 0.06 mm. The tensile strength  $f_t$  was kept fixed and the value of  $b_2$  obtained in the first step was used as an initial guess in the next step. Value of  $b_2$  was not fixed in the second step as it was observed to have an influence on the point of load recovery in the post-peak load response. In second step the crack opening values are predefined with a regular interval considering the sensitivity of load deflection diagram and corresponding stress values were found so as to get good match and predefining opening values also makes it easy to compare the crack bridging stresses developed by different fiber volumes.

The inverse analysis is performed on steel, polypropylene and hybrid FRC specimens of 0.5% volume fraction at 3, 7 and 28 days. The normalised stress vs crack opening for various fiber combinations at 3 day, 7 day and 28 day are shown in Figure 6.9, 6.10 and

6.11 respectively. The early age response shows a similar trend. At 28 days the hybrid FRC shows a superior response in early crack opening. It shows that the fibers in the blend indicating an early activation during crack opening.

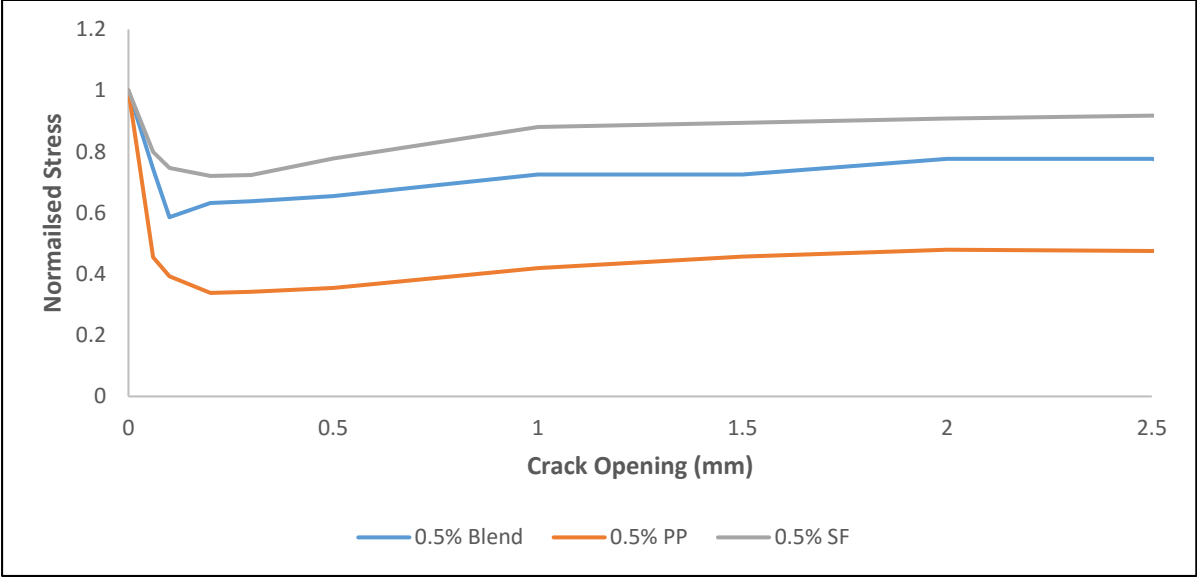


Figure 6.7 Stress crack opening relationship of steel, polypropylene and hybrid FRC at 0.5% volume fraction at 3 day

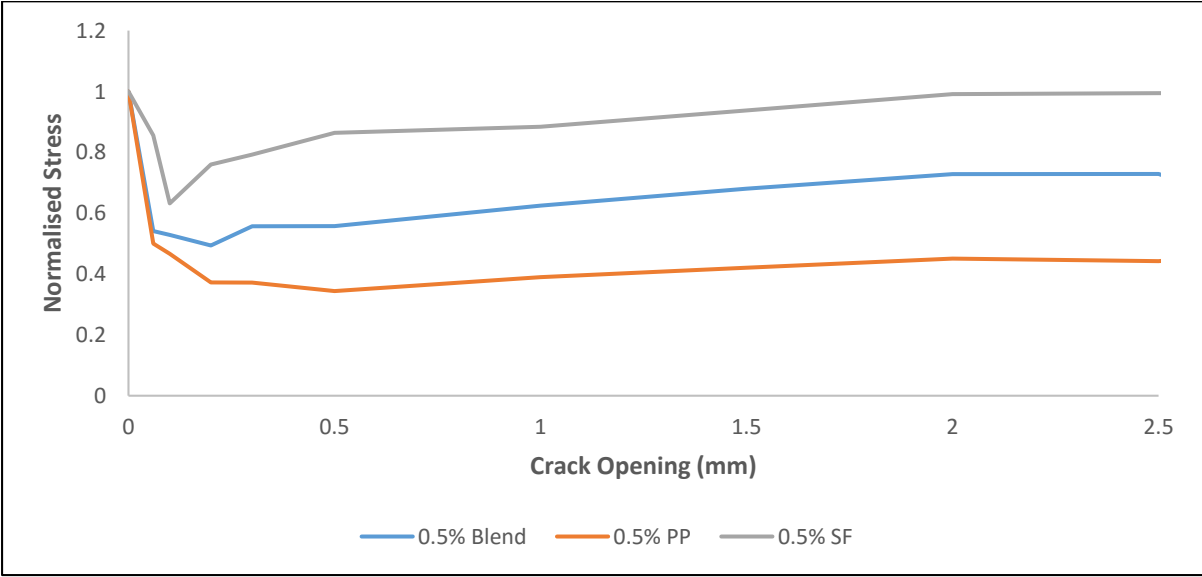


Figure 6.8 Stress crack opening relationship of steel, polypropylene and hybrid FRC at 0.5% volume fraction at 7 day

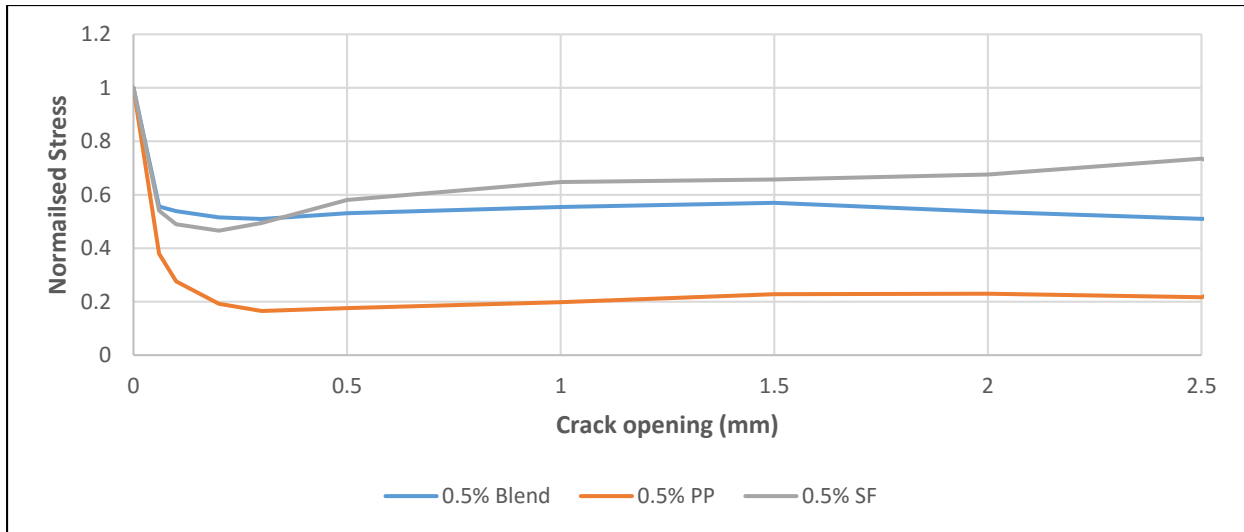


Figure 6.9 Stress crack opening relationship of steel, polypropylene and hybrid FRC at 0.5% volume fraction at 28 day

Table 6.1 Mean (Std Dev) values of Crack Opening parameters of Polypropylene, Blend and Steel FRC.

Crack Opening	3 Day			7 Day			28 Day		
	PP	Blend	SF	PP	Blend	SF	PP	Blend	SF
0	1.00 (0)	1.00 (0)	1.00 (0)	1.00 (0)	1.00 (0)	1.00 (0)	1.00 (0)	1.00 (0)	1.00 (0)
0.06	0.46 (0.103)	0.74 (0.037)	0.80 (0.027)	0.50 (0.034)	0.54 (0.098)	0.54 (0.044)	0.38 (0.034)	0.56 (0.024)	0.54 (0.015)
0.1	0.39 (0.050)	0.59 (0.005)	0.75 (0.080)	0.47 (0.015)	0.53 (0.090)	0.58 (0.063)	0.28 (0.031)	0.54 (0.118)	0.49 (0.027)

0.2	0.34 (0.116 )	0.63 (0.026 )	0.72 (0.072 )	0.37 (0.061 )	0.49 (0.131 )	0.43 (0.042 )	0.19 (0.042 )	0.52 (0.059 )	0.47 (0.020 )
0.3	0.34 (0.104 )	0.64 (0.036 )	0.72 (0.085 )	0.37 (0.055 )	0.56 (0.174 )	0.40 (0.043 )	0.17 (0.027 )	0.51 (0.083 )	0.49 (0.003 )
0.5	0.35 (0.121 )	0.66 (0.060 )	0.78 (0.123 )	0.34 (0.036 )	0.56 (0.151 )	0.42 (0.086 )	0.18 (0.047 )	0.53 (0.059 )	0.58 (0.018 )
1	0.42 (0.135 )	0.73 (0.074 )	0.88 (0.147 )	0.39 (0.041 )	0.62 (0.178 )	0.45 (0.016 )	0.20 (0.054 )	0.55 (0.051 )	0.65 (0.089 )
1.5	0.46 (0.148 )	0.75 (0.078 )	0.89 (0.079 )	0.42 (0.041 )	0.68 (0.187 )	0.49 (0.038 )	0.23 (0.056 )	0.57 (0.069 )	0.65 (0.135 )
2	0.48 (0.145 )	0.78 (0.085 )	0.91 (0.093 )	0.45 (0.052 )	0.73 (0.183 )	0.49 (0.098 )	0.23 (0.084 )	0.54 (0.077 )	0.66 (0.059 )
2.5	0.48 (0.113 )	0.72 (0.083 )	0.92 (0.092 )	0.44 (0.040 )	0.73 (0.153 )	0.48 (0.059 )	0.22 (0.084 )	0.51 (0.095 )	0.68 (0.040 )
Ft	1.18 (0.106 )	1.25 (0.034 )	1.23 (0.059 )	1.61 (0.005 )	1.47 (0.140 )	1.44 (0.116 )	2.07 (0.222 )	2.24 (0.104 )	2.27 (0.117 )

A comparison of the experimental and the numerically predicted load deflection responses of beams is shown in Figure 6.12. It can be seen that there is a good match between experimental and theoretical curves for all FRC beams. The difference in the area under curve between the experimental and the numerically predicted responses was mostly less than 1 percent. The model is able to capture the non-linearity prior to peak load, the load recovery point and also load recovery portion. But there is a small deviation

in the immediate post peak response after peak where the model is unable to capture the steep load drop. This may be improved by changing predefined crack opening values which are used in the calculation of the norm.

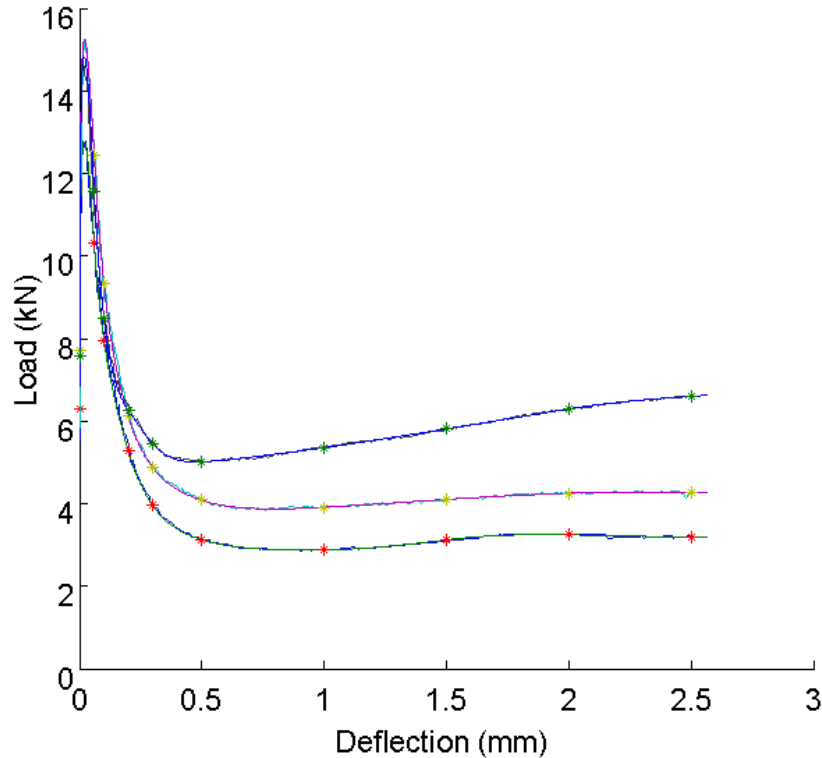


Figure 6.10 Experimental and matched theoretical curves for 0.5% Polypropylene FRC at 28 days.

Using the results of the inversion analysis, the relationship between the crack length and the crack opening are obtained. The crack length in the hinged crack model is defined by the depth at which the stress is equal to the tensile strength,  $f_t$ . Similarly, the crack opening is the crack opening displacement at the lowest portion of the beam. The relationship between the crack length and the crack opening displacement is plotted in Figure 6.13, 6.14 and 6.15. The results indicate that initially for a small increase in crack opening there is a large increase in the crack length. However, later there is a smaller increase in the crack length and the response is dominated by the opening of the crack.

The results also indicate that crack propagation along the depth of section is significantly affected by tensile strength. For a given crack opening, the crack length in specimens with a higher  $f_t$  are smaller.

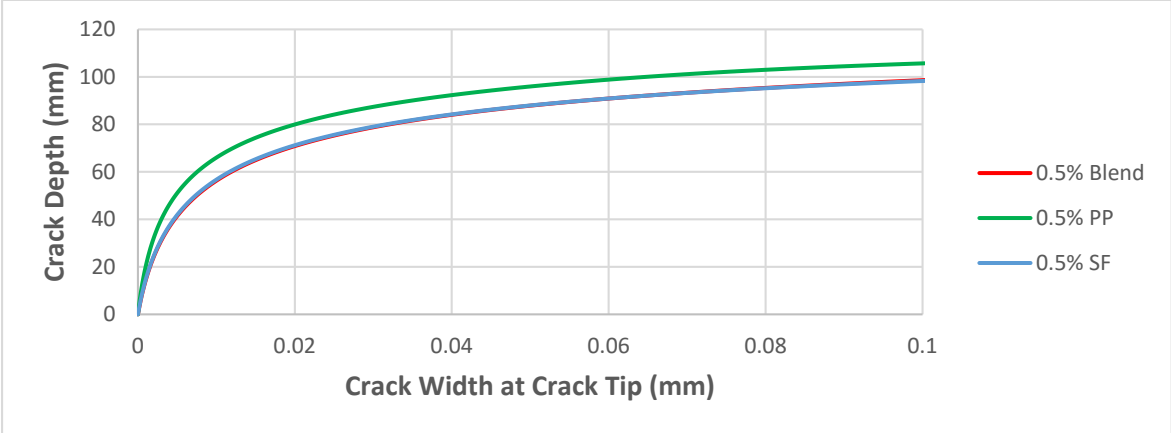


Figure 6.11 Crack Depth vs Crack Width for the mean crack opening parameters for polypropylene, steel and hybrid FRC at 3 day.

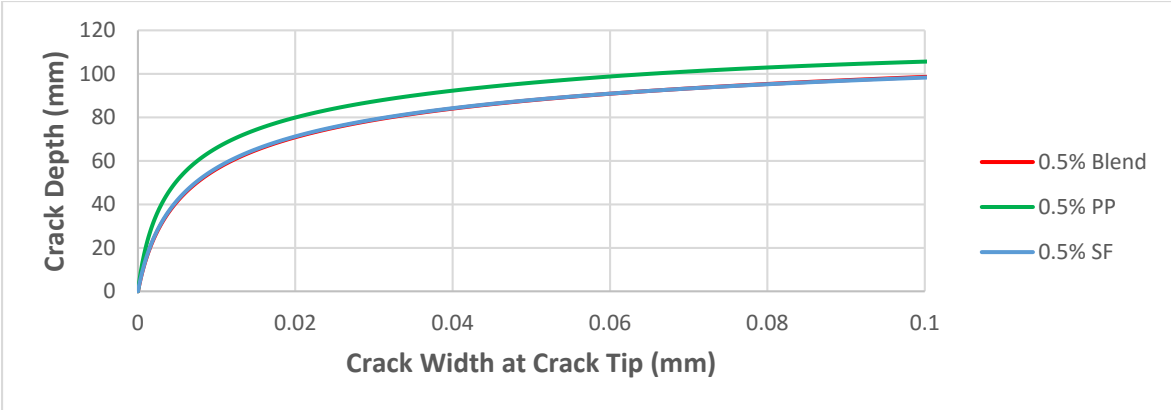


Figure 6.12 Crack Depth vs Crack Width for the mean crack opening parameters for polypropylene, steel and hybrid FRC at 7 day.



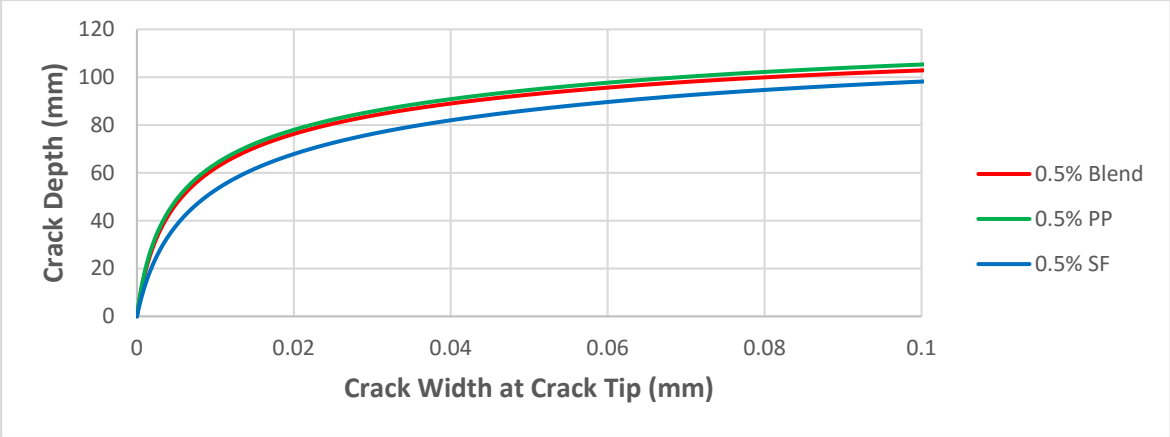


Figure 6.13 Crack Depth vs Crack Width for the mean crack opening parameters for polypropylene, steel and hybrid FRC at 28 day.

# Chapter 7

## Summary of findings and Future Works

For polypropylene FRC, the load drop in the post peak is accompanied with an increasing deflection, which is indicative of increasing compliance produced by the crack propagating along the height of the beam. Also load drop was found to increase as the concrete ages. For polypropylene FRC, the failure was observed to be produced by a single crack in the constant moment region. But multiple cracks were visible for specimens in both hybrid and steel FRC of higher volume content.

Steel FRC showed a superior performance in the early ages when compared to the hybrid and polypropylene FRC at both the fiber volume fractions i.e. 0.5% and 0.94%. Experimental results revealed that for a lower fiber volume fraction of 0.5%, the matured hybrid fiber reinforced concrete provided a superior response over steel FRC at 28 days. The hybrid FRC showed better performance till a deflection value of 0.9 mm and a crack opening of 0.6 mm. It is observed that the load deflection response of hybrid FRC was improving as the concrete ages.

Comparing the compressive strength values, the polypropylene FRC performed better in the early ages at both volume fractions, i.e. 0.5% and 0.94%. At 28 days, all the fiber combinations showed a comparable value, steel being the better. All the fiber combinations showed an improvement over the control specimen.

Failure in both control and macro polypropylene FRC beams were due to the formation of a single crack in the constant moment region. While failure for hybrid and

steel FRC beams were due to multiple cracks in constant moment region at higher volume fraction of 0.94%.

Directions for future research that emerge from the findings of this study are:

1. Investigate the shear response of the hybrid FRC at 0.5%.
2. Investigate the improvements in fracture behaviour of FRC with macro steel and polypropylene with micro polypropylene fibers.

## References

- [1] R. F. Zollo, "Fiber-reinforced concrete: an overview after 30 years of development," *Cement and Concrete Composites*, vol. 19, no. 2, pp. 107-122, 1997
- [2] B. Belletti, R. Cerioni, A. Medo and G. Plizzari, "Design Aspects on Steel Fiber-Reinforced Concrete Pavements," *Journal of Materials in Civil Engineering*, vol. 20, no. 9, pp. 599-607, 2008.
- [3] G. L. Sorelli, A. Meda and A. G. Plizzari, "Steel Fiber Concrete Slabs on Ground: A Structural Matter," *ACI Structural Journal*, vol. 103, no. 4, pp. 551-558, 2006.
- [4] L. Ferrara and A. Meda, "Relationships between fibre distribution, workability and the mechanical properties of SFRC applied to precast roof elements.," *Materials and Structures*, vol. 39, no. 4, pp. 411-420, 2006.
- [5] G. Ravindra, B. Bryan, G. Tomas, O. Jorge and J. Rolando, "Fiber Concrete Tunnel Lining: Construction of a Subway Line in Barcelona," *Concrete International*, vol. 28, no. 8, pp. 63-69, August 2006.
- [6] L. Taerwe and A. Van Gysel, "Influence of Steel Fibers on Design Stress-Strain Curve for High-Strength Concrete," *Journal of Engineering Mechanics*, vol. 122, no. 8, pp. 695-704, 1996.
- [7] A. C. 544, "State-of-the-Art Report on Fiber Reinforced Concrete," American Concrete Institute, 1996.
- [8] A. 544.3R-93, "Guide for Specifying, Proportioning, Mixing, Placing, and Finishing Steel Fiber Reinforced Concrete," American Concrete Institute, 1993.
- [9] Z. Bayasi and M. McIntyre, "Application of Fibrillated Polypropylene Fibers for Restraint of Plastic Shrinkage Cracking in Silica Fume Concrete," *Materials Journal*, vol. 99, no. 4, pp. 337-344, 7 1 2002.
- [10] V. S. Gopalaratnam and G. Ravindra , "On the characterization of flexural toughness in fiber reinforced concretes," *Cement and Concrete Composites*, vol. 17, no. 3, pp. 239-254, 1995.

- [11] S. P. Shah and C. Ouyang, "Mechanical Behavior of Fiber-Reinforced Cement-Based Composites," *Journal of the American Ceramic Society*, vol. 74, no. 11, pp. 2727-38,2947-53, November 2005.
- [12] C. D. Johnston, "Steel Fiber Reinforced Mortar and Concrete: A Review of Mechanical Properties," *Fiber Reinforced Concrete SP-44*, vol. 44, pp. 127-142, 1974.
- [13] G. R. Williamson, "The Effect of Steel Fibers on the Compressive Strength of Concrete," *Fiber Reinforced Concrete, SP-44*, vol. 44, pp. 195-208, 1974.
- [14] C. D. Johnston and R. J. Gray, "Uniaxial Tension Testing of Steel Fibre Reinforced Cementitious Composites," in *Proceedings, International Symposium on Testing and Test Methods of Fibre-Cement Composites.*, 1978.
- [15] J. N. Kar and A. K. Pal, "Strength of Fiber-Reinforced Concrete," *Journal of the Structural Division, ASCE*, vol. 98, no. 5, pp. 1053-1068, 1972.
- [16] J. P. Romualdi and J. A. Mandel, "Tensile Strength of Concrete Affected by Uniformly Distributed and Closely Spaced Short Lengths of Wire Reinforcement," *ACI Journal Proceedings*, vol. 61, no. 6, pp. 657-672, 1964.
- [17] C. D. Johnston and R. A. Coleman, "Strength and Deformation of Steel Fiber Reinforced Mortar in Uniaxial Tension," *Fiber Reinforced Concrete, SP-44 American Concrete Institute*, vol. 44, pp. 177-194, 1974.
- [18] C. D. Johnston, "Definition and Measurement of Flexural Toughness Parameters for Fiber Reinforced Concrete," *ASTM- Cement, Concrete and Aggregates*, vol. 4, no. 2, pp. 53-60, 1982.
- [19] V. Ramakrishnan, T. Brandshaug, W. V. Coyle and E. K. Schrader, "Comparative Evaluation of Concrete Reinforced with Straight Steel Fibers and Fibers with Deformed Ends Glued Together into Bundles," *American Concrete Institute*, vol. 77, no. 3, pp. 135-143, 1980.
- [20] C. D. Johnston and R. J. Gray, "Flexural Toughness First-Crack Strength of Fibre-Reinforced-Concrete Using ASTM Standard C 1018," in *Proceedings, Third International*

*Symposium on Developments in Fibre Reinforced Cement Concrete, RILEM*, , Sheffield, 1986.

[21] P. J. Hannant, "FIBRE CEMENTS AND FIBRE CONCRETES," Wiley(John) & Sons, Limited, Chichester, United Kingdom, 1978.

[22] H. Cifuentes, F. Garcia, O. Maeso and F. Medina, "Influence of the properties of polypropylene fibres on the fracture behaviour of low-, normal- and high-strength FRC," *Construction and Building Materials*, vol. 45, pp. 130-137, August 2013.

[23] B. H. Oh, J. C. Kim and C. Y. Choi, "Fracture behavior of concrete members reinforced with structural synthetic fibers," *Engineering Fracture Mechanics*, vol. 74, no. 1-2, pp. 243-257, January 2007.

[24] S. Singh, A. Shukla and R. Brown, "Pullout behavior of polypropylene fibers from cementitious matrix," *Cement and Concrete Research*, vol. 34, no. 10, pp. 1919-1925, October 2004.

[25] M. N. Soutsos, T. T. Le and A. P. Lampropoulos, "Flexural performance of fibre reinforced concrete made with steel and synthetic fibres," *Construction and Building Materials*, vol. 36, pp. 704-710, November 2012.

[26] F. Benacardino, L. Rizzuti, G. Spadea and R. N. Swamy, "Experimental evaluation of fiber reinforced concrete fracture properties," *Composites Part B: Engineering*, vol. 41, no. 1, pp. 17-24, January 2010.

[27] N. Buratti, C. Mazzotti and M. Savoia, "Post-cracking behaviour of steel and macro-synthetic fibre-reinforced concretes," *Construction and Building Materials*, vol. 25, no. 5, pp. 2713-2722, May 2011.

[28] A. Hillerborg, M. Modeer and P. E. Petersson, "Analysis of crack formation and crack growth in concrete by means of fracture mechanics and finite elements," *Cement and Concrete Research*, vol. 6, no. 6, pp. 773-781, November 1976.

- [29] R. T. 162\_TDF, "Test and design methods for steel fibre reinforced concrete, "Design of steel fibre reinforced concrete using the ( $\sigma$ -w method: principles and applications)", *Materials and Structures*, vol. 35, pp. 262-278, 2002.
- [30] R. Evans and M. Marathe, "Microcracking and stress-strain curves for concrete in tension," *Materials and Structures, Matériaux et Construction*, vol. 1, no. 1, pp. 61-64, 1968.
- [31] V. S. Gopalaratnam and S. P. Shah, "Post-Cracking Characteristics of Concrete in Uniaxial Tension," in *Engineering Mechanics in Civil Engineering*, New York, 1984.
- [32] P. Petersson, "Fracture energy of concrete: Practical performance and experimental results," *Cement and Concrete Research*, vol. 10, no. 1, pp. 91-101, 1980.
- [33] H. Reinhardt, "Fracture Mechanics of an Elastic Softening Material like Concrete," pp. 5-41, 01 01 1984.
- [34] K. Visalvanich and A. E. Naaman, "Fracture Model for Fiber Reinforced Concrete," *ACI Journal*, vol. 80, no. 2, pp. 128-138, 1983.
- [35] A. Hillerborg, "Analysis of fracture by means of the fictitious crack model, particularly for fibre reinforced concrete," *International Journal of Cement Composites*, vol. 2, no. 4, pp. 177-184, 1980.
- [36] A. R. Ingraffea and W. H. Gerstle, "Non-Linear Fracture Models for Discrete Crack Propagation," in *Application of Fracture Mechanics to Cementitious Composites, NATO ASI series*, 1985.
- [37] L. Oostergaard, D. Lange and H. Stang, "Early-age stress-crack opening relationship for high performance concrete," *Cement and Concrete Composites*, vol. 26, no. 5, pp. 563-572, 2004.
- [38] H. K. Seung , Z. Zhifang and S. P. Shah, "Effect of specimen size on fracture energy and softening curve of concrete: Part II. Inverse analysis and softening curve," *Cement and Concrete research*, vol. 38, no. 8-9, pp. 1061-1069, 2008.

- [39] M. Wecharatana and S. P. Shah, "A Model for Predicting Fracture Resistance of Fiber Reinforced Concrete," *Cement and Concrete Research*, vol. 13, no. 6, pp. 819-829, November 1983.
- [40] J. F. Olesen, "Fictitious Crack Propagation in Fiber-Reinforced Concrete Beams," *Journal of Engineering Mechanics*, vol. 127, no. 3, pp. 272-280, 01 March 2001.
- [41] I. Lofgren, H. Stang and J. F. Olesen, "Fracture Properties of FRC Determined through Inverse Analysis of wedge Splitting and Three-Point Bending Tests," *Journal of Advanced Concrete Technology*, vol. 3, no. 3, pp. 423-434, October 2005.
- [42] S. Matthys and T. Soetens, "Different methods to model the post-cracking behaviour of hooked-end steel fibre reinforced concrete," *Construction and Building Materials*, vol. 73, pp. 458-471, 2014.
- [43] J. Barros, V. Cunha, A. F. Ribeiro and J. A. B. Antunes, "Post-cracking behaviour of steel fibre reinforced concrete," *Materials and Structures*, vol. 38, no. 1, pp. 47-56, January-February 2005.
- [44] U. 11039-2, "Steel Fibre Reinforced Concrete - Test Method For Determination Of First Crack Strength And Ductility Indexes," 2003.
- [45] T. C. Chu, W. F. Ranson, M. A. Sutton and W. H. Peters, "Applications of Digital Image correlation technique to Experimental Mechanics," *Exp. Mech*, vol. 25, pp. 232-244, 1985.
- [46] A. Kobayashi, *Handbook on Experimental Mechanics*, Indiana: Prentice Hall / Society for Experimental Mechanics, Inc., Lebanon, 1993.
- [47] f. Pierron , B. Green, Wisnom MR and S. R. Hallet, "Full-field assessment of the damage process of laminated composite open-hole tensile specimens. Part I: methodology," *Composites*, vol. 38, pp. 2307-2320, 2007.
- [48] K. V. Subramaniam, C. Carloni and L. Nobile, "Interface Fracture and Debonding in the FRP-Concrete Interface: Influence of the FRP Laminate width on Load Capacity," *Engineering Fracture Mechanics*, vol. 74, no. 4, pp. 578-594, 2007.



- [49] N. Banthia and R. Gupta; Hybrid fiber reinforced concrete (HyFRC): fiber synergy in high strength matrices; *Materials and Structures*, Vol. 37, December 2004, pp 707-716]
- [50]: Glavind, M. and Aarre, T., 'High-strength concrete with increased fracture-toughness', in 'Fiber-reinforced cementitious materials: symposium, Boston, Massachusetts, 1990 / editors, Sidney Mindess, Jan Skalny' in *Materials Research Society Symposia Proceedings v. 211* (Materials Research Society, Pittsburgh, 1991) 39-46.
- [51]: Feldman, D. and Zheng, Z., 'Synthetic fibres for fibre concrete composites', in 'High performance polymers and polymer matrix composites: symposium held April 13-16, 1993, San Francisco, California, U.S.A. / editors, Ronald K. Eby et al.' in *Materials Research Society Symposia Proceedings v. 305* (Materials Research Society, Pittsburgh, 1993) 123-128.
- [52]: Banthia, N. and Soleimani, S.M., 'Flexural response of hybrid fiber reinforced cementitious composites', *ACI Materials Journal*, Submitted, 2003.
- [53] A. Sivakumar, Manu Santhanam\_A quantitative study on the plastic shrinkage cracking in high strength hybrid fibre reinforced concrete\_Cement & Concrete Composites 29 (2007) 575-581
- [54] Jean-Francois Trottier 1 and Nemkumar Banthia 2; Toughness Characterization of Steel-Fiber Reinforced Concrete; *J. Mater. Civ. Eng.* 1994.6:264-289
- [55]: N. Banthia, F. Majdzadeh, J.Wua, V. Bindiganavile, Fiber synergy in Hybrid Fiber Reinforced Concrete (HyFRC) in flexure and direct shear, *Cement & Concrete Composites* 48 (2014) 91-97
- [56]: Lawler J, Zampini D, Shah SP. Permeability of cracked hybrid fiber reinforced mortar under load. *ACI Mater J* 2002(July-August):379-85.

[57]: John Forbes Olesen, Fictitious Crack Propagation in Fiber-Reinforced Concrete Beams. J. Eng. Mech. 2001.127:272-280.

## Annexure I

### 3-Day Compressive Strength Results

Specimen	Mean Compressive Strength (MPa)	Std. Deviation (MPa)
Control	14.60	0.84
0.5% Blend (0.3% SF+0.2% PP)	19.48	0.25
0.5% PP	20.27	0.45
0.5% SF	18.39	0.24
0.94% Blend (0.5% SF+0.44% PP)	19.20	0.35
0.94% PP	20.43	1.50
0.94% SF	18.49	1.30

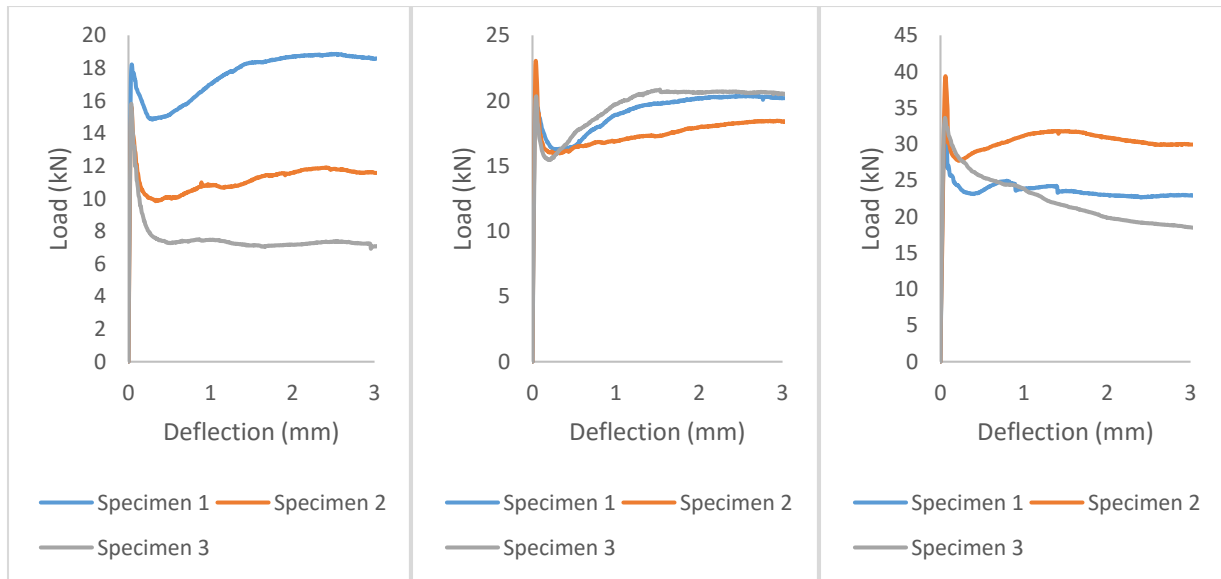
### 7-Day Compressive Strength Results

Specimen	Mean Compressive Strength (MPa)	Std. Deviation (MPa)
Control	20.37	0.93
0.5% Blend (0.3% SF+0.2% PP)	23.88	1.10
0.5% PP	29.12	0.54
0.5% SF	23.13	0.82
0.94% Blend (0.5% SF+0.44% PP)	25.63	2.10
0.94% PP	24.84	0.56
0.94% SF	22.56	0.67

### 28-Day Compressive Strength Results

Specimen	Mean Compressive Strength (MPa)	Std. Deviation (MPa)
Control	38.37	0.52
0.5% Blend (0.3% SF+0.2% PP)	39.69	0.39
0.5% PP	38.81	0.42
0.5% SF	40.57	0.35
0.94% Blend (0.5% SF+0.44% PP)	41.60	0.39
0.94% PP	40.42	0.71
0.94% SF	42.00	0.44

### Flexural Testing Response as per ASTM C1609 (Unnotched Beams)

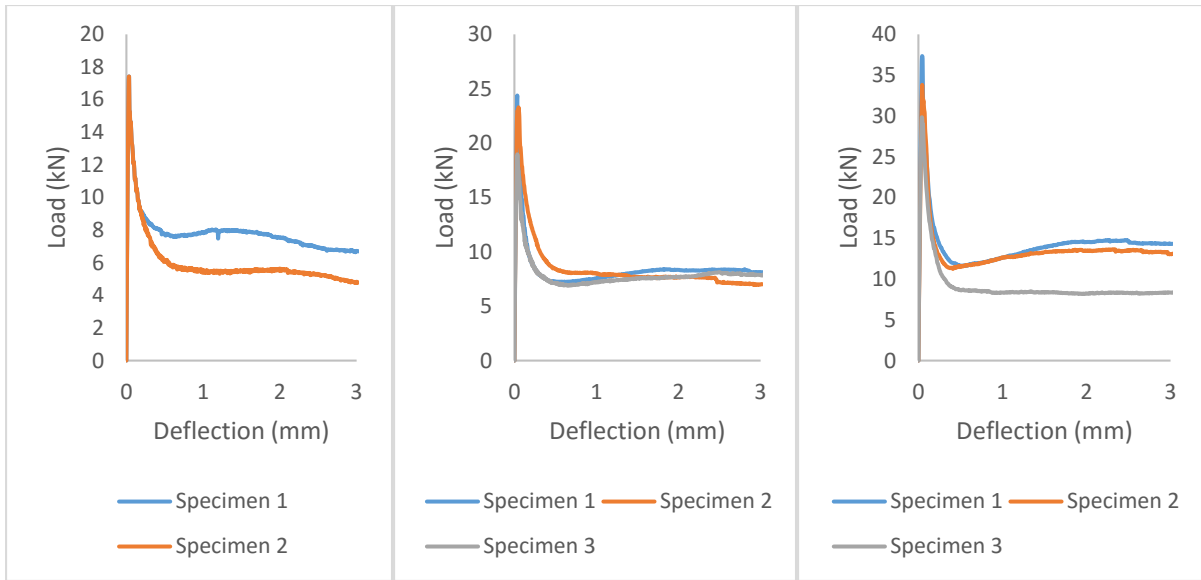


(a)

(b)

(c)

Load Deflection response of 0.5% volume fraction HyFRC at (a) 3 day (b) 7 day (c) 28 day

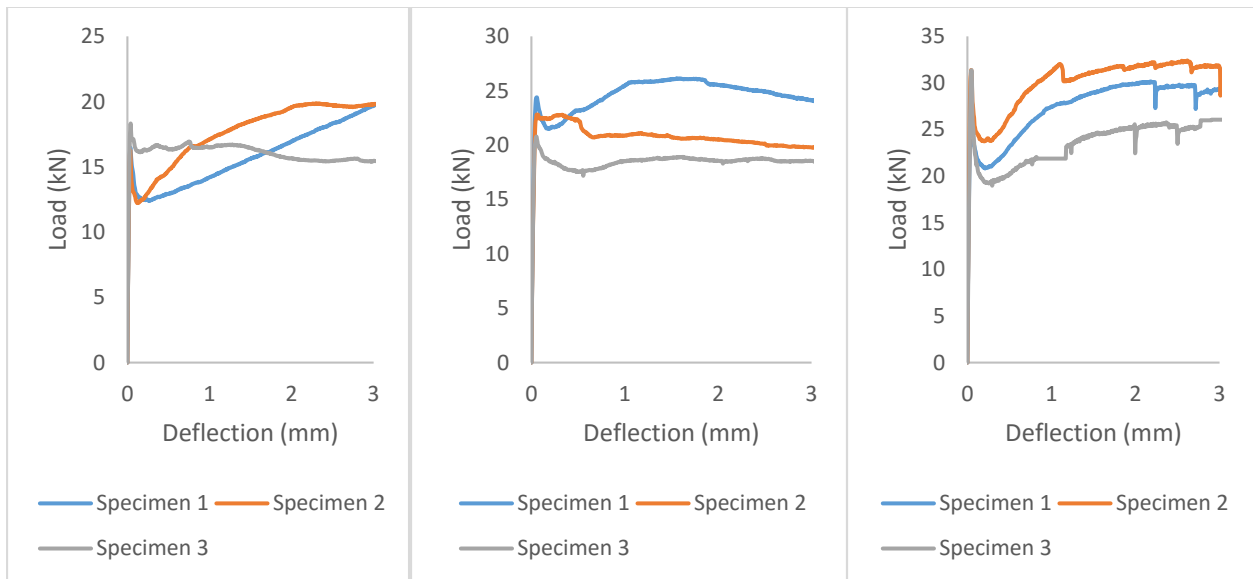


(a)

(b)

(c)

Load Deflection response of 0.5% volume fraction PPFRC at (a) 3 day (b) 7 day (c) 28 day

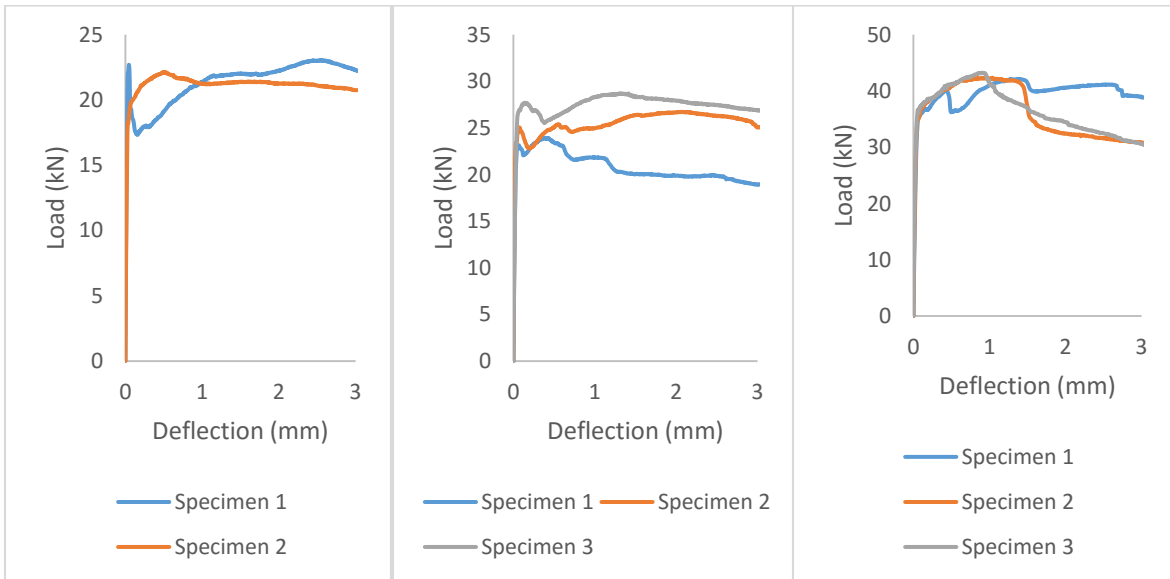


(a)

(b)

(c)

Load Deflection response of 0.5% volume fraction SFRC at (a) 3 day (b) 7 day (c) 28 day

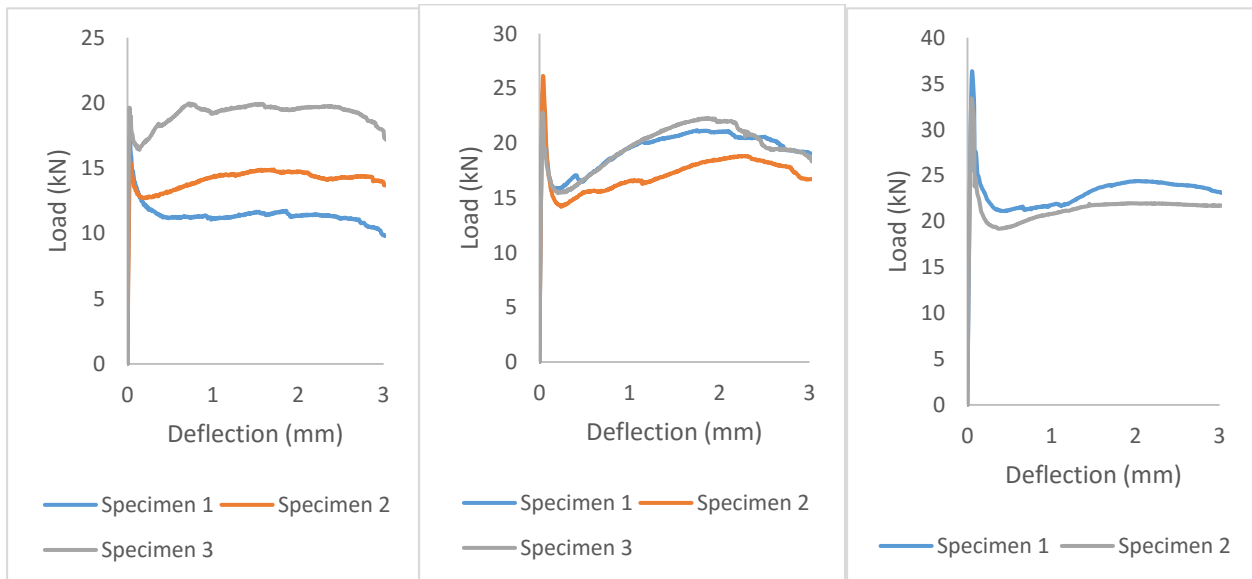


(a)

(b)

(c)

Load Deflection response of 0.94% volume fraction HyFRC at (a) 3 day (b) 7 day (c) 28 day

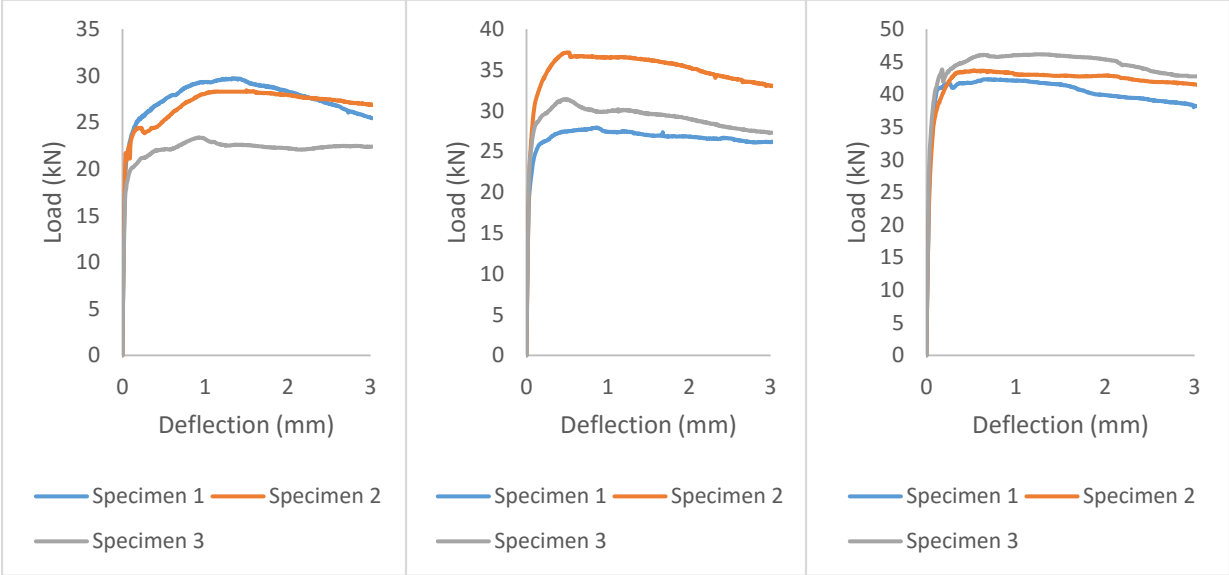


(a)

(b)

(c)

Load Deflection response of 0.94% volume fraction PPFRC at (a) 3 day (b) 7 day (c) 28 day



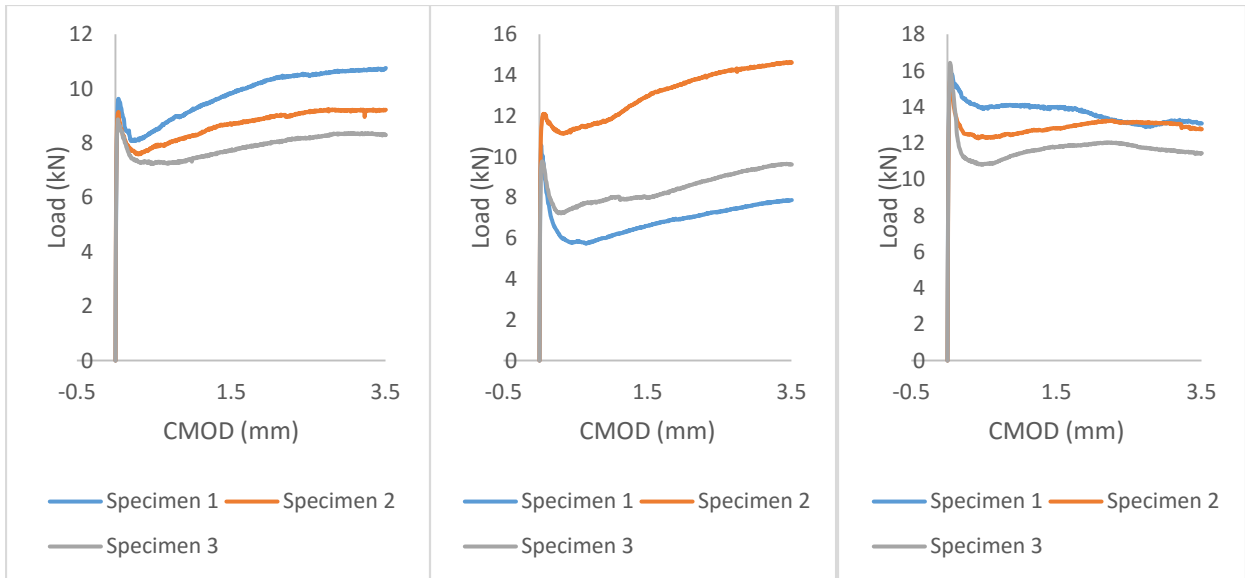
(a)

(b)

(c)

Load Deflection response of 0.94% volume fraction SFRC at (a) 3 day (b) 7 day (c) 28 day

Flexural Testing Response as per EN14651 (Notched Beams)

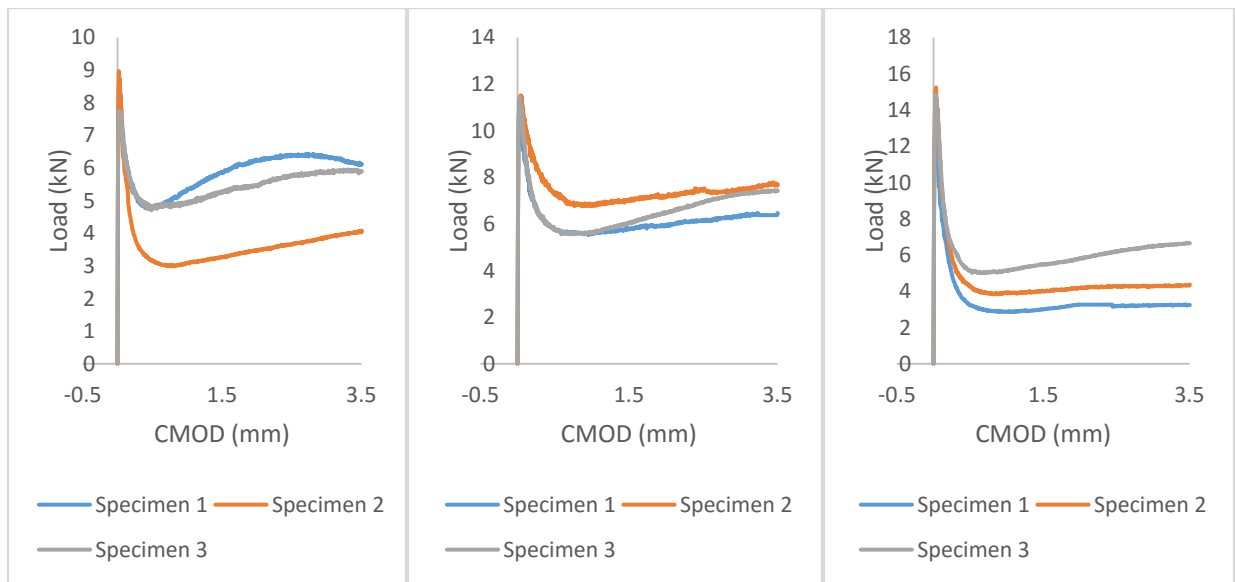


(a)

(b)

(c)

Load CMOD response of 0.5% volume fraction HyFRC at (a) 3 day (b) 7 day (c) 28 day



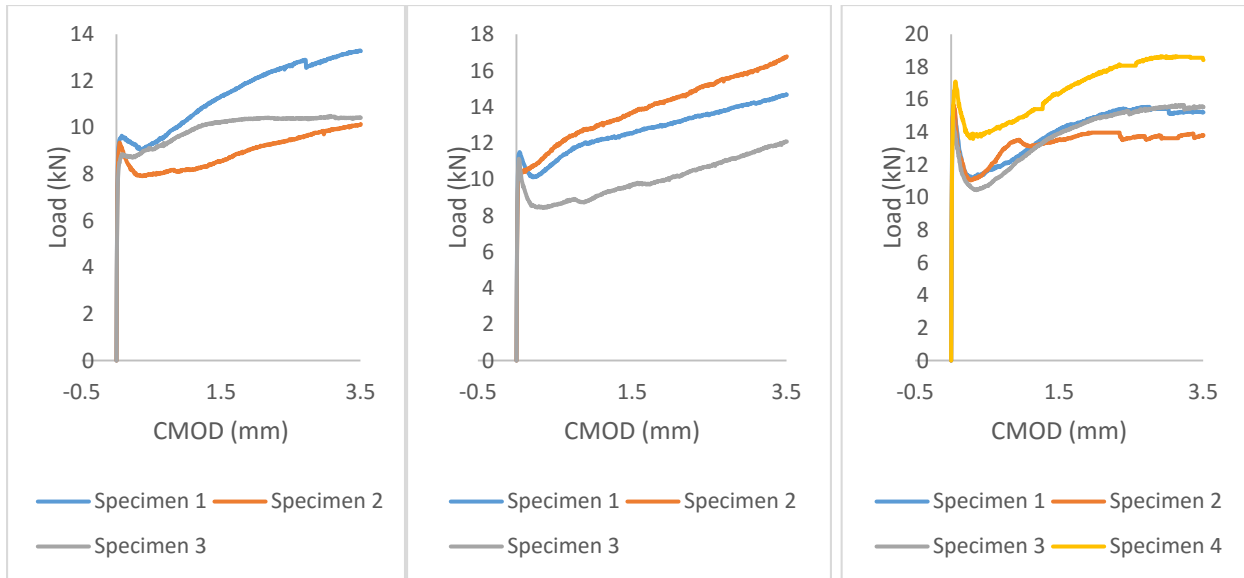
(a)

(b)

(c)

Load CMOD response of 0.5% volume fraction PPFRC at (a) 3 day (b) 7 day (c) 28 day



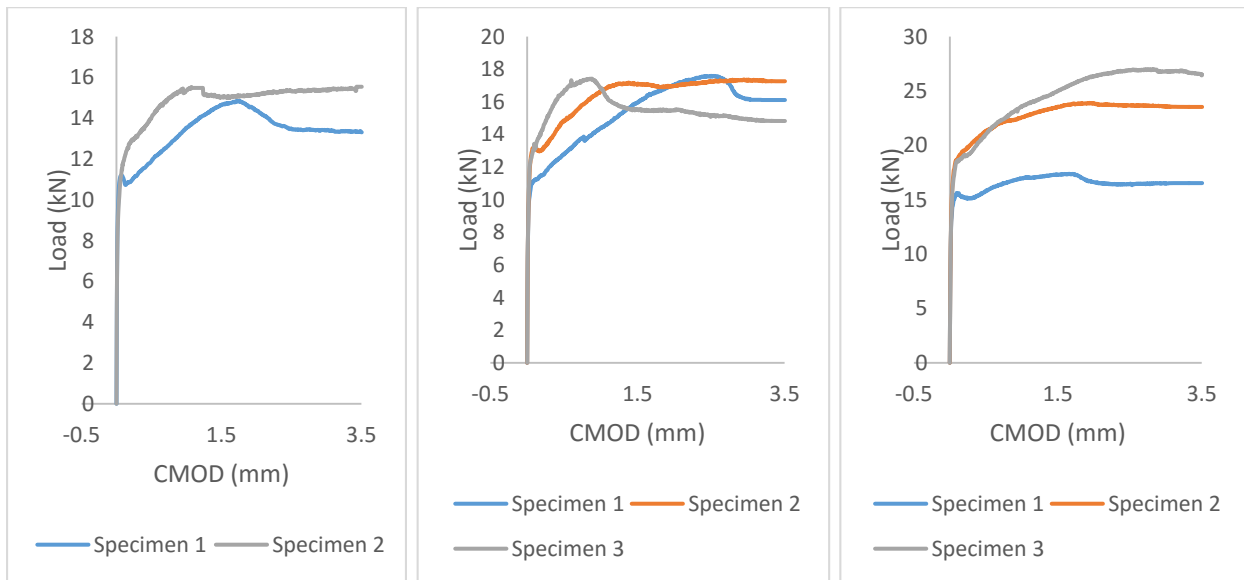


(a)

(b)

(c)

Load CMOD response of 0.5% volume fraction SFRC at (a) 3 day (b) 7 day (c) 28 day

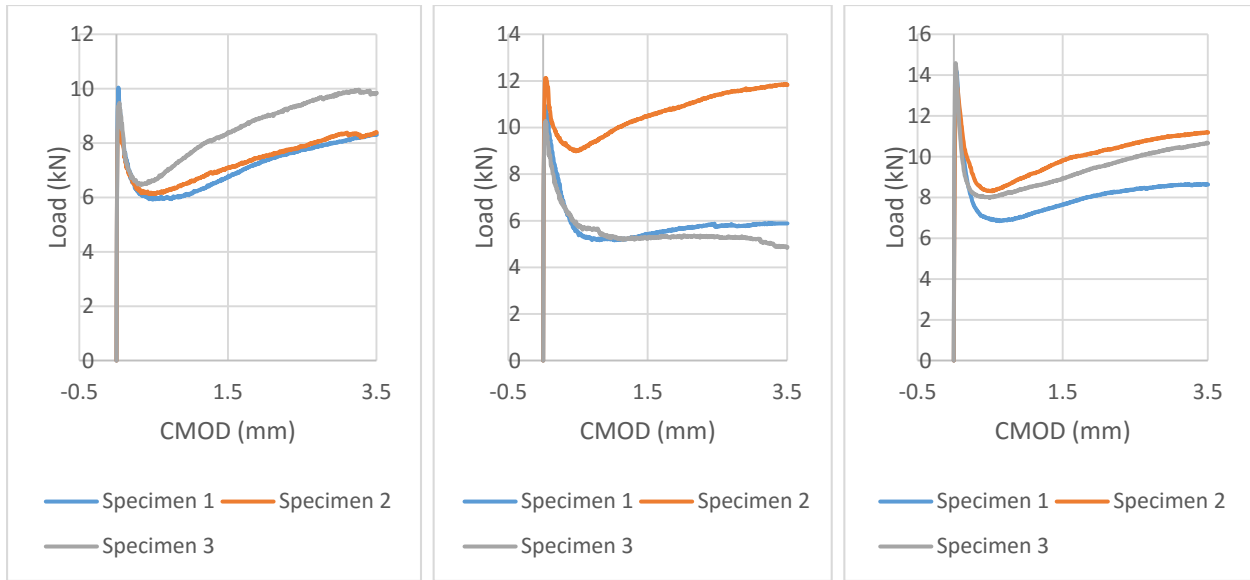


(a)

(b)

(c)

Load CMOD response of 0.94% volume fraction HyFRC at (a) 3 day (b) 7 day (c) 28 day

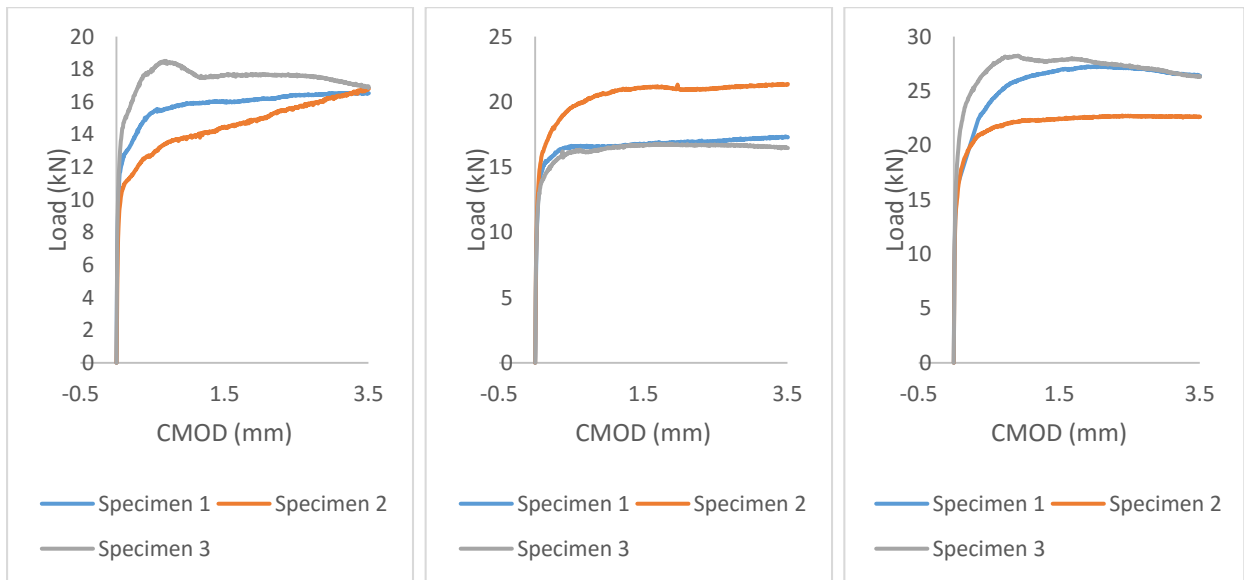


(a)

(b)

(c)

Load CMOD response of 0.94% volume fraction PPFRC at (a) 3 day (b) 7 day (c) 28 day



(a)

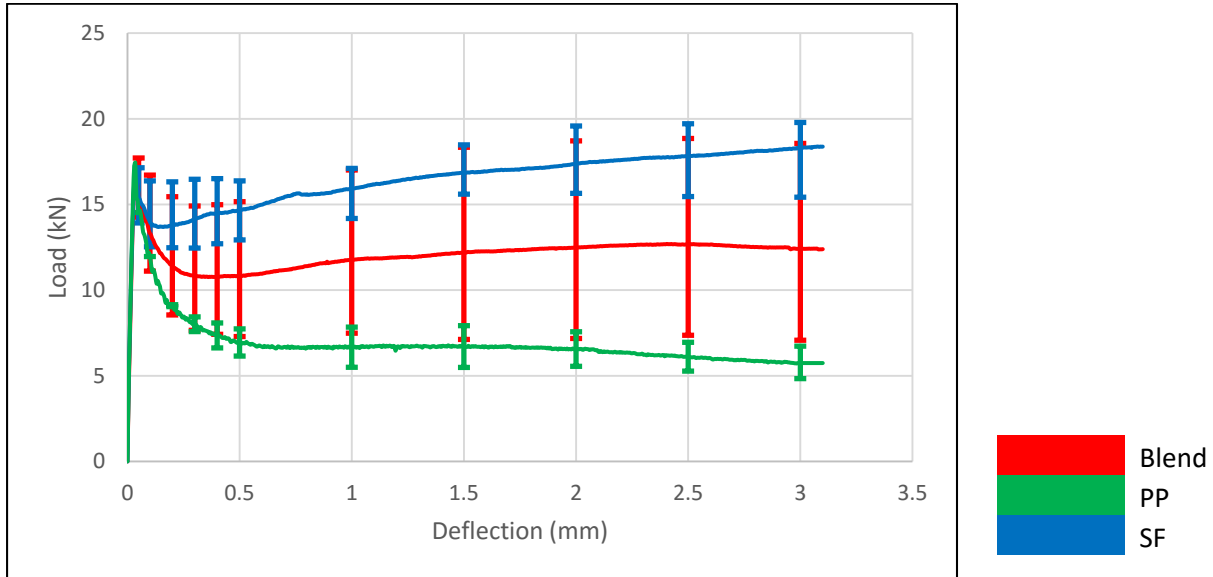
(b)

(c)

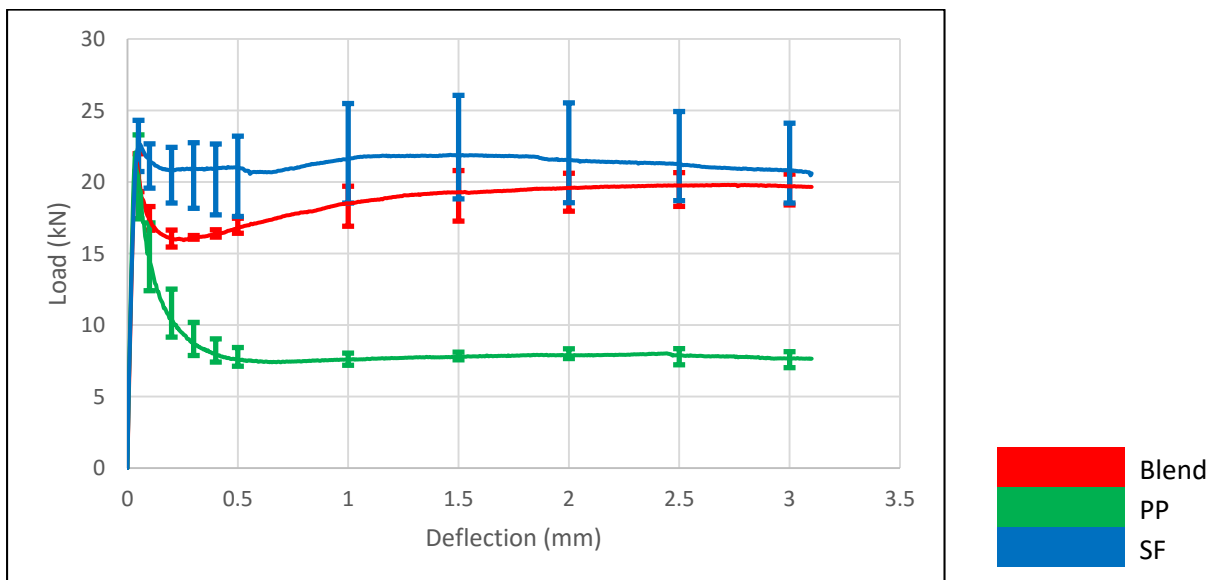
Load CMOD response of 0.94% volume fraction SFRC at (a) 3 day (b) 7 day (c) 28 day

## Annexure II

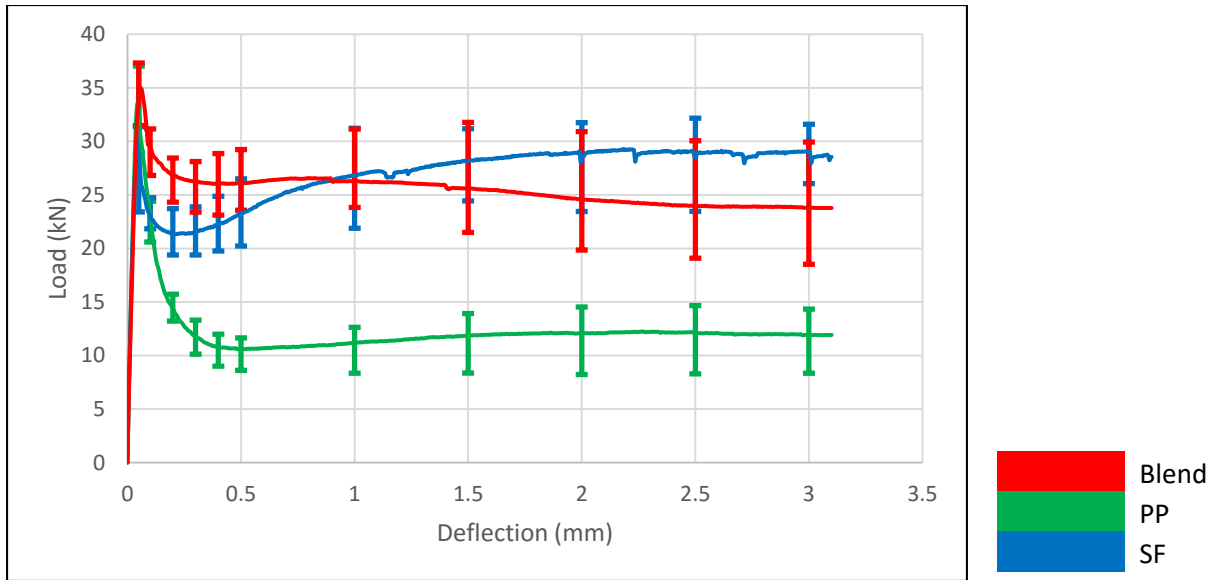
### EXPERIMENTAL RESULTS WITH ERROR BARS



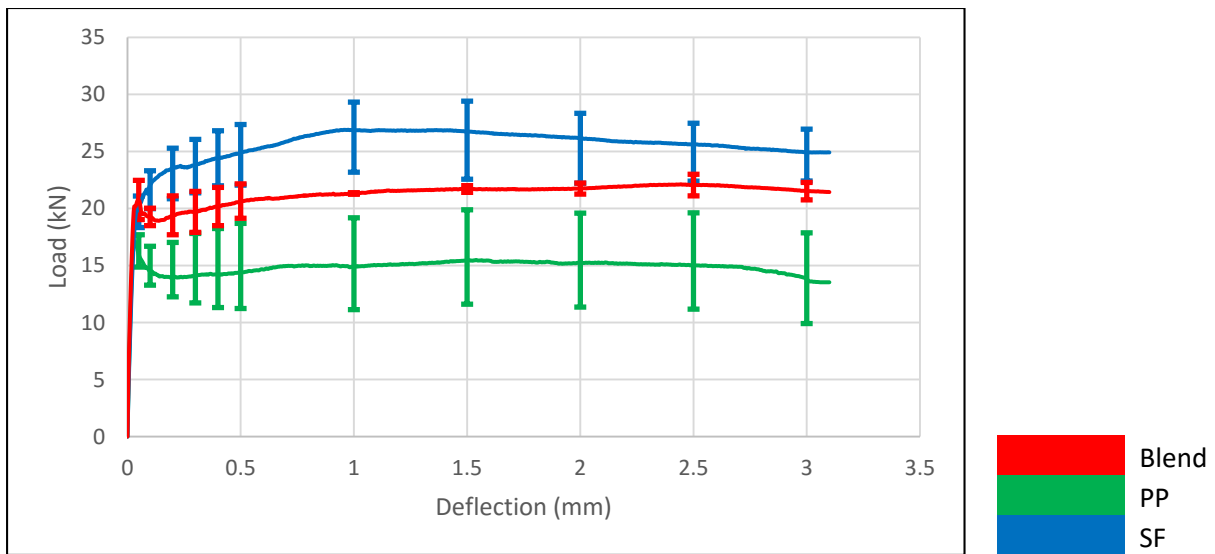
Load Deflection response of 0.5% volume fraction of steel, hybrid and polypropylene FRC at 3 day.



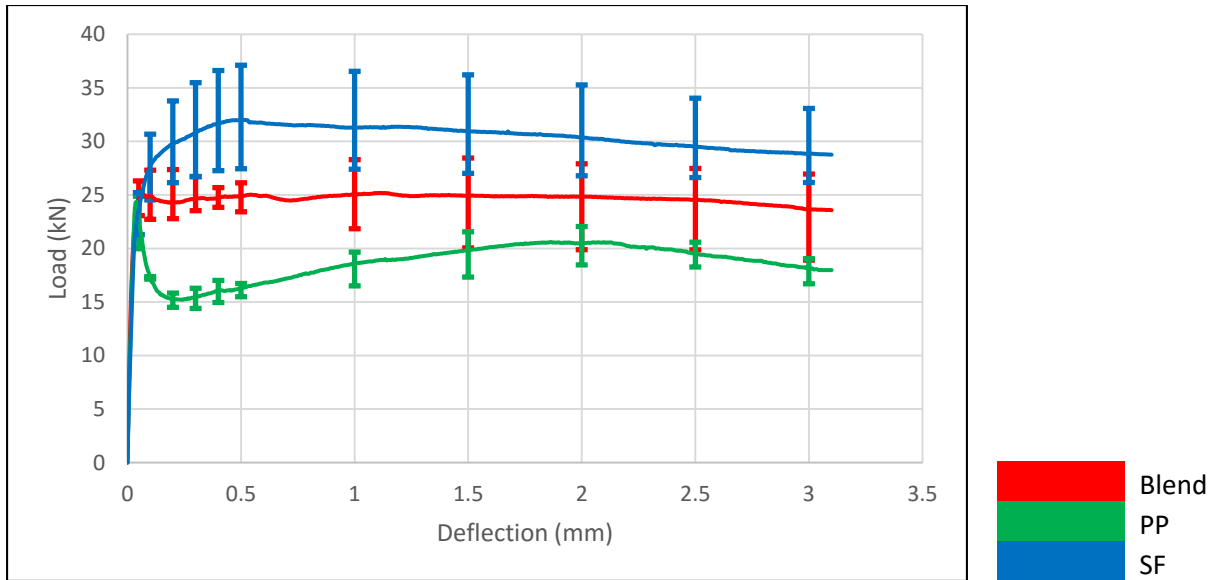
Load Deflection response of 0.5% volume fraction of steel, hybrid and polypropylene FRC at 7 day.



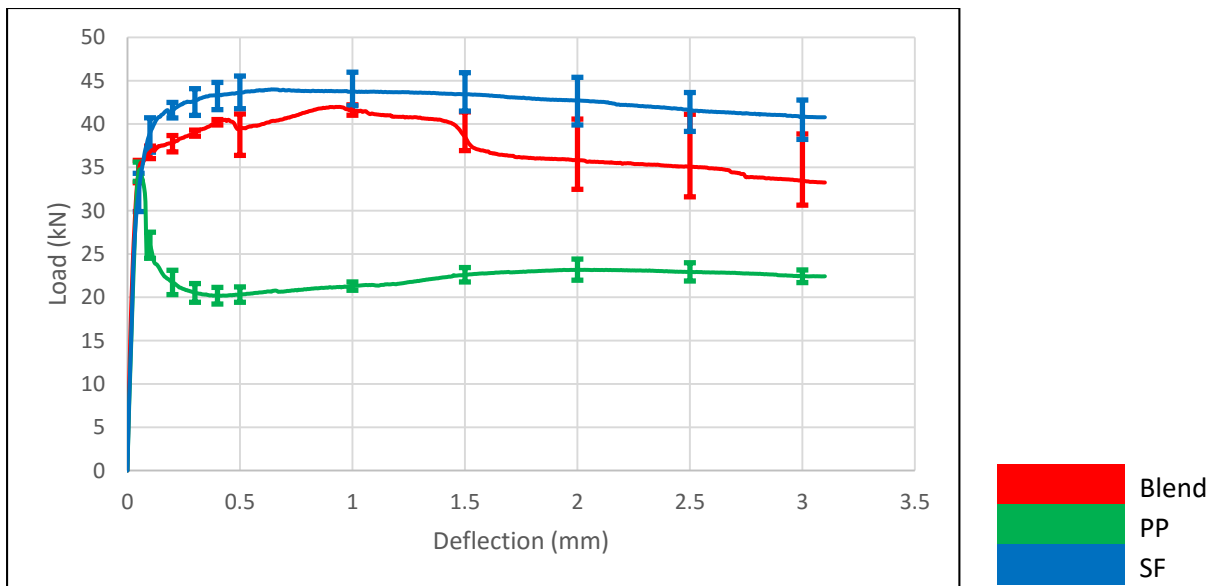
Load Deflection response of 0.5% volume fraction of steel, hybrid and polypropylene FRC at 28 day.



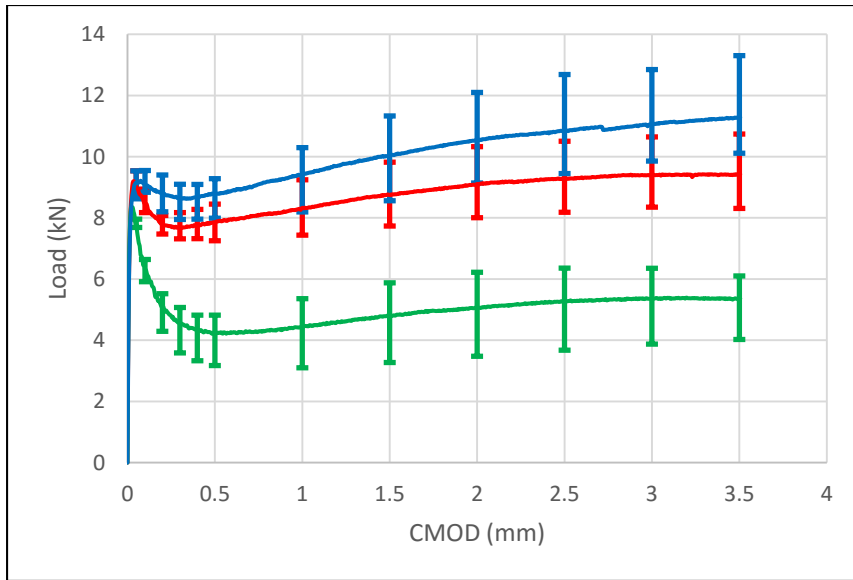
Load Deflection response of 0.94% volume fraction of steel, hybrid and polypropylene FRC at 3 day.



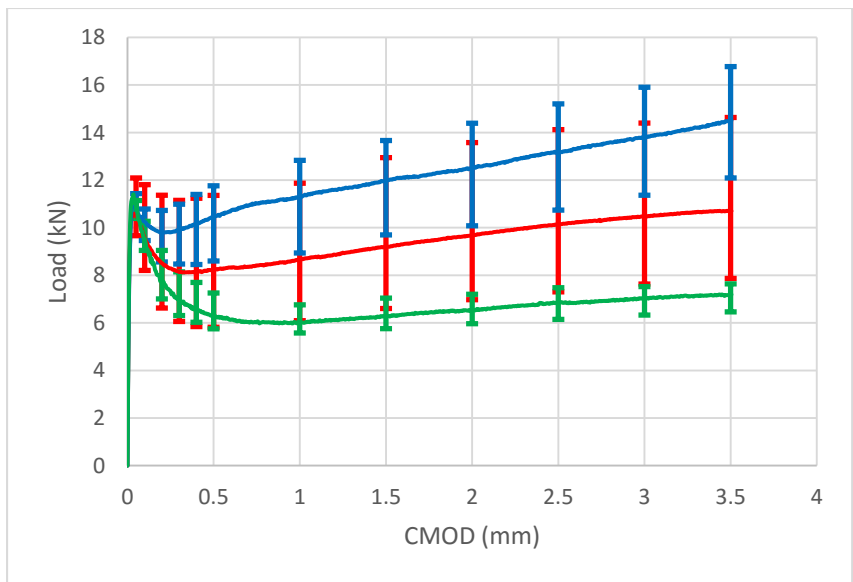
Load Deflection response of 0.94% volume fraction of steel, hybrid and polypropylene FRC at 7 day.



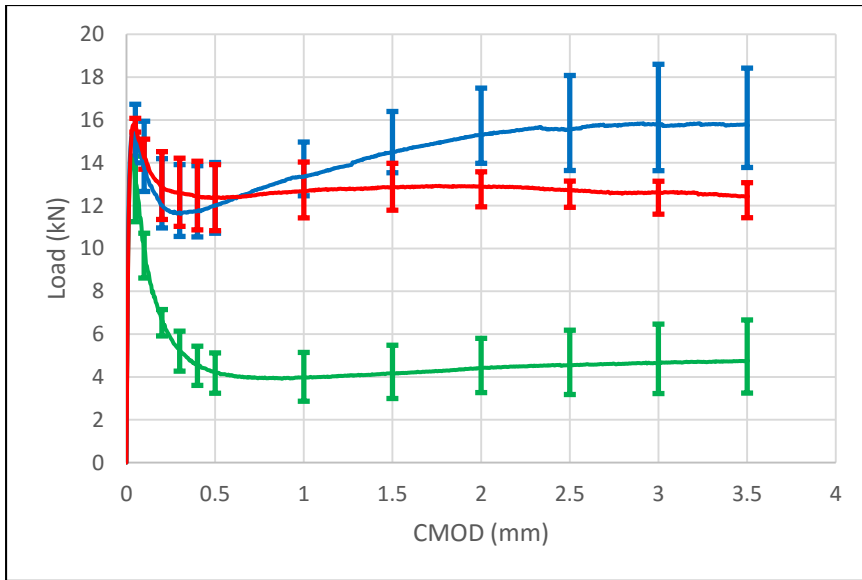
Load Deflection response of 0.94% volume fraction of steel, hybrid and polypropylene FRC at 28 day.



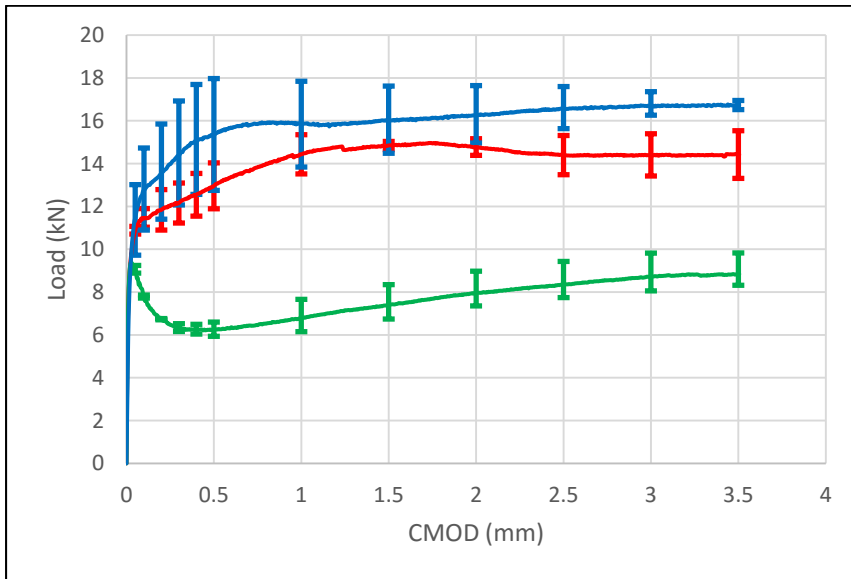
Load CMOD response of 0.5% volume fraction of steel, hybrid and polypropylene FRC at 3 day.



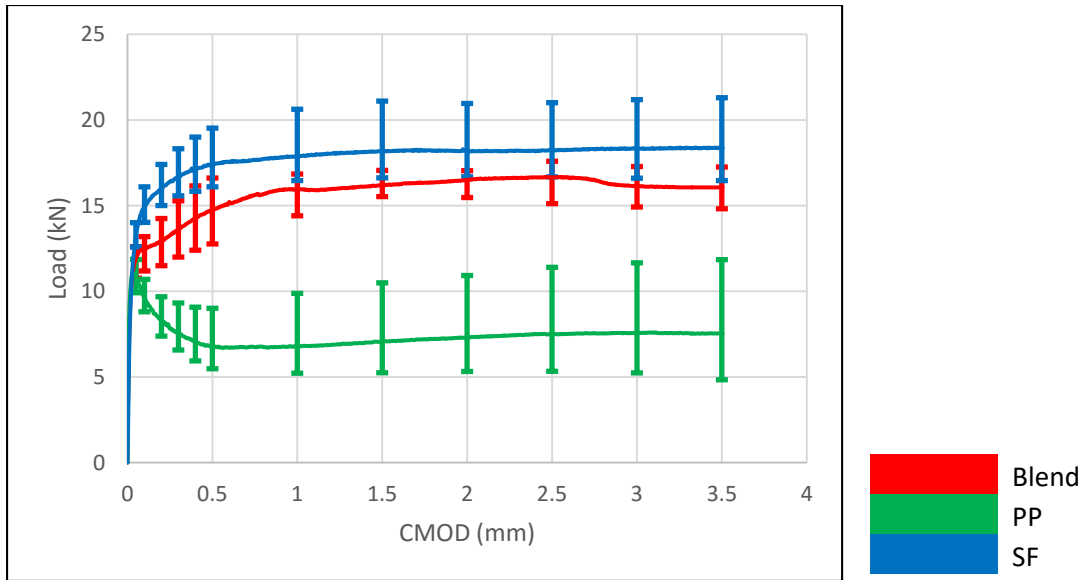
Load CMOD response of 0.5% volume fraction of steel, hybrid and polypropylene FRC at 7 day.



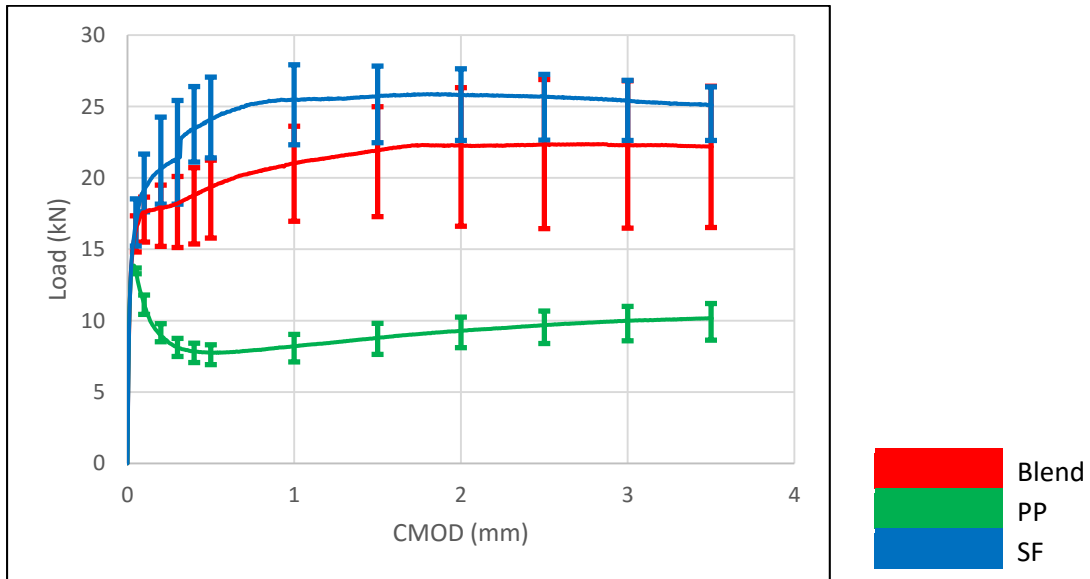
Load CMOD response of 0.5% volume fraction of steel, hybrid and polypropylene FRC at 28 day.



Load CMOD response of 0.94% volume fraction of steel, hybrid and polypropylene FRC at 3 day.



Load CMOD response of 0.94% volume fraction of steel, hybrid and polypropylene FRC at 7 day.



Load CMOD response of 0.94% volume fraction of steel, hybrid and polypropylene FRC at 28 day.



## Annexure III

### FIBER COUNT

#### 1. 0.5% VF Hybrid FRC

##### 1.1 3 Day

##### 1.1.1 Unnotched Specimen

##### Specimen 1

Steel Fiber						Fiber count
1	4	4	2	1	2	14
3	5	3	4	0	2	17
3	2	1	1	1	4	12
5	1	0	2	2	4	14
2	1	5	3	5	7	23
1	3	4	5	4	1	18
Sum						98

Polypropylene fiber						Fiber count
1	1	3	0	1	1	7
3	2	0	2	0	3	10
1	1	3	1	0	2	8
1	0	2	1	1	0	5
4	0	2	0	2	0	8
4	0	2	1	2	0	9
Sum						47

##### Specimen 2

Steel Fiber						Fiber count
1	0	0	1	4	1	7
5	3	2	2	1	0	13
0	0	1	3	2	1	7
0	1	0	2	1	1	5
1	1	3	2	1	0	8
1	4	4	2	2	5	18
Sum						58

Polypropylene fiber						Fiber count
1	0	1	1	1	0	4
1	0	3	1	0	0	5
0	2	1	3	1	1	8
0	0	1	3	0	0	4
2	0	1	3	1	3	10
0	3	0	2	0	4	9
Sum						40

Specimen 3

Steel Fiber						Fiber count
0	5	2	3	1	4	15
1	3	3	3	1	2	13
3	3	0	5	1	1	13
1	0	4	2	0	0	7
3	0	1	3	2	2	11
2	1	2	4	1	1	11
Sum						70

Polypropylene fiber						Fiber count
0	2	3	2	4	3	14
0	3	0	2	1	0	6
0	0	1	2	0	1	4
2	0	12	0	0	2	16
0	2	1	1	0	0	4
3	1	1	0	2	0	7
Sum						51

1.1.2 Notched Specimen

Specimen 1

Steel Fiber						Fiber count
2	9	5	3	2	3	24
6	10	3	3	3	3	28
2	1	2	6	1	1	13
4	8	0	2	1	1	16
3	4	4	4	4	3	22
0	0	0	0	0	0	0
Sum						103

Polypropylene fiber						Fiber count
2	4	3	2	1	2	14
3	8	1	7	6	5	30
0	2	1	7	2	1	13
3	4	2	2	1	1	13
3	6	4	6	2	1	22
0	0	0	0	0	0	0
Sum						92

Specimen 2

Steel Fiber						Fiber count
4	2	2	4	1	3	16
5	1	1	4	2	4	17
3	4	2	0	3	2	14
2	0	0	1	2	2	7
5	3	3	1	6	7	25
0	0	0	0	0	0	0
Sum						79

Polypropylene fiber						Fiber count
4	3	3	2	1	2	15
2	5	1	4	3	3	18
0	1	3	6	1	1	12
2	4	0	2	1	3	12
2	3	3	4	2	4	18
0	0	0	0	0	0	0
Sum						75

### Specimen 3

Steel Fiber						Fiber count	Polypropylene fiber						Fiber count
5	4	6	1	3	11	30	3	4	2	3	4	3	19
2	6	2	3	4	2	19	3	7	1	2	3	4	20
4	5	4	2	2	1	18	1	3	1	6	1	1	13
8	2	8	4	8	1	31	3	4	0	3	2	1	13
5	4	4	2	2	5	22	3	3	1	4	5	1	17
0	0	0	0	0	0	0	0	0	0	0	0	0	0
Sum						120	Sum						82

### 1.2 7 Day

#### 1.2.1 Unnotched Specimen

### Specimen 1

Steel Fiber						Fiber count	Polypropylene fiber						Fiber count
2	2	4	5	1	1	15	1	0	0	0	1	0	2
0	2	4	3	1	4	14	1	1	0	1	2	3	8
0	3	4	3	4	2	16	0	2	0	2	3	1	8
2	0	5	2	1	1	11	0	0	1	4	2	1	8
2	1	1	3	1	1	9	0	1	1	2	0	1	5
4	1	2	2	5	3	17	2	0	1	3	3	1	10
Sum						82	Sum						41

### Specimen 2

Steel Fiber						Fiber count	Polypropylene fiber						Fiber count
2	4	1	1	4	0	12	2	1	0	0	3	2	8
2	3	1	1	5	0	12	1	0	0	1	2	3	7
0	0	2	3	2	1	8	1	2	2	0	1	1	7
2	5	2	3	2	2	16	2	2	0	1	4	2	11
4	0	0	6	1	1	12	3	0	0	0	1	1	5
2	4	8	1	1	0	16	0	0	0	1	0	1	2
Sum						76	Sum						40

### Specimen 3

Steel Fiber						Fiber count
4	4	2	2	1	1	14
8	4	3	1	1	4	21
1	4	3	2	5	1	16
2	1	2	5	0	1	11
1	1	2	5	3	1	13
0	1	2	0	3	3	9
Sum						84

Polypropylene fiber						Fiber count
3	2	0	0	0	1	6
1	0	2	2	1	0	6
0	4	0	4	2	4	14
2	1	2	0	0	1	6
1	2	1	1	1	4	10
0	3	0	0	0	3	6
Sum						48

### 1.2.2 Notched Specimen

#### Specimen 1

Steel Fiber						Fiber count
1	2	7	6	8	5	29
2	5	5	4	4	5	25
0	3	5	2	2	3	15
4	0	1	0	1	0	6
0	6	1	1	0	0	8
0	0	0	0	0	0	0
Sum						83

Polypropylene fiber						Fiber count
2	1	0	1	3	4	11
1	2	3	0	0	1	7
0	1	3	0	1	0	5
3	3	0	0	2	1	9
0	2	0	1	0	0	3
0	0	0	0	0	0	0
Sum						35

#### Specimen 2

Steel Fiber						Fiber count
1	3	2	3	3	2	14
0	1	1	2	3	6	13
1	3	1	5	2	1	13
4	4	3	7	0	7	25
1	1	6	6	4	3	21
0	0	0	0	0	0	0
Sum						86

Polypropylene fiber						Fiber count
2	2	2	2	1	1	10
0	0	0	1	1	3	5
1	1	2	0	0	1	5
3	0	3	2	2	2	12
1	0	2	4	3	1	11
0	0	0	0	0	0	0
Sum						43

### Specimen 3

Steel Fiber						Fiber count
2	3	0	4	2	0	11
1	1	2	1	0	1	6
2	1	2	0	3	3	11
1	3	4	1	0	3	12
2	4	1	4	3	0	14
0	0	0	0	0	0	0
Sum						54

Polypropylene fiber						Fiber count
1	0	2	0	1	0	4
0	1	2	2	0	0	5
0	2	2	1	1	0	6
0	1	1	1	2	0	5
3	0	2	3	1	0	9
0	0	0	0	0	0	0
Sum						29

### 1.3 28 Day

#### 1.3.1 Unnotched Specimen

### Specimen 1

Steel Fiber						Fiber count
3	7	9	1	1	3	24
0	2	0	2	1	4	9
2	3	4	0	1	0	10
0	2	0	4	2	2	10
3	1	3	5	2	3	17
1	4	0	0	1	3	9
Sum						79

Polypropylene fiber						Fiber count
5	3	1	2	3	1	15
2	0	1	1	1	2	7
2	4	2	1	2	3	14
1	2	0	1	0	2	6
2	0	2	0	0	1	5
2	3	0	0	1	1	7
Sum						54

### Specimen 2

Steel Fiber						Fiber count
0	3	2	0	3	2	10
4	4	4	5	1	1	19
2	1	4	2	4	2	15
4	6	5	5	6	4	30
2	2	1	1	2	2	10
1	3	0	0	3	1	8
Sum						92

Polypropylene fiber						Fiber count
1	4	0	1	4	0	10
3	1	1	4	2	1	12
2	2	1	2	0	2	9
2	3	1	1	3	2	12
1	1	1	1	1	1	6
4	1	2	2	1	4	14
Sum						63

### Specimen 3

Steel Fiber						Fiber count
2	2	2	5	5	4	20
3	4	3	2	2	4	18
2	6	4	5	3	3	23
1	0	2	3	2	4	12
3	5	7	4	3	6	28
0	2	3	7	2	3	17
Sum						118

Polypropylene fiber						Fiber count
3	0	2	2	5	0	12
1	0	4	5	1	3	14
5	1	0	2	2	0	10
1	0	0	2	1	0	4
3	1	4	1	1	2	12
1	0	2	1	3	1	8
Sum						60

### 1.3.2 Notched Specimen

#### Specimen 1

Steel Fiber						Fiber count
2	3	1	2	5	2	15
1	0	2	4	6	4	17
1	1	1	5	8	3	19
1	0	1	6	4	14	26
1	5	1	0	3	1	11
0	0	0	0	0	0	0
Sum						88

Polypropylene fiber						Fiber count
2	0	2	4	1	3	12
1	2	1	0	0	1	5
2	0	0	2	1	0	5
2	0	0	1	2	1	6
2	1	0	2	2	0	7
0	0	0	0	0	0	0
Sum						35

#### Specimen 2

Steel Fiber						Fiber count
3	1	2	5	3	7	21
2	1	0	3	3	1	10
1	2	1	4	1	2	11
1	1	3	2	1	0	8
3	2	0	1	4	7	17
0	0	0	0	0	0	0
Sum						67

Polypropylene fiber						Fiber count
1	0	5	0	2	2	10
2	2	1	1	1	1	8
4	0	4	1	3	1	13
0	1	1	0	0	4	6
1	4	2	2	1	3	13
0	0	0	0	0	0	0
Sum						50

### Specimen 3

Steel Fiber						Fiber count
0	7	3	1	1	4	16
0	1	1	3	4	5	14
2	2	1	0	2	5	12
0	0	1	2	6	2	11
4	2	1	1	2	7	17
0	0	0	0	0	0	0
Sum						70

Polypropylene fiber						Fiber count
1	1	1	0	3	0	6
1	1	2	1	2	1	8
2	0	0	0	0	1	3
0	0	1	2	2	2	7
1	0	0	0	2	2	5
0	0	0	0	0	0	0
Sum						29

## 2. 0.5% VF PP FRC

### 2.1 3 Day

#### 2.1.1 Unnotched Specimen

Specimen 1						Fiber count
2	4	1	6	4	3	20
1	0	0	6	10	5	22
6	2	4	1	1	4	18
1	6	2	5	1	5	20
6	3	1	1	1	2	14
5	3	6	3	7	3	27
Sum						121

Specimen 2						Fiber count
2	0	1	3	1	0	7
4	1	11	1	3	0	20
0	3	0	0	4	0	7
1	2	0	2	2	1	8
2	0	1	2	0	3	8
2	3	3	0	0	2	10
Sum						60

#### 2.1.2 Unnotched Specimen

Specimen 1						Fiber count
2	12	4	7	4	2	31
4	7	3	4	7	4	29
4	2	1	7	7	2	23
1	4	1	3	3	3	15
1	5	2	9	7	1	25
0	0	0	0	0	0	0
Sum						123

Specimen 2						Fiber count
9	4	1	1	0	3	18
5	0	0	1	1	4	11
5	5	5	0	1	0	16
2	1	4	6	0	2	15
5	3	3	3	3	5	22
0	0	0	0	0	0	0
Sum						82

Specimen 3						Fiber count
4	6	3	2	3	8	26
4	6	1	3	2	2	18
6	6	4	4	2	1	23
6	6	7	5	6	1	31
4	2	2	3	3	7	21
0	0	0	0	0	0	0
Sum						119

## 2.2 7 Day

### 2.2.1 Unnotched Specimen

Specimen 1						Fiber count
1	1	1	2	4	7	16
0	1	0	2	0	4	7
1	0	0	5	1	4	11
2	1	6	2	1	9	21
1	3	1	1	1	2	9
1	1	1	1	2	3	9
Sum						73

Specimen 2						Fiber count
1	2	4	1	1	2	11
3	0	2	2	2	1	10
2	0	1	1	0	6	10
1	0	4	0	3	2	10
2	3	1	2	1	7	16
4	2	0	0	0	7	13
Sum						70

Specimen 3						Fiber count
6	2	0	4	2	2	16
4	1	0	1	8	5	19
1	1	1	2	2	4	11
1	4	3	4	5	1	18
3	1	3	0	4	1	12
5	1	3	1	0	1	11
Sum						87



## 2.2.2 Unnotched Specimen

Specimen 1						Fiber count
3	3	2	4	4	6	22
1	6	6	8	1	8	30
6	6	1	2	3	8	26
5	3	2	2	3	5	20
6	4	6	6	2	9	33
0	0	0	0	0	0	0
Sum						131

Specimen 2						Fiber count
5	4	3	3	1	1	17
4	4	0	4	2	5	19
10	6	1	0	4	8	29
9	5	3	1	1	3	22
11	8	0	3	6	14	42
0	0	0	0	0	0	0
Sum						129

Specimen 3						Fiber count
2	6	9	5	7	5	34
7	3	0	5	1	8	24
10	3	2	2	2	2	21
7	8	12	10	7	1	45
9	5	5	1	2	2	24
0	0	0	0	0	0	0
Sum						148

## 2.3 28 Day

### 2.3.1 Unnotched Specimen

Specimen 1						Fiber count
6	4	5	5	7	4	31
5	4	4	4	3	3	23
4	1	2	2	2	4	15
3	2	2	4	4	4	19
3	0	4	1	2	4	14
2	3	4	6	2	2	19
Sum						121

Specimen 2						Fiber count
4	0	4	2	5	2	17
4	3	4	6	2	2	21
7	4	5	2	2	3	23
2	5	2	1	2	3	15
2	6	4	5	2	2	21
2	5	3	5	3	9	27
Sum						124

Specimen 3						Fiber count
0	1	2	1	6	1	11
0	3	5	2	3	1	14
3	1	1	2	5	2	14
0	1	0	2	7	4	14
2	0	1	4	2	5	14
1	2	1	3	5	8	20
Sum						87

### 2.3.2 Unnotched Specimen

Specimen 1						Fiber count
2	1	3	1	1	5	13
1	2	25	1	2	4	35
1	1	4	4	6	3	19
0	1	0	1	5	1	8
6	1	2	0	1	8	18
0	0	0	0	0	0	0
Sum						93

Specimen 2						Fiber count
0	6	7	2	0	6	21
0	0	4	0	2	5	11
4	3	6	2	5	0	20
4	5	3	1	1	0	14
0	2	2	1	4	2	11
0	0	0	0	0	0	0
Sum						77

Specimen 3						Fiber count
6	4	2	5	2	4	23
2	3	3	1	1	1	11
3	1	1	4	2	2	13
1	3	1	4	3	1	13
3	7	3	6	2	1	22
0	0	0	0	0	0	0
Sum						82

### 3. 0.5% VF SFRC

#### 3.1 3 Day

##### 3.1.1 Unnotched Specimen

Specimen 1						Fiber count
6	6	5	3	5	1	26
7	2	7	2	5	8	31
9	1	4	8	7	4	33
3	4	8	3	5	10	33
1	4	4	7	7	3	26
6	4	6	1	4	2	23
Sum						172

Specimen 2						Fiber count
6	4	2	0	3	2	17
3	10	2	3	5	10	33
3	8	0	5	7	4	27
1	4	5	5	2	4	21
8	9	5	5	5	6	38
4	6	5	1	5	9	30
Sum						166

Specimen 3						Fiber count
4	3	7	5	11	6	36
2	1	6	2	4	6	21
3	5	6	0	5	6	25
5	7	6	2	3	6	29
2	4	5	4	4	0	19
3	4	4	4	2	2	19
Sum						149

##### 3.1.2 Notched Specimen

Specimen 1						Fiber count
2	1	15	4	6	2	30
3	6	2	9	0	8	28
3	5	7	13	9	2	39
4	4	4	2	3	2	19
3	4	11	7	4	2	31
0	0	0	0	0	0	0
Sum						147

Specimen 2						Fiber count
5	9	3	0	7	1	25
7	8	1	3	4	5	28
6	3	7	1	2	1	20
3	7	3	5	2	4	24
0	4	8	2	1	5	20
0	0	0	0	0	0	0
Sum						117

Specimen 3						Fiber count
6	6	6	5	3	0	26
4	5	3	2	5	1	20
9	4	8	4	6	7	38
4	7	2	7	6	6	32
4	0	4	8	7	6	29
0	0	0	0	0	0	0
Sum						145

### 3.2 7 Day

#### 3.2.1 Unnotched Specimen

Specimen 1						Fiber count
4	9	4	2	12	3	34
1	3	3	7	3	1	18
7	2	3	4	1	5	22
1	8	6	3	3	2	23
5	3	2	4	4	3	21
7	6	1	6	10	6	36
Sum						154

Specimen 2						Fiber count
2	5	8	11	3	2	31
0	6	8	3	5	8	30
7	3	8	4	4	3	29
3	4	6	6	5	4	28
6	4	7	5	5	5	32
7	2	5	5	5	5	29
Sum						179

Specimen 3						Fiber count
1	4	5	5	2	4	21
4	3	5	5	6	6	29
0	4	8	7	9	6	34
5	5	1	6	6	6	29
3	5	9	4	3	7	31
7	3	2	6	6	0	24
Sum						168

### 3.2.2 Notched Specimen

Specimen 1						Fiber count
6	2	3	14	4	4	33
1	4	4	5	9	2	25
6	3	4	1	5	3	22
5	4	0	7	7	3	26
6	3	3	7	0	5	24
0	0	0	0	0	0	0
Sum						130

Specimen 2						Fiber count
5	9	3	2	1	1	21
2	10	9	0	1	5	27
4	9	9	6	1	4	33
13	8	11	5	4	5	46
2	10	2	8	2	1	25
0	0	0	0	0	0	0
Sum						152

Specimen 3						Fiber count
12	9	4	1	4	3	33
4	1	1	6	6	4	22
6	6	4	6	5	2	29
7	9	2	8	2	1	29
3	6	3	6	0	4	22
0	0	0	0	0	0	0
Sum						135

### 3.3 28 Day

#### 3.3.1 Unnotched Specimen

Specimen 1						Fiber count
3	4	6	3	0	5	21
9	8	6	1	2	8	34
4	6	2	4	1	3	20
5	6	7	5	1	7	31
2	0	12	9	2	4	29
1	2	0	2	3	7	15
Sum						150

Specimen 2						Fiber count
5	3	7	17	12	8	52
8	4	2	3	3	0	20
5	2	4	9	8	1	29
10	0	0	7	2	5	24
6	3	1	5	2	2	19
4	2	9	2	3	2	22
Sum						166

Specimen 3						Fiber count
4	5	5	4	1	2	21
1	3	8	6	2	0	20
4	2	7	8	2	5	28
6	3	0	12	8	0	29
7	1	2	7	2	2	21
2	0	1	4	2	3	12
Sum						131

### 3.3.2 Notched Specimen

Specimen 1						Fiber count
6	2	3	14	4	4	33
1	4	4	5	9	2	25
6	3	4	1	5	3	22
5	4	0	7	7	3	26
6	3	3	7	0	5	24
0	0	0	0	0	0	0
Sum						130

Specimen 2						Fiber count
5	9	3	2	1	1	21
2	10	9	0	1	5	27
4	9	9	6	1	4	33
13	8	11	5	4	5	46
2	10	2	8	2	1	25
0	0	0	0	0	0	0
Sum						152

Specimen 3						Fiber count
12	9	4	1	4	3	33
4	1	1	6	6	4	22
6	6	4	6	5	2	29
7	9	2	8	2	1	29
3	6	3	6	0	4	22
0	0	0	0	0	0	0
Sum						135

#### 4. 0.94% VF HyFRC

##### 4.1 3 Day

##### 4.1.1 Unnotched Specimen

##### Specimen 2

Steel Fiber						Fiber count
0	0	4	0	2	6	12
0	2	0	2	4	4	12
0	0	6	4	6	6	22
6	4	4	6	4	6	30
2	8	4	16	6	12	48
0	4	4	4	2	4	18
Sum						142

Polypropylene fiber						Fiber count
0	2	0	4	2	8	16
0	4	2	0	4	8	18
0	4	6	0	6	6	22
4	0	6	2	4	4	20
0	4	6	10	10	2	32
0	10	8	6	0	0	24
Sum						132

##### Specimen 2

Steel Fiber						Fiber count
6	8	2	6	4	8	34
2	2	2	6	0	6	18
6	2	2	0	2	8	20
10	0	6	4	4	8	32
4	2	2	0	8	4	20
6	8	2	2	2	4	24
Sum						148

Polypropylene fiber						Fiber count
4	0	4	8	0	4	20
2	4	2	0	2	0	10
0	2	0	0	0	0	2
4	2	2	4	0	4	16
8	0	0	0	2	2	12
2	6	0	0	0	2	10
Sum						70

### 4.1.2 Notched Specimen

#### Specimen 1

Steel Fiber						Fiber count	Polypropylene fiber						Fiber count
12	6	14	2	10	14	58	2	4	6	2	6	2	22
4	0	2	6	0	8	20	4	0	0	0	4	4	12
2	2	2	2	2	4	14	2	4	2	0	0	6	14
4	4	0	0	0	4	12	0	0	2	0	2	6	10
4	10	4	10	12	2	42	2	8	2	10	4	2	28
0	0	0	0	0	0	0	0	0	0	0	0	0	0
Sum						146	Sum						86

#### Specimen 2

Steel Fiber						Fiber count	Polypropylene fiber						Fiber count
4	4	2	0	6	6	22	0	4	2	6	6	8	26
0	2	2	10	6	4	24	2	2	2	6	6	10	28
10	0	0	2	0	4	16	4	2	0	0	0	10	16
8	10	8	6	0	4	36	6	0	0	2	0	2	10
4	4	8	6	2	2	26	6	0	6	4	2	2	20
0	0	0	0	0	0	0	0	0	0	0	0	0	0
Sum						124	Sum						100

#### Specimen 3

Steel Fiber						Fiber count	Polypropylene fiber						Fiber count
2	4	16	6	8	8	44	2	8	2	2	2	4	20
2	0	8	6	6	10	32	2	2	4	4	2	4	18
2	0	4	6	12	10	34	0	0	0	0	6	10	16
4	0	2	8	6	14	34	10	2	4	8	4	8	36
8	8	6	0	2	10	34	6	6	4	4	0	8	28
0	0	0	0	0	0	0	0	0	0	0	0	0	0
Sum						178	Sum						118



## 4.2 7 Day

### 4.2.1 Unnotched Specimen

#### Specimen 1

Steel Fiber						Fiber count
2	2	0	3	9	6	22
6	6	4	10	4	6	36
3	5	1	2	0	2	13
2	1	2	3	8	1	17
1	2	4	2	2	2	13
3	9	5	5	2	14	38
Sum						139

Polypropylene fiber						Fiber count
3	3	1	4	2	5	18
4	6	2	1	1	3	17
3	0	2	2	2	2	11
4	3	1	2	4	3	17
0	5	2	0	4	5	16
4	6	3	2	1	4	20
Sum						99

#### Specimen 2

Steel Fiber						Fiber count
2	5	6	2	8	3	26
2	0	3	3	0	1	9
1	0	5	3	4	5	18
1	5	0	5	4	6	21
2	2	3	9	4	3	23
7	4	13	7	5	3	39
Sum						136

Polypropylene fiber						Fiber count
4	1	5	1	6	0	17
1	1	2	0	1	1	6
1	1	2	1	2	2	9
2	4	2	5	2	3	18
5	2	5	5	4	4	25
2	2	8	6	3	6	27
Sum						102

#### Specimen 3

Steel Fiber						Fiber count
9	7	7	4	4	5	36
8	4	5	8	5	3	33
4	7	1	1	2	0	15
8	8	1	2	2	1	22
8	1	0	4	2	6	21
5	10	6	11	7	7	46
Sum						173

Polypropylene fiber						Fiber count
3	4	3	8	9	4	31
5	1	1	7	1	7	22
1	2	3	4	0	0	10
0	0	1	0	3	1	5
3	3	3	5	11	5	30
2	3	10	7	3	4	29
Sum						127

## 4.2.2 Notched Specimen

### Specimen 1

Steel Fiber						Fiber count
6	7	4	4	4	0	25
1	2	2	3	4	7	19
3	12	5	6	2	2	30
3	2	3	6	2	2	18
0	6	10	3	4	1	24
0	0	0	0	0	0	0
Sum						116

Polypropylene fiber						Fiber count
3	2	3	3	0	1	12
0	4	7	8	3	1	23
3	4	7	6	0	4	24
4	2	2	0	3	4	15
1	2	5	1	4	3	16
0	0	0	0	0	0	0
Sum						90

### Specimen 2

Steel Fiber						Fiber count
4	2	1	2	1	11	21
6	1	0	0	1	2	10
5	3	4	4	1	3	20
6	4	2	5	4	5	26
6	4	4	5	7	5	31
0	0	0	0	0	0	0
Sum						108

Polypropylene fiber						Fiber count
6	4	1	1	3	5	20
7	0	0	0	2	1	10
3	3	2	4	0	3	15
2	2	1	3	0	3	11
7	4	10	3	9	5	38
0	0	0	0	0	0	0
Sum						94

### Specimen 3

Steel Fiber						Fiber count
5	7	4	4	6	5	31
3	9	6	12	11	4	45
11	11	5	7	6	6	46
7	5	6	4	4	3	29
6	7	9	7	6	2	37
0	0	0	0	0	0	0
Sum						188

Polypropylene fiber						Fiber count
4	6	7	7	6	5	35
5	4	4	7	4	11	35
1	4	6	4	3	5	23
12	3	3	2	1	3	24
5	6	4	4	1	3	23
0	0	0	0	0	0	0
Sum						140

### 4.3 28 Day

#### 4.3.1 Unnotched Specimen

##### Specimen 1

Steel Fiber						Fiber count
1	2	6	8	8	8	33
5	4	4	8	6	9	36
1	3	4	1	6	3	18
4	5	2	4	5	3	23
5	9	0	1	1	5	21
5	8	14	8	8	12	55
Sum						186

Polypropylene fiber						Fiber count
6	9	8	3	4	2	32
8	4	5	4	2	2	25
3	0	1	1	0	2	7
2	0	1	3	6	2	14
0	5	2	2	11	4	24
4	6	3	2	1	4	20
Sum						122

##### Specimen 2

Steel Fiber						Fiber count
2	5	6	2	8	3	26
2	0	3	3	5	1	14
1	1	2	0	1	5	10
1	4	1	4	3	6	19
2	3	7	10	5	3	30
7	3	13	7	5	3	38
Sum						137

Polypropylene fiber						Fiber count
3	5	3	1	6	0	18
2	1	2	1	0	0	6
1	1	2	2	3	0	9
5	2	2	4	2	1	16
1	6	3	0	6	5	21
4	6	6	4	4	2	26
Sum						96

##### Specimen 3

Steel Fiber						Fiber count
9	7	7	4	4	5	36
1	4	1	1	5	3	15
2	5	10	4	4	4	29
7	1	0	0	2	1	11
3	0	0	0	2	6	11
3	6	4	10	10	6	39
Sum						141

Polypropylene fiber						Fiber count
4	3	2	3	3	2	17
4	1	3	5	1	6	20
0	2	1	1	1	0	5
1	1	5	1	4	2	14
5	7	3	1	7	4	27
2	3	10	7	3	4	29
Sum						112

### 4.3.2 Notched Specimen

#### Specimen 1

Steel Fiber						Fiber count
6	7	4	4	4	0	25
1	2	2	3	4	7	19
3	12	5	6	2	2	30
3	2	3	6	2	2	18
0	6	10	3	4	1	24
0	0	0	0	0	0	0
Sum						116

Polypropylene fiber						Fiber count
3	2	3	3	0	1	12
0	2	0	8	3	1	14
3	3	4	6	0	4	20
4	4	1	0	3	4	16
1	2	5	1	4	3	16
0	0	0	0	0	0	0
Sum						78

#### Specimen 2

Steel Fiber						Fiber count
4	2	1	2	1	11	21
6	1	0	3	4	9	23
5	3	4	6	2	4	24
6	4	2	4	7	6	29
7	4	4	8	11	7	41
0	0	0	0	0	0	0
Sum						138

Polypropylene fiber						Fiber count
6	4	1	1	3	5	20
7	0	0	3	3	1	14
3	3	2	5	4	3	20
2	2	1	3	2	3	13
7	4	10	5	7	5	38
0	0	0	0	0	0	0
Sum						105

#### Specimen 3

Steel Fiber						Fiber count
4	10	9	3	4	3	33
6	7	8	7	11	4	43
6	5	4	5	7	3	30
4	2	4	2	4	5	21
3	7	6	9	6	2	33
0	0	0	0	0	0	0
Sum						160

Polypropylene fiber						Fiber count
4	6	7	7	6	5	35
5	4	4	7	4	11	35
1	4	6	4	3	5	23
12	3	3	2	1	3	24
5	6	4	4	1	3	23
0	0	0	0	0	0	0
Sum						140

5. 0.94% VF PPFRC

5.1 3 Day

5.1.1 Unnotched Specimen

Specimen 1						Fiber count
6	2	5	1	9	8	31
1	2	6	1	6	9	25
8	3	2	1	0	10	24
9	5	2	3	2	2	23
4	6	5	6	2	12	35
5	2	6	7	4	4	28
Sum						166

Specimen 2						Fiber count
12	7	1	7	6	5	38
8	5	4	11	3	6	37
8	6	5	4	8	10	41
6	3	6	10	5	9	39
5	7	5	4	6	3	30
4	6	4	4	14	9	41
Sum						226

Specimen 3						Fiber count
7	6	9	3	7	10	42
8	6	2	8	4	1	29
7	6	7	6	5	5	36
9	4	13	5	6	6	43
3	2	10	8	6	6	35
5	6	4	6	8	3	32
Sum						217

5.1.2 Unnotched Specimen

Specimen 1						Fiber count
8	5	4	10	2	15	44
6	5	1	5	4	7	28
18	2	2	2	7	6	37
5	2	3	3	8	5	26
5	3	3	12	6	6	35
0	0	0	0	0	0	0
Sum						170

Specimen 2						Fiber count
6	15	9	17	1	0	48
2	5	5	8	1	2	23
2	7	1	4	15	8	37
6	9	7	10	1	5	38
8	4	7	9	2	0	30
0	0	0	0	0	0	0
Sum						176

Specimen 3						Fiber count
8	7	5	6	6	4	36
6	6	6	10	7	6	41
3	2	10	5	6	3	29
4	8	10	12	6	9	49
2	16	5	8	2	6	39
0	0	0	0	0	0	0
Sum						194

## 5.2 7 Day

### 5.2.1 Unnotched Specimen

Specimen 1						Fiber count
3	7	9	3	3	5	30
2	12	6	5	8	2	35
1	10	8	8	9	6	42
9	8	7	9	8	2	43
7	7	5	6	7	8	40
9	1	7	7	5	2	31
Sum						221

Specimen 2						Fiber count
11	5	8	2	5	9	40
4	8	4	3	7	11	37
8	3	1	2	5	9	28
5	3	5	3	1	8	25
4	6	1	8	4	2	25
6	3	5	3	2	6	25
Sum						180

Specimen 3						Fiber count
5	5	5	5	5	7	32
4	6	5	5	10	7	37
2	4	6	4	2	3	21
5	7	5	5	2	2	26
12	9	5	8	2	4	40
5	4	4	2	1	3	19
Sum						175

### 5.2.2 Notched Specimen

Specimen 1						Fiber count
6	3	3	4	8	7	31
8	3	7	5	2	6	31
8	7	6	6	3	1	31
3	6	6	3	4	6	28
2	2	7	7	1	3	22
0	0	0	0	0	0	0
Sum						143

Specimen 2						Fiber count
4	6	3	6	6	10	35
5	5	1	7	5	6	29
4	3	4	4	4	7	26
8	5	5	9	1	7	35
6	2	6	1	5	8	28
0	0	0	0	0	0	0
Sum						153

Specimen 3						Fiber count
7	6	3	5	3	6	30
3	7	3	1	1	1	16
6	3	3	1	0	3	16
5	3	1	3	3	5	20
3	2	1	4	3	9	22
0	0	0	0	0	0	0
Sum						104

### 5.3 28 Day

#### 5.3.1 Unnotched Specimen

Specimen 1						Fiber count
1	6	6	3	4	8	28
1	4	4	0	2	4	15
3	5	2	0	2	5	17
6	4	6	3	9	6	34
6	5	5	9	14	6	45
10	6	5	11	2	4	38
Sum						177

Specimen 2						Fiber count
9	4	7	7	5	6	38
1	5	5	3	2	10	26
9	5	12	2	15	7	50
2	7	1	4	5	7	26
3	5	8	10	3	2	31
2	3	12	6	8	7	38
Sum						209

Specimen 3						Fiber count
1	7	5	5	3	6	27
3	2	8	3	3	7	26
13	2	6	15	11	6	53
3	8	6	7	6	10	40
3	7	5	7	4	5	31
6	7	8	4	6	3	34
Sum						211

### 5.3.2 Notched Specimen

Specimen 1						Fiber count
16	0	2	6	6	5	35
6	1	0	2	6	5	20
15	3	5	1	9	6	39
6	1	4	2	2	4	19
5	1	4	8	0	5	23
0	0	0	0	0	0	0
Sum						136

Specimen 2						Fiber count
9	6	9	3	6	4	37
5	2	9	8	9	2	35
4	10	4	3	2	2	25
7	10	7	6	4	8	42
10	4	8	3	6	3	34
0	0	0	0	0	0	0
Sum						173

Specimen 3						Fiber count
5	7	10	4	5	11	42
4	4	9	6	4	11	38
9	5	15	6	4	13	52
4	1	2	2	6	17	32
6	3	6	3	6	5	29
0	0	0	0	0	0	0
Sum						193



## 6. 0.94% VF SFRC

### 6.1 3 Day

#### 6.1.1 Unnotched Specimen

Specimen 1						Fiber count
9	10	2	6	3	6	36
10	5	10	7	11	10	53
5	8	14	20	13	11	71
6	7	8	9	14	8	52
3	4	6	4	2	3	22
1	2	5	1	9	2	20
Sum						254

Specimen 2						Fiber count
7	4	1	6	3	4	25
8	8	3	14	5	2	40
7	4	5	5	13	1	35
3	2	2	12	7	1	27
11	3	3	18	7	1	43
7	7	7	11	6	2	40
Sum						210

Specimen 3						Fiber count
13	4	14	8	16	17	72
3	3	17	4	6	9	42
9	11	8	3	3	6	40
7	7	15	1	3	10	43
1	4	9	11	6	11	42
8	5	19	3	10	2	47
Sum						286

#### 6.1.2 Notched Specimen

Specimen 2						Fiber count
4	17	12	12	16	23	84
2	8	6	10	5	17	48
6	13	6	11	12	17	65
11	5	12	5	13	5	51
10	4	5	6	11	8	44
0	0	0	0	0	0	0
Sum						292

Specimen 3						Fiber count
12	11	11	5	12	14	65
9	4	7	8	10	10	48
7	2	8	3	10	4	34
3	4	7	6	17	1	38
0	6	9	8	13	5	41
0	0	0	0	0	0	0
Sum						226

## 6.2 7 Day

### 6.2.1 Unnotched Specimen

Specimen 1						Fiber count
7	12	14	3	6	13	55
14	6	7	7	4	7	45
13	9	3	4	6	10	45
5	1	7	13	4	9	39
3	3	3	11	10	4	34
15	4	4	7	10	10	50
Sum						268

Specimen 2						Fiber count
8	3	5	5	1	5	27
7	5	3	1	7	22	45
7	2	5	8	1	11	34
14	3	5	9	3	13	47
4	8	6	15	3	1	37
3	5	4	1	4	9	26
Sum						216

Specimen 3						Fiber count
7	7	7	13	13	14	61
16	10	4	16	11	6	63
16	2	9	8	7	6	48
7	10	6	7	9	16	55
3	3	11	2	8	12	39
1	5	1	2	3	9	21
Sum						287

### 6.2.2 Notched Specimen

Specimen 1						Fiber count
17	16	5	8	2	10	58
19	10	5	6	10	3	53
5	9	10	8	9	2	43
5	12	11	4	3	3	38
7	11	4	8	5	7	42
0	0	0	0	0	0	0
Sum						234

Specimen 2						Fiber count
24	22	19	13	20	13	111
7	12	10	8	10	5	52
1	3	13	1	2	8	28
4	2	6	3	14	7	36
6	5	11	2	7	20	51
0	0	0	0	0	0	0
Sum						278

Specimen 3						Fiber count
11	1	13	18	18	16	77
8	11	12	8	9	10	58
13	7	19	9	8	8	64
8	11	10	3	4	5	41
8	12	8	11	13	8	60
0	0	0	0	0	0	0
Sum						300

### 6.3 28 Day

#### 6.3.1 Unnotched Specimen

Specimen 1						Fiber count
1	6	6	3	4	8	28
1	4	4	0	2	4	15
3	5	2	0	2	5	17
6	4	6	3	9	6	34
6	5	5	9	14	6	45
10	6	5	11	2	4	38
Sum						177

Specimen 2						Fiber count
9	4	7	7	5	6	38
1	5	5	3	2	10	26
9	5	12	2	15	7	50
2	7	1	4	5	7	26
3	5	8	10	3	2	31
2	3	12	6	8	7	38
Sum						209

Specimen 3						Fiber count
1	7	5	5	3	6	27
3	2	8	3	3	7	26
13	2	6	15	11	6	53
3	8	6	7	6	10	40
3	7	5	7	4	5	31
6	7	8	4	6	3	34
Sum						211

### 6.3.2 Notched Specimen

Specimen 1						Fiber count
16	0	2	6	6	5	35
6	1	0	2	6	5	20
15	3	5	1	9	6	39
6	1	4	2	2	4	19
5	1	4	8	0	5	23
0	0	0	0	0	0	0
Sum						136

Specimen 2						Fiber count
9	6	9	3	6	4	37
5	2	9	8	9	2	35
4	10	4	3	2	2	25
7	10	7	6	4	8	42
10	4	8	3	6	3	34
0	0	0	0	0	0	0
Sum						173

Specimen 3						Fiber count
5	7	10	4	5	11	42
4	4	9	6	4	11	38
9	5	15	6	4	13	52
4	1	2	2	6	17	32
6	3	6	3	6	5	29
0	0	0	0	0	0	0
Sum						193